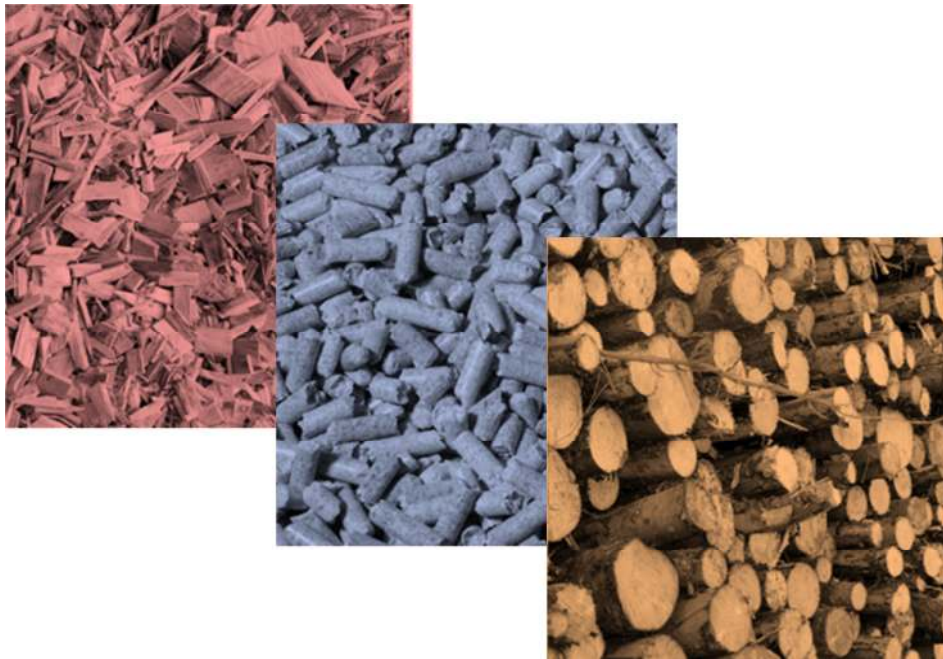


# CHALMERS



## Development of a tar decomposition model for application in a Chemical-Looping Reformer operated with raw gas from a biomass gasifier

*Master of Science Thesis*

MARIA INÊS ADRIÃO PESTANA

Department of Energy and Environment  
*Division of Energy Technology*  
CHALMERS UNIVERSITY OF TECHNOLOGY  
Göteborg, Sweden, 2011  
Master's Thesis 2011:T2011-363



MASTER'S THESIS 2011:NN

Development of a tar decomposition model for application in a  
Chemical-Looping Reformer operated with raw gas from a biomass gasifier

Master's Thesis

MARIA INÊS ADRIÃO PESTANA

Department of Energy and Environment  
*Division of Energy Technology*  
CHALMERS UNIVERSITY OF TECHNOLOGY  
Göteborg, Sweden 2011

Development of a tar decomposition model for application in a Chemical-Looping Reformer operated with raw gas from a biomass gasifier  
Master's Thesis  
MARIA INÊS ADRIÃO PESTANA

© MARIA INÊS ADRIÃO PESTANA, 2011

Master's Thesis 2011:NN  
Department of Energy and Environment  
Division of Energy Technology

Chalmers University of Technology  
SE-412 96 Göteborg  
Sweden  
Telephone: + 46 (0)31-772 1000

Cover:  
Woody biomass types – wood chips, wood pellets and logs. Referred to in the introduction from biomass to Synthetic Natural Gas (SNG).

Chalmers Reproservice  
Göteborg, Sweden 2011

## Development of a tar decomposition model for application in a Chemical-Looping Reformer operated with raw gas from a biomass gasifier

MARIA INÊS ADRIÃO PESTANA  
Department of Energy and Environment  
Division of Energy Technology  
Chalmers University of Technology  
SE-412 96 Göteborg (Sweden)

### ABSTRACT

The production of Synthetic Natural Gas (SNG) represents one of the promising alternatives for biofuel manufacture. The transport sector is where SNG has been identified as having the highest potential in terms of profitability and use efficiency, making it the main aim of production. The key process steps to yield SNG are thermal gasification of biomass followed by methanation of the product gas. But, before reaching methanation the producer gas has to be cleaned from the presence of organic hydrocarbons called tars as well as other contaminants, eliminating them from the mixture of permanent gases. Tars are usually referred to as condensable hydrocarbons that start to condense already at temperatures around 350°C. As the tar condenses it creates operating problems like clogging and blockage of equipment downstream the gasifier. A system for cleaning the producer gas from biomass gasification was developed at Chalmers University of Technology, using a Chemical-Looping Reformer (CLR) for catalytic cracking of tar components. The system was developed for further implementation in the industry with the aim of making it a quicker solution for tar cleaning.

The objective of the work was to develop a model for catalytic decomposition of tars, using data available by experiments occurring within the CLR-System at Chalmers. The system is fed with producer gas from Chalmers 2-4MW<sub>th</sub> biomass gasifier, which goes into the dual-fluidized bed process in which the system consists. The available data for the work was achieved by running the CLR-System with a manganese-based catalyst in the fuel reactor (FR) at three different working temperatures and two oxygen concentrations for reforming of the catalyst in the air reactor (AR). Development of the decomposition model was done firstly by grouping the analyzed tar molecules according to structures, conversions and amount and secondly by study of models describing decomposition processes. From implementation of the developed model ruling first order differential equations in the mathematical software MatLab, it was possible to verify to what extent the model correctly describes the decomposition processes inside the reactor and to have a first impression on how fast the reactions are or how each reaction interacts with the others. Experimental data and simulation results only differed by around 15% maximum. It was conclusive that increasing temperatures and higher oxygen concentrations perform better than lower values, but can also have an influence on the composition of the permanent gases. It was possible to detect some trends on the decomposition pattern but no correlation between working conditions and cracking processes can be made. Finally, temperature seems to have a higher influence on the results than oxygen concentration.

KEYWORDS: Tars; Catalytic Cracking/Decomposition; Manganese-Based Catalyst; Biomass Gasification; Synthetic Natural Gas (SNG); Chemical-Looping Reformer (CLR)



## ACKNOWLEDGMENT

I would like to thank the research team working at the Chemical-Looping Reformer System at Chalmers for all the help and support during the completion of this thesis. Nicolas Berguerand, Fredrik Lind, Mikael Israelsson, Martin Seemann and Henrik Thunman thank you so much for having received me in the department and for participating in the project.

I would like to thank also to my family for all the support while I was in Sweden. Especially to my parents, José and Isabel, for giving me this unique opportunity both for visiting and working in a new environment which made me grow as a person and gave me new experiences. To my sister Leonor, my grandparents Carlos and Pilar and my aunts Helena and Regina for all the support and “saudade” during this period.

Finally, I would like to thank all my friends. My friends from Portugal, who helped me adapt to a new place and kept in touch making me feel I was not so far away. To all my new friends from all over the world, who made me feel I was at home in Göteborg. I’ll miss all the Erasmus community.





# TABLE OF CONTENTS

<b>ABSTRACT</b> .....	i
<b>ACKNOWLEDGMENT</b> .....	iii
<b>NOMENCLATURE &amp; ABBREVIATIONS</b> .....	xi
Nomenclature.....	xi
Abbreviations .....	xi
<b>1. INTRODUCTION</b> .....	1
1.1. Background.....	1
1.2. From Biomass to Synthetic Natural Gas (SNG).....	4
1.2.1. <i>Biomass</i> .....	4
1.2.2. <i>Gasification</i> .....	8
1.2.3. <i>Gas Conditioning</i> .....	11
1.2.4. <i>Methanation &amp; Gas Upgrading</i> .....	16
1.3. Literature Survey .....	17
1.3.1. <i>Chemical-Looping Combustion (CLC) &amp; Chemical-Looping Reforming (CLR)</i> .....	17
1.3.2. <i>Oxygen Carriers</i> .....	20
1.3.3. <i>Tar Models</i> .....	23
1.4. Objective.....	24
1.5. Methodology .....	24
1.6. Thesis Outline and Structure .....	25
<b>2. CHEMICAL-LOOPING REFORMING (CLR) SYSTEM AT CHALMERS</b> .....	27
2.1. Description of Experimental Set-up .....	28
2.2. Measurement Techniques.....	30
2.2.1. Permanent Gases .....	30
2.2.2. Solid-Phase Adsorption (SPA).....	31
2.3. Experimental Results and Analysis .....	33
2.3.1. Error Analysis of SPA-Sampling Results .....	33
2.3.2. Decomposition Trends .....	35
<b>3. DECOMPOSITION MODEL</b> .....	40
3.1. Development of Model .....	40
3.2. Implementation of Model in MatLab .....	47
<b>4. RESULTS &amp; DISCUSSION</b> .....	50
4.1. Analysis of Best Results for Each Working System Conditions.....	50

4.2. Evaluation of Kinetic Constants and Simulation Errors for all Best Results .....	58
<b>5. CONCLUSIONS &amp; FUTURE WORK .....</b>	<b>63</b>
<b>REFERENCES .....</b>	<b>67</b>
<b>APPENDIXES:</b>	
APPENDIX I – WORLD SHARES OF FUELS’ PRODUCTION.....	73
APPENDIX II – GAS CLEANING TECHNOLOGIES .....	74
APPENDIX III – CLR SYSTEM .....	76
APPENDIX IV – RESULTS OF PREVIOUS STUDIES .....	77
APPENDIX V – DETAILED INFORMATION ON IDENTIFIED TAR MOLECULES.....	79
APPENDIX VI – RELATIVE STANDARD DEVIATION TABLES .....	81
APPENDIX VII – ADDITIONAL RESULTS FOR TARS CALCULATIONS.....	84

# TABLE OF FIGURES

Figure 1 - European Union consumption of energy in 2010 .....	1
Figure 2 - Worldwide energy consumption in 2010.....	1
Figure 3 - Simplified scheme of Biomass to SNG configuration (with gas cooling, depending on the gas conditioning/cleaning technology) [1] .....	3
Figure 4 - Typical process efficiencies from wood to SNG production [1] .....	3
Figure 5 - Biomass constituents .....	5
Figure 6 - Woody biomass: a) wood chips; b) wood pellets; c) logs .....	6
Figure 7 - Biomass carbon cycle .....	7
Figure 8 - Chalmers allothermic/indirect gasification system.....	9
Figure 9 - Tar maturation scheme proposed by Elliott [23] .....	12
Figure 10 - Tar yield as a function of the maximum temperature exposure [24].....	12
Figure 11 - Tar cleaning concept by primary methods [26] .....	14
Figure 12 - Illustration of the need of primary and secondary methods with technology development in time [20] .....	14
Figure 13 - Tar cleaning concept by secondary methods [26] .....	15
Figure 14 - Schematic view of chemical-looping combustion process with two interconnected fluidized beds: 1) air reactor; 2) cyclone; 3) fuel reactor [31] .....	18
Figure 16 - Equilibrium gas composition of the fuel reactor (FR) exhaust depending on the air/fuel ratio for pure methane according to J. Bolhar-Nordenkamp et al. (40).....	19
Figure 15 - The necessary heat extraction from the reactor system versus the global air/fuel ratio for pure methane according to J. Bolhar-Nordenkamp et al. [65] .....	19
Figure 17 - Conversion of CH <sub>4</sub> to CO <sub>2</sub> versus the temperature for different metal oxides [32].....	21
Figure 18 - Mass ratio of active oxygen for different systems of metal oxides [38].....	21
Figure 19 - Reduction and oxidation conversions for Mn-based oxygen carrier supported by ZrO <sub>2</sub> sintered at 950° (-), 1100° (- -), 1200° (...) and 1300°C (- .. -) [34] .....	22
Figure 20 - System Components [17] .....	29
Figure 21 - Circulation of the catalyst in the system [16].....	30
Figure 22 - Permanent gases measurement set.....	31
Figure 23 - Septum-tight port for gastight syringe insertion in the raw gas line .....	32
Figure 24 - SPA sampling and analysis scheme for tar components [21].....	33
Figure 25 - RSD result values of grouped tars for 23% manganese catalyst at 700°C .....	34
Figure 26 - RSD result values of grouped tars for 23% manganese catalyst at 750°C .....	34

Figure 27 - RSD result values of grouped tars for 23% manganese catalyst at 800°C .....	34
Figure 28 - 23% Manganese tar conversions [%] .....	36
Figure 29 - Relative concentrations of grouped tars for operating temperature 700° at different O <sub>2</sub> concentrations.....	36
Figure 30 - Relative concentrations of grouped tars for operating temperature 750° at different O <sub>2</sub> concentrations.....	36
Figure 31 - Relative concentrations of grouped tars for operating temperature 800° at different O <sub>2</sub> concentrations.....	37
Figure 32 - FID signal during analysis cycle [60] .....	41
Figure 33 - Tar groups: a) Benzene; b) Naphthalene; c) Branched molecules of 1 and 2 rings; d) Non-alternant molecules of 1 and 2 rings; e) Polycyclic Aromatic Hydrocarbons (PAHs) of 3 and 4 rings; f) Phenolic compounds .....	43
Figure 34 - Developed model for tar breakdown.....	45
Figure 35 - Overall view of MatLab model .....	47
Figure 36 - Schematics of the calculation of the best kinetic constants on the iterative loop for the manganese catalyst.....	48
Figure 37 - Tested set of kinetic constants and respective error for each tar group.....	50
Figure 38 - Development of each group's concentrations at 700°C and 1% O <sub>2</sub> on the whole considered time span.....	51
Figure 39 - Zoom on the development of each group's concentrations at 700°C and 1% O <sub>2</sub> .....	52
Figure 40 - Development of each group's concentrations at 700°C and 2.2% O <sub>2</sub> on the whole considered time span .....	53
Figure 41 - Zoom on the development of each group's concentrations at 700°C and 2.2% O <sub>2</sub> .....	53
Figure 42 - Development of each group's concentrations at 750°C and 1% O <sub>2</sub> on the whole considered time span.....	54
Figure 43 - Zoom on the development of each group's concentrations at 750°C and 1% O <sub>2</sub> .....	54
Figure 44 - Development of each group's concentrations at 750°C and 2.2% O <sub>2</sub> on the whole considered time span .....	55
Figure 45 - Zoom on the development of each group's concentrations at 750°C and 2.2% O <sub>2</sub> .....	56
Figure 46 - Development of each group's concentrations at 800°C and 1% O <sub>2</sub> on the whole considered time span.....	56
Figure 47 - Zoom on the development of each group's concentrations at 800°C and 1% O <sub>2</sub> .....	57
Figure 48 - Development of each group's concentrations at 800°C and 2.2% O <sub>2</sub> on the whole considered time span .....	58
Figure 49 - Zoom on the development of each group's concentrations at 800°C and 2.2% O <sub>2</sub> .....	58
Figure 50 - World energy production shares of: a) coal; b) natural gas; c) oil; d) biofuels.....	73

Figure 51 - Gas cleaning technologies (23).....	76
Figure 52 - CLR-System .....	76
Figure 53 - CLR-System after operation .....	76
Figure 54 - Chalmers gasifier product gas from gasification of wood chips and wood pellets.....	77
Figure 55 - CLR reference experiments with silica-sand [33]: a) at 740°C; b) at 815°C .....	77
<b>Figure 56</b> - Previous models by Corella et al.: a) Two-Lump model [27]; b) Six-Lump model [53].....	78
Figure 57 - Group concentrations before and after CLR-System on the two oxygen concentrations and at: a) 700°C; b) 750°C; c) 800°C .....	87
Figure 58 - Group conversions of total amount of tars on the two oxygen concentrations and at: a) 700°C; b) 750°C; c) 800°C .....	88

## TABLE OF TABLES

Table 1 - Description of gases.....	2
Table 2 - Process performance indicators available for biofuel production processes [5].....	4
Table 3 - Summary of woody biomass types [10,11] .....	6
Table 4 - Specific technical data of Chalmers' gasifier .....	10
Table 5 - Chemical components in biomass tars [22].....	11
Table 6 - List of different tar classes from GC/MS analysis [22].....	13
Table 7 - Maximum oxygen transport capacity of different concentrations of manganese based oxygen carriers .....	22
Table 8 - Summary of properties of M4MgZ1150 particles [38].....	22
Table 9 - Oxygen carriers tested at Chalmers University of Technology .....	23
Table 10 - Geometrical measures of the dual-fluidized bed reactor .....	28
Table 11 - Representative tar molecules present in gas .....	41
Table 12 - Set of kinetic constants and respective simulation relative errors for all operating conditions' best results .....	59
Table 13 - "Intrinsic reactivity rate" of each group of tars.....	60
Table 14 - Information on identified tar molecules .....	79
Table 15 - RSD result values for the samples of manganese catalyst at 700°C.....	81
Table 16 - RSD result values for the samples of manganese catalyst at 750°C.....	82
Table 17 - RSD result values for the samples of manganese catalyst at 800°C.....	83
Table 18 - Tar values and grouping for 23% manganese at 700°C and three situations: reference from the gasifier, 1% oxygen concentration and 2,2% oxygen concentration .....	84
Table 19 - Tar values and grouping for 23% manganese at 800°C and three situations: reference from the gasifier, 1% oxygen concentration and 2,2% oxygen concentration .....	85
Table 20 - Tar values and grouping for 23% manganese at 750°C and three situations: reference from the gasifier, 1% oxygen concentration and 2,2% oxygen concentration .....	86

# NOMENCLATURE & ABBREVIATIONS

## Nomenclature

$C_nH_m$	Tar Components
$Me_xO_y$	Oxidized Metal Oxide Catalyst
$Me_xO_{y-1}$	Reduced Metal Oxide Catalyst
$X_i$	Conversion Rate of each Tar Group [%]
$\tau$	Residence Time
$C_{i,0}$	Concentration of each Tar Group in the Raw Gas [ $g/m^3_{normal}$ ]
$C_i$	Concentration of each Tar Group in the Producer Gas [ $g/m^3_{normal}$ ]
$r_j$	First order reaction of $jth$ Group
$k_{ij}$	Kinetic Reaction Rate Constant from the $ith$ Group to the $jth$ Group [ $m^3_{tar}/g_{catalyst}S$ ]
$RSD$	Relative Standard Deviation [%]
$x_i$	Value of $ith$ Sample [ $\mu g$ ]
$\bar{x}$	Mean Value of the Samples [ $\mu g$ ]
$n$	Number of Samples

## Abbreviations

CNG	Compressed Natural Gas
SNG	Synthetic Natural Gas
CHP	Combined Heat and Power
GHG	Greenhouse Gas
MSW	Municipal Solid Wastes
SRF	Short Rotation Forestry
SRC	Short Rotation Coppicing
EF	Entrained Flow (Gasifier)

CFB	Circulating Fluidized Bed (Gasifier)
CLC	Chemical-Looping Combustion
FR	Fuel (or Reformer or Catalyst) Reactor
AR	Air (or Regenerator) Reactor
CLR	Chemical-Looping Reforming
TGA	Thermo-gravimetric Analyzer
ILS	Inferior Loop Seal (Lower Loop Seal, LLS)
SLS	Superior Loop Seal (Upper Loop Seal, ULS)
SPA	Solid-Phase Adsorption
PAHs	Polycyclic Aromatic Hydrocarbons
LC	Liquid Chromatographic (group separation)
GC	(Capillary) Gas Chromatography
FID	Flame-ionization Detection
TD	Thermal Desorption
MS	Mass Spectrometry
SI	International System Units

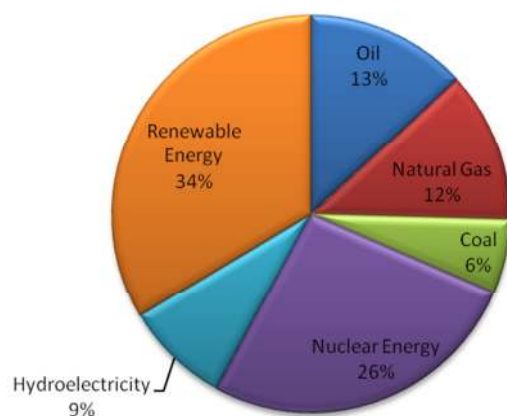


# 1. INTRODUCTION

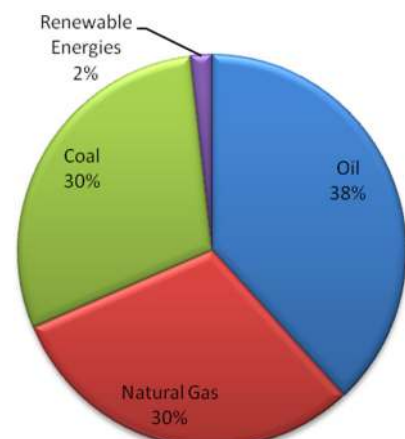
## 1.1. Background

Natural gas is increasingly important as a primary source. It is used for electricity production, industrial and domestic heating purposes, as chemical feedstock and is gaining importance in the transport sector as compressed natural gas (CHG) [1]. According to BP Statistical Review of World Energy [2] the consumption of natural gas will increase over any other energy source (in absolute numbers). The global consumption of natural gas will be doubled in 2030 and, in the period till 2020, the European demand for natural gas will increase with annually 2-3%, as a result of changing feedstocks in the electricity sector.

According to the same source, the European Union contributes with 1.3% of the proved reserves of natural gas and with 5.5% of the total world production of natural gas in 2010. However the European Union's share of the total world consumption in 2010 reached 15.5%. This means that, currently, the European Union covers approximately 5% of its own consumption. Nevertheless, due to increasing demand for natural gas and the decreasing resources, the import dependency in the European Union will increase to approximately 70% in 2020 [1,3]. The energy consumption shares worldwide and in European Union are presented in Figures Figure 1 and Figure 2.



**Figure 1** - European Union consumption of energy in 2010



**Figure 2** - Worldwide energy consumption in 2010

Compared to other fossil fuels, such as coal or oil, natural gas presents some advantages. Gas-fired power stations are cheaper than coal-fired plants and natural gas has by far the smallest impact on the environment [3]. However, a sustainable alternative is required as the natural gas reserves are finite and their use still contributes to greenhouse gas emissions [1]. Nowadays, the global reserves are large enough to accommodate the growing demand in natural gas but they still are finite [3].

The substitution of natural gas by a renewable equivalent is an interesting option to reduce the use of fossil fuels and the consequent gas emissions. This is called green natural gas and comprises both biogas and Synthetic Natural Gas (SNG) [3]. A summarized description of these three types of fuel is shown in Table 1.

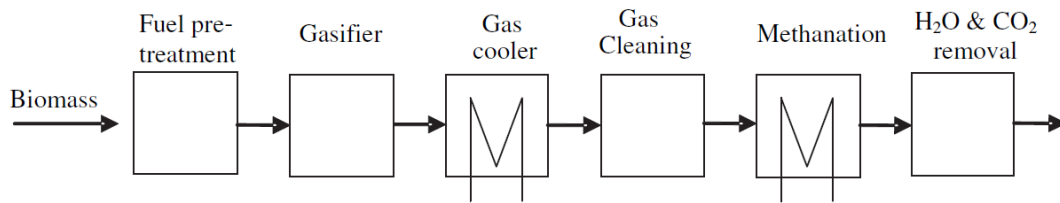
**Table 1** - Description of gases

Type of gas	Description
Natural Gas	<ul style="list-style-type: none"> <li>• Produced from gas fields, contains mainly CH<sub>4</sub>;</li> <li>• Variable composition, depending on gas field.</li> </ul>
Biogas	<ul style="list-style-type: none"> <li>• Produced by digestion, contains mainly CH<sub>4</sub> and CO<sub>2</sub>.</li> </ul>
SNG	<ul style="list-style-type: none"> <li>• “Synthetic Natural Gas”, contains mainly CH<sub>4</sub>;</li> <li>• Produced via gasification and methanation;</li> <li>• Main source: coal (or biomass).</li> </ul>
Bio-SNG	<ul style="list-style-type: none"> <li>• SNG from biomass</li> </ul>

The production of SNG represents one of the auspicious alternatives for biofuel manufacture. Today with the present economic situation, the transport sector is identified as being the most interesting customer for SNG, as this fuel shows promising results for integration in heavy fuel vehicles and, thereby, reduce the diffuse emissions of carbon dioxide, which is associated with the transport sector. However, there are also applications in the stationary sector as it can be used for industrial purposes as a small-scale alternative for electric power generation, through combustion, or for heating purposes, through combined heat and power (CHP) production [4,5].

The process steps to yield SNG, shown in Figure 3, are thermal gasification of biomass followed by gas conditioning, methanation and gas upgrading of the product gas [3,5,6] and, among its various advantages, the following stand out:

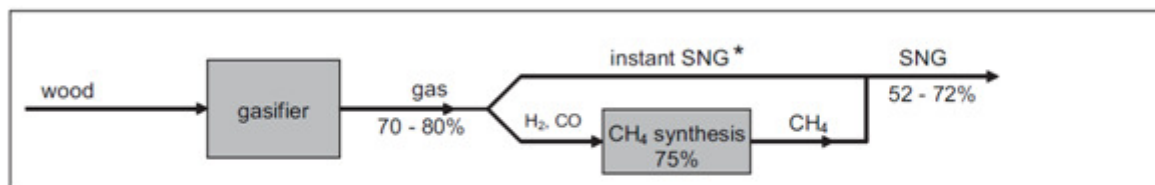
- a high conversion efficiency;
- a large diversity of ready-to-use applications in different sectors;
- its production aims at an effective reduction of CO<sub>2</sub> and other anthropogenic greenhouse gas (GHG) emissions [6], accompanied by an overall reduction in the use of fossil fuels;



**Figure 3** - Simplified scheme of Biomass to SNG configuration (with gas cooling, depending on the gas conditioning/cleaning technology) [1]

There are other potential advantages of SNG over other biofuels: it can readily be blended with natural gas [7] and, therefore, distributed through the existing grid [3] and that the level of experience for storage is already high, through previous experience with natural gas [5]. All these factors combined could lead to a smooth transition from fossil fuels to bio, renewable fuels [6], allowing extended security of gas supply, especially for Europe which is increasingly dependent on import [8]. A potential limitation for total substitution of natural gas for SNG in the future is the requirement of large amounts of biomass for gasification [3].

In the final upgrading step, part of the biomass carbon is removed as  $\text{CO}_2$ . Thus, the production of Bio-SNG can be considered  $\text{CO}_2$  negative, which contributes for the GHG reduction. This will increase the biomass demand which in turn will increase the biomass prices. Consequently, a high overall efficiency is a prerequisite for any biomass conversion process [1]. Typical general efficiencies for biomass from wood gasification to SNG production are shown in Figure 4.



\* mainly  $\text{CH}_4$ , but also olefins and aromatics

**Figure 4** - Typical process efficiencies from wood to SNG production [1]

SNG is not the only possible product from biomass conversion processes. In order to evaluate an SNG production process in comparison with alternative biofuel production routes it is important to define suitable generic performance indicators [5]. Three most common performance indicators are presented in Table 2. These are not directly comparable but, in order to provide useful guidance when selecting a production process, all efficiencies have to be interpreted while also taking other aspects, such as economics, into account [5].

Different future energy scenarios might favor different process designs. Therefore, an economic evaluation of the process needs to account for uncertainties regarding future development of fuel and electricity prices, as well as costs related to energy and environmental policy instruments, such as carbon dioxide emissions costs etc. [5].

**Table 2** - Process performance indicators available for biofuel production processes [5]

Performance indicator	Advantages	Disadvantages
Cold gas efficiency (fuel conversion efficiency)	Easy to calculate; Clear idea of fuel yield.	Does not account for by-products; No information about overall process efficiency.
Thermal/energetic efficiency (first law efficiency)	Possible to account for by-products; Relatively easy to calculate.	Detailed information about system boundaries necessary; Limited information about overall process efficiency.
Exergetic efficiency (second law efficiency)	Possible to account for by-products; Information on overall process efficiency.	Efficiency related to a reference state (definition necessary); Detailed information on system boundaries necessary.

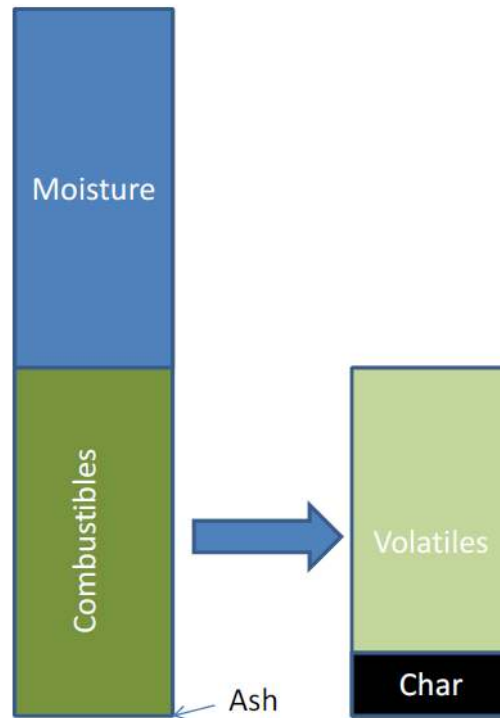
## 1.2. From Biomass to Synthetic Natural Gas (SNG)

### 1.2.1. Biomass

As said before, the production of SNG includes four major steps – gasification of biomass, gas conditioning and methanation of the product gas, followed by gas upgrading. For the aim of this work, it is the gas cleaning technologies that will be focused upon.

Biomass refers to all organic materials that originate from plants. Therefore, biomass is one of the most abundant natural resources worldwide [9]. Biomass has several potential advantages when compared to other renewable energy resources. One of the main advantages is that it can be used for heat, power and combined heat and power (CHP) production, as well as being able to produce continuous energy and, therefore, not have intermittency problems, like those associated with wind, solar etc. It is also controllable so it can be adjusted to meet demand and can be applied to a wide range of scales from 50kW domestic systems, medium 500kW plant to MW scale power stations [10].

When biomass is submitted to a conversion process, its different constituents, represented in Figure 5, play an important role in the performance efficiency and in the producer gas components. When biomass arrives to the conversion unit it consists of 10 to 70% moisture (water) and a remaining share of combustible components, which are the dry part of biomass. This moisture is released from the fuel as water-vapor when the fuel is heated. The volatiles constitute between 50 and 95% of the combustibles in biomass, which are released when the fuel is heated. Char is the combustible part of the fuel remaining after the volatiles have left and it consists of nearly pure carbon that can be combusted together with oxygen to produce carbon dioxide and heat. Char can also be gasified to hydrogen and carbon monoxide by supplying steam and heat. Finally, the ash content in most biomasses is very low, usually below 1% of the dry mass. Nevertheless, it is known to be problematic.



**Figure 5** - Biomass constituents

Biomass feedstocks can be divided in four main categories – organic residues and wastes; forestry production/residues; agricultural residues and wastes and energy crops.

The organic residues and wastes can be understood as municipal solid wastes (MSW), this is, a combination of domestic, light industrial and demolition solid wastes generated within a community. Presently, the three main ways of treatment of this waste is through disposal in landfills, combustion or disposal in anaerobic digesters. Incineration of this waste is considered problematic because of the potential effect on health and impact on environment from the release of emissions that carry dangerous pollutants, such as dioxins, heavy metals, particulates, nitrogen oxides, etc. Therefore, it is advisable and economically feasible that the use of biomass from MSW comes from large commercial power plants. These residues, wastes and co-products arise from commercial and industrial process and manufacturing operations. They can be divided into two categories – woody wastes which are essentially the same as wood fuel, and non woody wastes, that are material such as paper pulp/wastes, textiles and sewage sludge [10,11].

The second category, forestry production/residues, incorporates the biggest variety of woody biomass sources. With the decrease in demand for paper pulp and construction timber, the amount of forestry products available to use as wood fuel increases. Besides these, forestry residues also arise from forestry operations such as thinning plantations (plantations of smaller-diameter trees) and trimming felled trees to prevent forest fires and accelerate growth. These residues and wastes offer a large potential for energy supply. Also, sawmill products can be used as a biomass fuel either as sawdust to be compressed into pellets or off-cuts suitable for chipping [10,11]. Therefore, the forestry related biomass can be classified as presented in Table 3.

**Table 3** - Summary of woody biomass types [10,11]

Biomass	Characteristics
Wood	Is the most common form of biomass and has been used for thousands of years; it includes several products such as wood, sawdust and bark that has not been chemically treated or finished; it can be obtained from a number of sources such as forestry, sawmills and timber merchants.
Logs (Figure 6.c)	Can be bought directly from a supplier and be directly burnt after drying period to reduce moisture.
Sawdust	Typical by-product from wood processing or manufacture; can have either a high or low moisture content, depending on origin; has low energy content but has a large surface area to volume ratio meaning it can be burnt easily.
Wood Chips (Figure 6.a)	Offer a much more uniform fuel than logs, that can flow and be automatically fed; are convenient to transport; have large surface area to volume ratio; the characteristics of wood chips depend o the original source, from which they are made, and on the chipper.
Wood Pellets and Briquettes (Figure 6.b)	Need to be made from a fine dry feedstock, usually sawdust or other by-products of wood processing industry; the production of wood pellets is more energy intensive than that of other wood fuel production; wood pellets have higher calorific value than woodchips; are less bulky to store, easier to handle and more suited to automatic handling systems because of the consistent size; have low moisture content (8%-10%) and have a consistent density and heat content.



Figure 6.a



Figure 6.b



Figure 6.c

**Figure 6** - Woody biomass: a) wood chips; b) wood pellets; c) logs

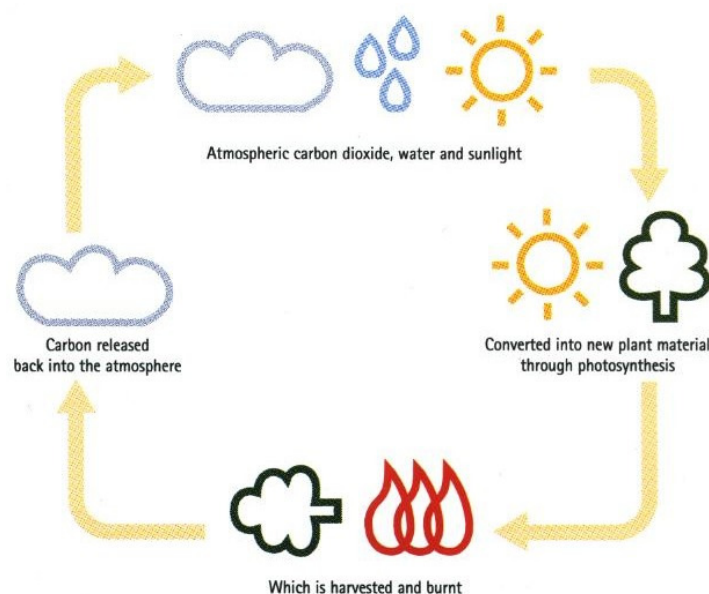
Agricultural residues and wastes are defined as the by-products of the agricultural system and can be split in two types – dry and wet. Dry residues consist of parts of arable crops that are not used for the primary production of food or fiber. These include straw, a by-product or the dry stalk of a cereal plant, such as wheat or barley; poultry litter which is wood shavings or straw used in deep litter broiler houses; corn stover which is stalk and leaf residues from harvesting maize for grain. The wet residues typically consist of animal slurry and farmyard manure and grass silage. They are primarily

used as fertilizers and have high moisture content. Food waste is also included and it is characterized by residues and wastes occurring at all points in the food supply chain. It has a high moisture content and, depending on the sugar or oil levels, it can be used for the production of several types of biofuels [10,11].

Lastly, energy crops are crops/plants that are purposefully planted to be used as fuel or to be converted to biofuel. The primary objective when selecting energy crops is to obtain the highest possible amount of energy. Methods of growing energy crops include short rotation forestry (SRF) which involves planting trees close together and felling them when they have reached a certain diameter (takes about 8-20 years depending on tree species), and short rotation coppicing (SRC) which generally involves cutting back species in the first year to encourage rapid, thick growth in the following three years, after which it is ready to be harvested [10,11].

Although biomass is being traditionally used as energy source, especially for cooking and heating, particularly in the developing countries, the use of biomass-related biofuels is increasing and has both its advantages and disadvantages when it comes to the environmental impact associated with the full biofuel supply chain from field to wheel [12]. Biomass thermochemical conversion for the production of fuels has a number of realizable social, political and economic benefits. It is possible to utilize biomass to generate a number of product and revenue streams that could revitalize rural economies, increase national security by reducing the dependence on foreign oil imports and improve the global environment by reducing fossil fuel emissions, including greenhouse gases and oxides of nitrogen and sulfur [13].

The large amount of biomass necessary for the production of biofuels, requiring a greater land area available, also leads to an increase in the emissions of GHG during the transportation from the exploitation sites to the production facilities. However, these emissions are largely compensated, as the croplands are considered net GHG sinks and because the production processes and usage of the resulting fuels in the transportation sector are considered to be “clean burning” processes [9,12]. All these factors make the whole carbon cycle from field to wheel a “closed” cycle, accounting for zero global emissions, as demonstrated by Figure 7.



**Figure 7** - Biomass carbon cycle

As a result, with respect to global issues of sustainable energy and reduction in greenhouse gas, biomass is getting increased attention as a potential source of renewable energy. Despite this, biomass is not yet competitive with fossil fuels [14]. World production shares of the main fuels, coal, natural gas, oil and biofuels are shown in Appendix I.

### **1.2.2. Gasification**

In order to produce Synthetic Natural Gas (SNG) from biomass, it is necessary to convert the biomass first. Different biomass conversion processes produce heat, electricity and fuels. Among all biomass conversion processes, gasification is one of the most promising ones. Biomass gasification is recognized as an effective way of converting biomass with low heating value into combustible gas [15]. Indeed, it is recognized as an effective route for converting the heterogeneous bound energy within lignocelluloses to a gaseous fuel [16]. In other words, biomass gasification technologies convert lignocellulosic materials such as wood, corn stover and switchgrass into a medium-Btu gas that can be used in a number of energy applications such as fuel for process heat, steam, cogeneration of electricity and the synthesis of liquid products that can be used in producing transportation fuels [17].

Consequently, gasification technologies are expected to play a key role in expanding the use of biomass as a major renewable energy source [18]. Some advantages of using gasification processes are the comparatively low investment and costs of operation and maintenance, the reliable techniques and compact structure and a lower demand on gas quality, as the producer gas is sent to further treatments [15].

Biomass contains more volatile matter than coal and its main constituents, the high-oxygen cellulose and hemicellulose, also have higher reactivities. Therefore, biomass is gasified at lower temperatures, under much less severe operating conditions. The choice of the gasifier, gasifying medium, such as air, steam or oxygen, and operating conditions depend on both the provided feedstock and the wished quality of the final Syngas [5]. The gasifying reactions are mainly endothermic and, consequently, there is a necessary heat input [18]. There are three principal design concepts for gasification: entrained flow gasifier (EF), a circulating fluidized bed (CFB) or else through indirect gasifiers (allothermic gasification).

#### *Entrained Flow Gasification*

The entrained flow gasification requires an energy intensive pretreatment to produce fine powder out of the biomass. Therefore, torrefaction processes followed by milling are usually chosen due to the relatively low energy requirement. After the dried biomass is fed into the torrefaction reactor and milled, it is pressurized and pneumatically fed into the entrained flow gasifier. The typical operating temperature of this type of gasifier is between 1300-1500°C. At lower temperatures the fuel is not completely converted and the viscosity of the produced slag can become too high. On the other hand, at higher temperatures, the cold gas efficiency decreases. Therefore, the selected operating temperature is a tradeoff between fuel conversion and cold gas efficiency. The system pressure is around 3MPa and the gasification agent that is normally used is oxygen. Ashes and particulates in the producer gas are removed by filters and adsorbents [1].



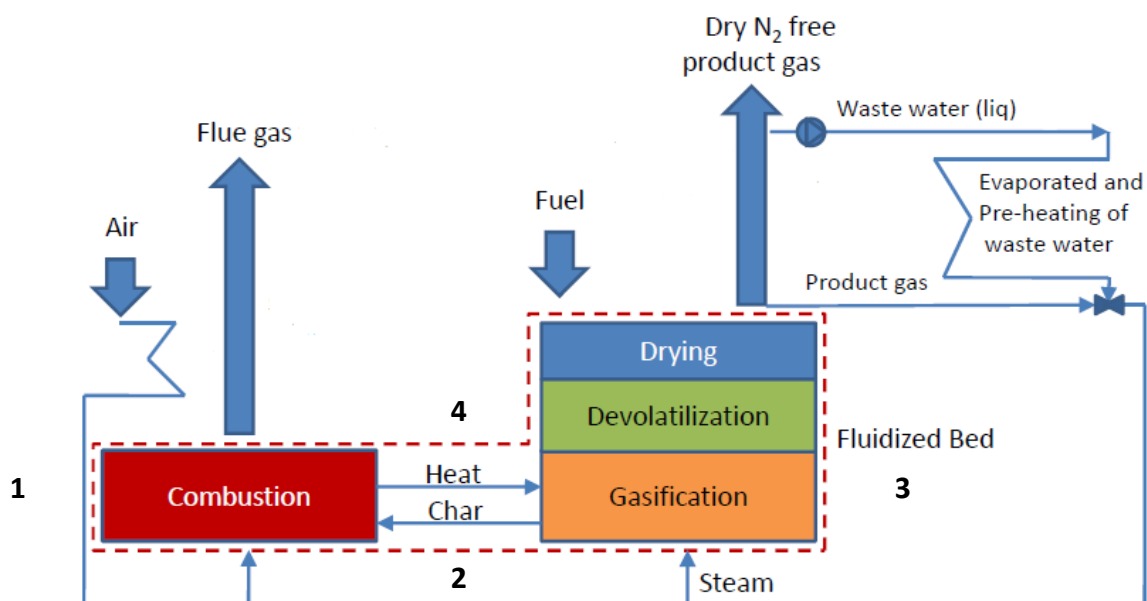
### Circulating Fluidized Bed Gasification

The conventional circulating fluidized bed gasifier uses air as the gasification medium. If oxygen is used it has to be diluted with the stream, not to increase the chance of formation of local hot spots in the fluidized bed which results in an increased risk of agglomeration of the bed material. In this system, biomass is pressurized and fed into the gasifier. The operating conditions are characterized by a lower pressure than the previous system, of around 1MPa and also lower temperatures of around 850°C. Most of the dust (carbon containing ash) is removed from the producer gas by a cyclone or dissolved in oil [1].

### Allothermic/Indirect Gasification

The system based on the allothermic gasifier has three reactors – the riser, the fluidized bed combustor and the burner. The biomass is directly fed into the riser where a small amount of superheated steam is added. Hot bed material (typically sand) enters the riser from the combustor reactor, through a hole located under the biomass feeding point, and it heats the biomass to temperatures around 850°C. The producer gas leaves the riser following for the upcoming cleaning stages. The bed material together with the degasified biomass particles (char) returns to the combustor where char is burnt, heating the bed material, and leaves as flue gas. The heated bed material leaves the fluidized bed from the bottom and is sent to the riser again. The system operates at atmospheric pressure [1].

The system used at Chalmers for the gasification of biomass is based on the allothermic/indirect gasification. The specifications of this gasifier are summarized in Table 4. Figure 8 shows the main components of the system. The component (1) is the fluidized bed combustor where the bed consists of, for example, quartz sand and where the unconverted biomass from reactor (3), the char, is transported and burnt, heating the bed material. Component (2) and component (4) are seals for the transportation of the bed material between reactors. Component (3) is a fluidized bed reactor where biomass is fed together with steam and where, during the heat up of the biomass, the desired product is obtained, this is, most of its mass as gas in the form of moisture and volatiles.



**Figure 8** - Chalmers allothermic/indirect gasification system

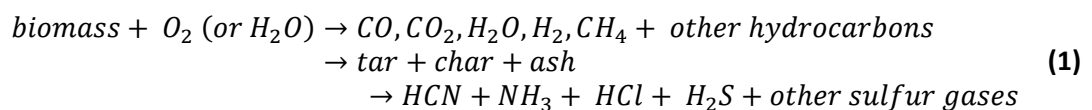
**Table 4** - Specific technical data of Chalmers' gasifier

Technical data	Measurements
Fuel load: 0 – 4 MW (0 - 1 ton/h) (tested: 0-2.3 MW)	Product gas composition
Optional fluidization media: - Steam - Flue gases - Air (not yet tested)	Solid flux
Temperature in Gasifier: 550-950 °C (tested 725 - 860 °C)	Fuel feed
Residence time: - Adjustable solid flux - Adjustable bed height	Temperatures and Pressures
Fuel: - Dry pellets (tested: Wood and Bark) - Wet biomass (tested: Wood chips)	In plant gas and bed sampling
Bed material (tested: silica sand)	Extraction of gas slip flow

Running of the system allowed for comparison of the performance of the gasifier and supplied information on the several components of product gas after the gasification of both wood pellets and wood chips, as demonstrated in Figure 54 in Appendix IV.

It is very important to distinguish two main types of gasification gases – the product gas, formed at low temperature gasification, and the biosyngas, formed at high temperature [19]. The product gas is used for production of synthetic natural gas (SNG) and electricity while the biosyngas is applied for production of Fischer-Tropsch diesel, methanol, ammonia and hydrogen, for various uses in chemical industry and for the production of electricity [19].

The composition of the product gas will vary with each operating conditions [5] but its constituents are permanent gases, such as N<sub>2</sub>, CO, H<sub>2</sub>, CO<sub>2</sub>, CH<sub>4</sub>, and C<sub>2</sub>H<sub>n</sub> as well as char, ash, soot, particulates, steam, volatile organic compounds and condensable organic hydrocarbons [20], as represented by the generalized Equation 1.



These condensable organic compounds, often called “tars”, start condensing at around temperatures below 350°C [21] and tend to cause plugging, fouling and corrosion problems in the pipes [20,5]. Also, the following methanation process is highly sensitive to impurities in the gas [5].

Gas conditioning is a general term for removing the unwanted impurities from biomass gasification product gas and generally involves an integrated, multi-step approach that depends on the end use of the product gas [13].

For the purpose of this thesis, the focus will be on removing or eliminating tars without regard to acid gas, ammonia, alkali metal and particulate removal, although, in some cases, the strategies used for removing the various classes of impurities overlap [13].

### 1.2.3. Gas Conditioning

Tars can be easily defined as undesirable and problematic organic products of biomass gasification, although there are a large number of definitions in the literature [19]. Tars are formed during gasification, when biomass is heated, in a series of complex reactions, causing carbon bonds to break and form tars. They can be understood as a complex heterogeneous mixture of organic molecules, such as hydrocarbons from 1 to 5-ring aromatic compounds, oxygen and sulphur-containing hydrocarbons and poly-aromatics (PAHs), which can be found in a variety of concentrations depending on the formation conditions (temperature, pressure, feedstock, gasifier, gasifier agent, equivalence ratio and residence time) [16,22].

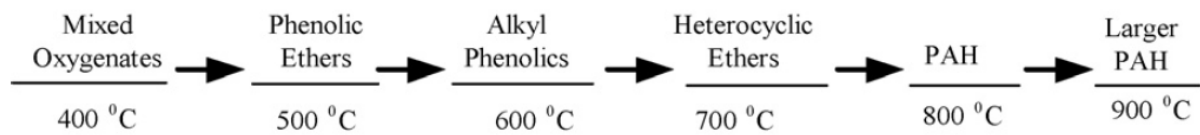
Some of the most influential parameters for the tar composition are the process temperature and the gasifier type. Table 5 features the variety of reported levels of tar in producer gas from different biomass gasification processes [23].

**Table 5** - Chemical components in biomass tars [23]

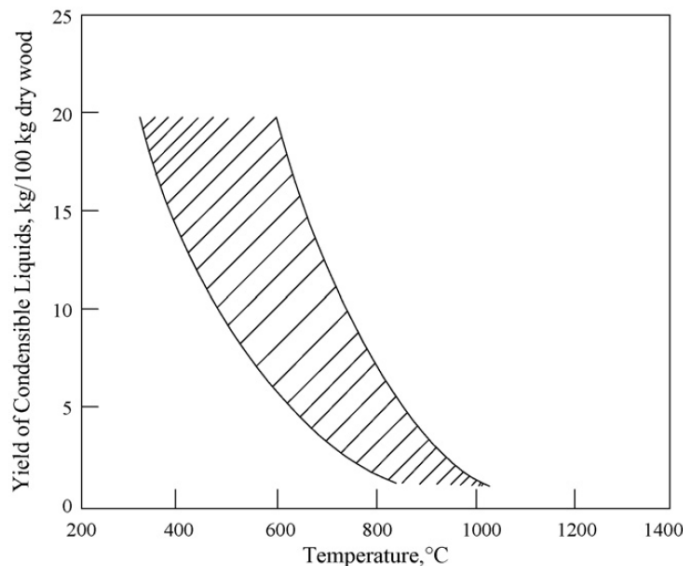
Conventional flash pyrolysis (450–500°C)	Acids; aldehydes; ketones; furans; alcohols; complex oxygenates; phenols; guaiacols; syringols; complex phenols
High-temperature flash pyrolysis (600–650°C)	Benzenes; phenols; catechols; naphthalenes; biphenyls; phenanthrenes; benzofurans; benzaldehydes
Conventional steam gasification (700–800°C) *	Naphthalenes; acenaphthylenes; fluorenes; phenanthrenes; benzaldehydes; phenols; naphthofurans; benzanthracenes
High-temperature steam gasification (900–1000°C)	Naphthalene; acenaphthylene; phenanthrene; fluoranthene; pyrene; acephenanthrylene; benzanthracenes; benzopyrenes; 226 MW PAHs; 276 MW PAHs

\*Conventional steam gasification is the process used at Chalmers University of Technology and which provided the raw gas at study in this thesis.

Due to increased reaction temperature in the gasifier, secondary reactions occur in the gas phase which convert oxygenated tar compounds to light hydrocarbons, aromatics, oxygenates and olefins subsequently forming higher hydrocarbons and larger PAH in tertiary processes [23]. Milne [24] summarized the tar formation scheme proposed by Elliott, demonstrated in Figure 9, which shows the transition of biomass pyrolysis products and gasifier tars as a function of the process temperature from primary products to phenolic compounds to aromatic hydrocarbons. A conceptual relationship between the yield of tars and the reaction temperature was derived by Baker et al. [25], shown in Figure 10.



**Figure 9** - Tar maturation scheme proposed by Elliott [24]



**Figure 10** - Tar yield as a function of the maximum temperature exposure [25]

There have been several attempts to identify and classify tar compounds based on specific criteria, e.g. reactivity, solubility, condensability etc.

Table 6 shows the classes of chemical components based on results from the gas chromatography (GC)/ mass spectrometry (MS) analysis of the collected tars [23].

**Table 6** - List of different tar classes from GC/MS analysis [23]

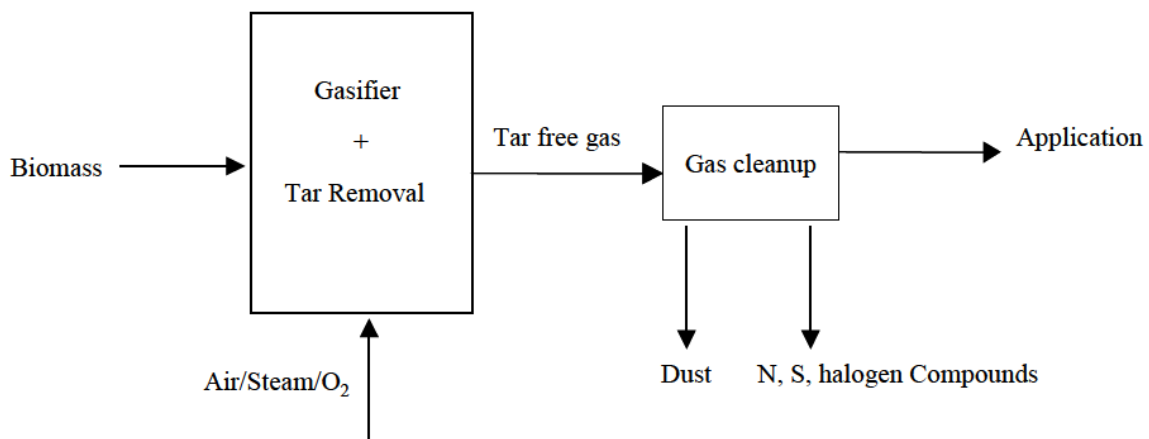
Class name	Property	Representative compounds
GC-undetectable	Very heavy tars, cannot be detected by GC	Biomass fragments; Heaviest tars
Heterocyclic aromatics	Tars containing hetero atoms	Phenol; Cresols; Pyridine; Quinoline; Isoquinoline; Dibenzophenol
Light aromatic (1 ring)	Usually light hydrocarbons with single ring; do not pose a problem regarding condensability and solubility	Toluene; Ethylbenzene; Xylenes; Styrene
Light PAH compounds (2-3 rings)	2 and 3 rings compounds; condense at low temperature even at very low concentration	Indene; Naphthalene; Methyl-naphthalene; Biphenyl; Acenaphthalene; Fluorene; Phenanthrene; Anthracene
Heavy PAH compounds (4-7 rings)	Larger than 3-ring, these components condense at high-temperatures at low concentrations	Fluoranthene; Pyrene; Chrysene; Perylene; Coronene
GC-detectable, not identified compounds	-	Unknowns

From all impurities present in the product gas, and even though they only account for a small percentage of the product gas, it is the tar components that are the most difficult to eliminate because they will clog up during conversion processes [26]. The tars can cause quite a few problems such as cracking in the pores of filters, forming coke and causing plugging of the filters, condensing in the cold spots and plugging the cold spots. These result in serious operational interruptions and maintenance costs. Another vital issue regarding tars is that they contain carcinogenic compounds that have to be removed to achieve health and environmental demands [19].

As a consequence, regardless of how “tar” is defined, tar removal, conversion or destruction is seen as one of the greatest technical challenges to overcome for the successful development of commercial advanced gasification technologies [23]. Therefore, product gas conditioning, as one of the most critical steps in the whole biofuel production process efficiency, is attracting a lot of attention by researchers worldwide, trying to develop new, optimized and more economic processes [26]. However, the methods used should affect the formation of useful gaseous products [14].

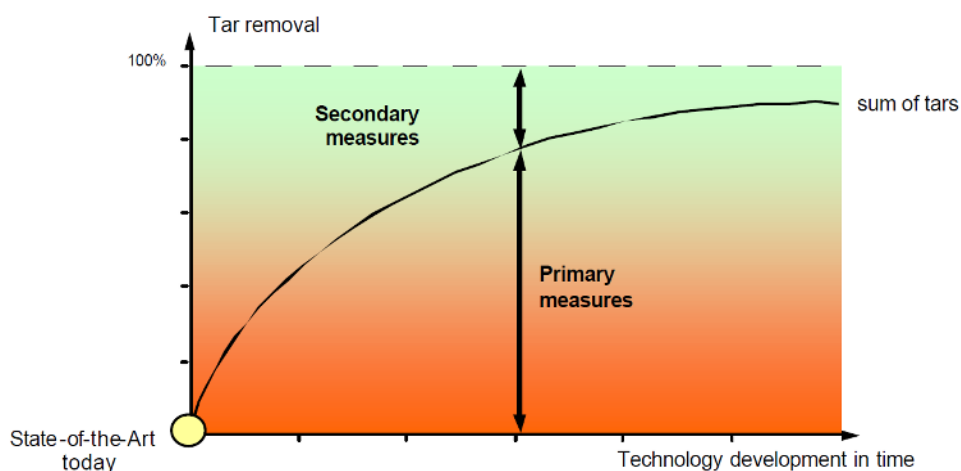
Upgrading the raw gas to a gaseous fuel or to a primary gas suitable for liquid fuel production has to involve gas cleaning either as a primary or as a secondary measure [16]. Primary methods can be broadly understood as treatments inside the gasifier and secondary methods as hot gas cleaning after the gasifier.

Primary methods can be defined as all the measures taken in the gasification step itself to prevent or convert tar formed in the gasifier. Many researchers, such as Devi et al. [14], who focus on primary methods, prospect of operating an integrated biomass gasification installation without struggling with tar anywhere downstream [21]. An ideal primary method concept eliminates the use of secondary treatments as shown in Figure 11. To get the best quality exit gas, the gasifier performance has to be optimized. For an optimized performance of the gasifier, the main attractive factors are the proper selection of the operating conditions, the use of a proper bed additives or a catalyst during gasification and a proper gasifier design [14]. Although measures inside the gasifier may be fundamentally more ideal and some of the measures result in low tar emissions, primary methods suffer from disadvantages related to limits in feedstock flexibility and scale-up, the



production of waste streams, a decrease in cold gas efficiency, complex gasifier constructions and narrow operating windows [21]. And, although primary measures can reduce the tar content considerably, demonstrated in Figure 12, it is foreseen that complete removal is not feasible without applying secondary methods [21].

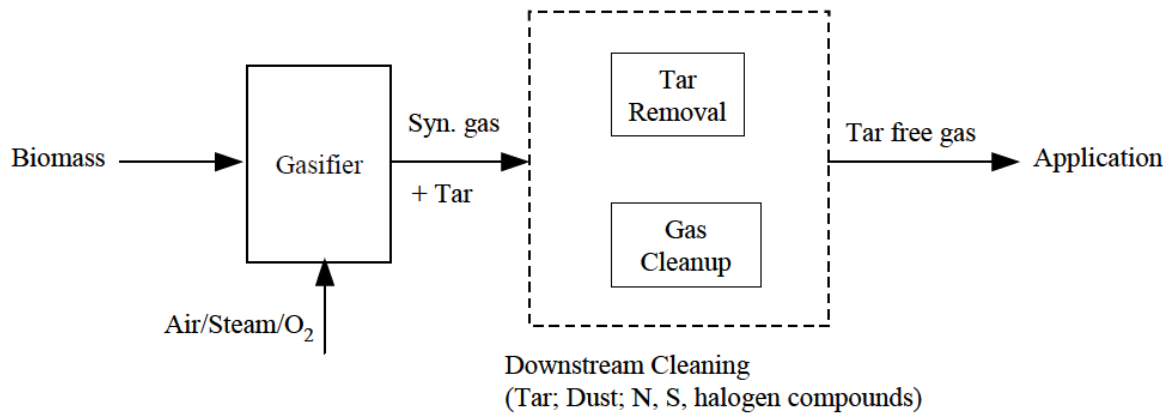
**Figure 11** - Tar cleaning concept by primary methods [26]



**Figure 12** - Illustration of the need of primary and secondary methods with technology development in time [21]

Secondary methods are conventionally used as treatments to the hot product gas from the gasifier, shown in Figure 13. Although downstream gas cleaning methods are reported to be very effective in

tar reductions, in some cases they are not economically viable or the tar problem is shifted to the treatment of wastewater. However, a secondary measure can be feasible without needing primary measures [21] and, therefore, it should be the basis for tar removal from biosyngas and primary measures could possibly be used for its optimization. These methods can be chemical or physical treatments [21,14].



**Figure 13** - Tar cleaning concept by secondary methods [14]

There exist several conventional techniques for mechanical secondary gas conditioning, such as standard cyclones, baffle, ceramic or fabric filters and rotating separators for particulates removal or regenerative sorbents or washing techniques used to reduce sulphur concentrations [5]. For instance, a combination of several physical removal techniques such as sorbents, scrubbers, filters, wet electronic separators, hot gas cyclones or catalysts can be used to reform the tars [4,5,26]. Traditional technologies for gas conditioning are summarized in the diagram of Appendix I.

Usually, hot gas conditioning processes are preferred to the wet methods as they convert the tars to useful product gas, transferring their energetic content to the flue gas as  $H_2$ ,  $CO$  and  $CH_4$  mainly. Instead, wet methods, despite being an effective gas conditioning process, they condense the tars out of the product gas, transferring them to a liquid waste flow proving difficult to dispose [27]. Wastewater minimization and treatment are important considerations of wet methods, increasing the overall costs and complexity of the system. Additionally, this methods are usually coupled with thermodynamic penalties, such as that associated with rapid cooling of the raw gas [28]. Therefore, wet methods are preferred when the end use of the gas requires cooling to near ambient temperatures [13].

On the other hand, hot gas conditioning eliminates tars by converting them into desired product gas components thus retaining their chemical energy in the product gas and avoiding treatment of an additional waste stream. Hot gas cleaning methods are preferred when the end use requires that the product gas remains at high temperature, at or slightly below the gasifier exit temperature. One hot method used is thermal cracking. This requires temperatures higher than typical gasifier exit temperatures ( $> 1100^\circ C$ ) which can be obtained from adding oxygen to the process and consuming some of the product gas to provide additional heat [13]. However, thermal destruction of tars may also produce soot, an unwanted impurity in the product gas stream.

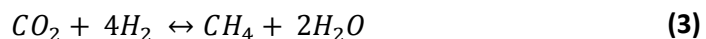
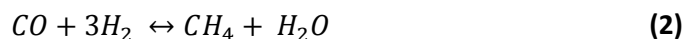
A second hot gas conditioning process, and usually a preferred method for reducing tars is to catalytically decompose them at or near the preferred gasifier temperature [17]. Catalytic tar decomposition is considered as the technology with the highest potential to contribute to the solution of the tar fraction problem [18]. As an attractive hot gas conditioning technique, it offers several advantages such as thermally integrating the catalyst reactor temperatures with the gasifier exit temperature, the composition of the product gas can be catalytically adjusted for the utilization step and steam can be added to the catalyst reactor to ensure complete reforming of tars, making it a catalytic steam reforming process. When tar cracking catalysts are used, the only thing that is reformed is the tars themselves while low hydrocarbons, e.g. methane, ethane and propane are left intact [19].

Different approaches for integrating catalytic tar destruction into biomass gasification systems have been investigated, being the system under study in this thesis one new alternative for this technology. Also, numerous catalysts have been studied for tar destruction activity at a broad range of scales [13]. A summary of the literature pertaining to the most interesting catalysts used for catalytic reforming is presented next.

#### **1.2.4. Methanation & Gas Upgrading**

A major process step, besides gasification, within the SNG production from biomass is the conversion of the product gas, after gas conditioning, to methane. There are two possible configurations: the use of a series of fixed bed reactors, which work adiabatically, usually in a temperature range of about 250-500°C, with a recycled flow for inter-cooling temperature control, or a fluidized bed reactor that works isothermally with internal cooling. The fluidized bed reactors have some advantages considering the reduced tendency of catalyst deactivation by deposition of coal on the active surface [5].

The methanation process main purpose is to convert the CO and H<sub>2</sub> in the cleaned gas to methane. This is processed by the following Reactions 2 and 3, which are strongly exothermic [1].



Due to its strong exothermicity, the methanation process represents an important source of heat that has to be considered when integrating the different sub-processes of SNG production [5]. The different operating conditions of the two methanation technologies lead to a change in temperature levels and quantities of recoverable heat and to differences in the overall processes' power consumption [7]. In previous work by Heyne [7], these two methanation technologies have been compared for their performance within the production process of SNG from biomass gasification. The results concluded that both techniques would be equally applicable from a process integration perspective, as they showed similar SNG production and ratio between the theoretical power production from process heat and the actual power consumption of the overall process.



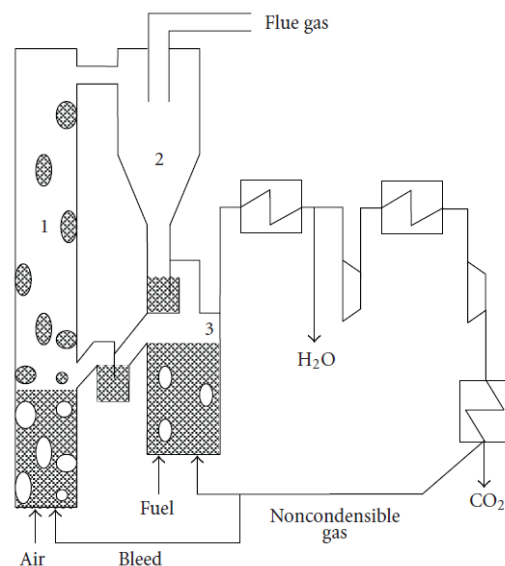
After methanation the gas needs to be adapted to natural gas grid quality required specifications. Therefore, the gas is sent to the following step in the whole process which is gas upgrading. The main step in gas upgrading is the removal of carbon dioxide, which represents a substantial fraction of the gas after methanation [5]. Common solutions for carbon capture currently are amine-based scrubbing techniques, pressure swing adsorption or membrane-based processes. During gas upgrading, the purpose is for the gas to be dried and traces of hydrogen and carbon dioxide to be removed in case the concentration exceeds the specifications for the envisaged application [5].

Conclusions from a study on the whole SNG production line, performed by Heyne [5], said that the pressure level at which the produced SNG is to be delivered is also an important parameter. High pressure is both advantageous and necessary for optimal operation of some of the process step options, therefore, pressure levels within the different sub-processes have to be chosen with care. In order to achieve this, compression work and process equipment size are important parameters, influencing investment and running costs.

### 1.3. Literature Survey

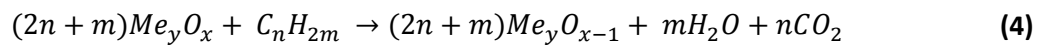
#### 1.3.1. Chemical-Looping Combustion (CLC) & Chemical-Looping Reforming (CLR)

Chemical-looping combustion (CLC) is a novel combustion technology with inherent separation of the greenhouse gas  $\text{CO}_2$ . CLC is a combustion technology where a solid oxygen carrier is used to transfer oxygen from the combustion air to the fuel, thus avoiding direct contact between air and fuel [29,30,31]. The process is composed of two fluidized reactors, a high-velocity riser or an air reactor (AR) and a low-velocity fluidized bed or a fuel reactor (FR), represented in Figure 14 by the numbers (1) and (3), respectively. A two interconnected fluidized beds configuration have an advantage over alternative designs, because the process requires a good contact between gas and solids as well as a flow of solid material between the two reactors. The critical design parameters for this system are considered to be: the amount of bed material necessary in the reactors which is inversely proportional to the rate of reaction of the oxygen carrier; the recirculation rate of the oxygen carriers between air and fuel reactor which is inversely proportional to the mass fraction of oxygen that is released/captured by the oxygen carrier during a cycle; the amount of non-condensable gas that needs to be re-circulated to the fuel reactor; and the dimensions of the reactors and the pressure drops [29,32].

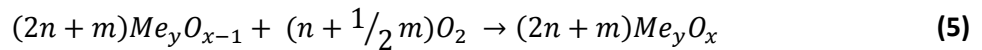


The fuel is fed into the fuel reactor where it is oxidized by the lattice oxygen of the oxygen carriers **Figure 14** - Schematic view of chemical-looping combustion process with two interconnected fluidized beds: 1) air reactor; 2) cyclone; 3) fuel reactor [31]

according to Reaction 4. The fuel needs to be in a gaseous form and can be either syngas from coal gasification, natural gas or refinery gas. Here the metal oxide ( $Me_xO_y$ ) is reduced to a metal or a metal-oxide with lower oxygen content.



Once the fuel oxidation is completed, the reduced metal oxide is transported to the air reactor where it is re-oxidized according to Reaction 5.



A full conversion from  $Me_xO_y$  to  $Me_xO_{y-1}$  and back to  $Me_xO_y$ , as indicated in Reactions 4 and 5, is not necessarily obtained in a real system.

The volumetric gas flow in the air reactor is approximately 10 times larger than that of the gaseous fuel. So, in order to keep a reasonable size of the reactors, a high velocity is chosen in the air reactor [29]. The gas velocity in this riser provides the driving force for the circulation of particles between the two beds. The particles carried away from the riser are recovered by a cyclone, number (2) in Figure 14, and are led to the fuel reactor. From the fuel reactor the particles are returned to the air reactor by means of gravity, therefore, the fuel reactor has to be located at a sufficiently high level.

Reaction 4 is either endothermic or exothermic, depending on type of fuel and oxygen carrier, while Reaction 5 is always exothermic. The total amount of heat evolved from Reaction 4 and 5 is the same as for normal combustion, where the oxygen is in direct contact with the fuel, this is, the CLC system does not bring any enthalpy gains.

The advantage of the chemical-looping combustion (CLC) system is that the fuel and the combustion air are never mixed, resulting in a series of benefits:

- As the combustion takes place without a flame,  $NO_x$  formation should be avoided;
- The air oxidizing the metal produces a flue gas containing only  $N_2$  and some unused  $O_2$ , which are discharged in a different stream, at the exit of the air reactor;
- The inherent separation of the gases from the oxidation of the fuel,  $CO_2$  and  $H_2O$ , which leave the system in a separate stream, at the exit of the fuel reactor;
- The  $H_2O$  can be easily removed by condensation and pure  $CO_2$  is obtained without any loss of energy for separation;
- $CO_2$  is not diluted with  $N_2$ , as it happens in any normal combustion, making it easier to recover;

- The remaining non-condensable gas from the fuel exit stream, such as unreacted methane, can be recycled to the fuel reactor.

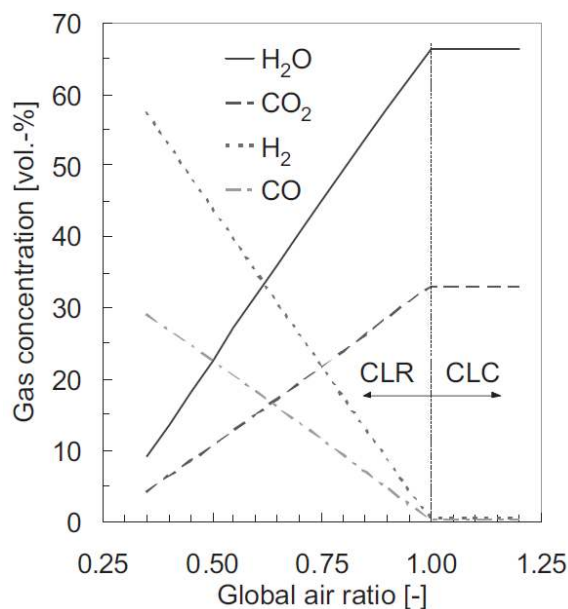
Therefore, compared to other technologies for capture of CO<sub>2</sub>, CLC is potentially much cheaper since no costly gas-separation equipment is necessary [29,30,31].

The chemical-looping reforming (CLR) system is a novel technique based on the same basic principles as the CLC. It is used for partial oxidation, steam reforming and thermal and catalytic cracking of the tar components by using an oxygen carrier in the form of a circulating metal oxide between the two reactors [33].

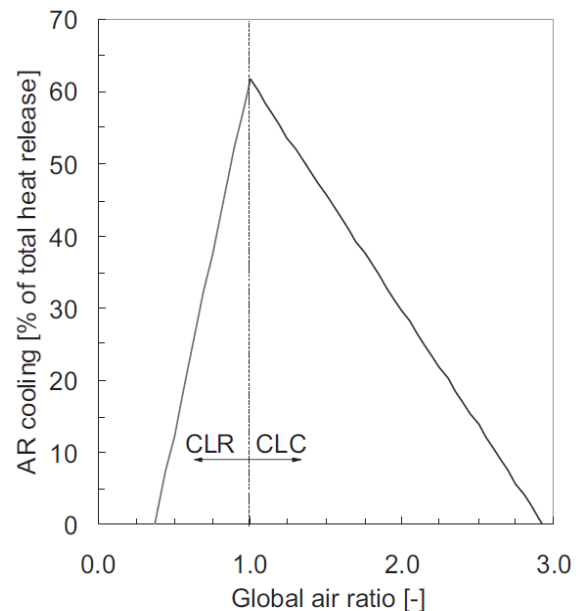
Distinct differences between the two systems, CLC and CLR are:

- The main objective is the production of syngas which consists of a hydrogen, H<sub>2</sub>, and carbon monoxide, CO, mixture, instead of heat;
- In the fuel reactor of the CLR process, the fuels are partially oxidized using a solid oxygen carrier to produce synthesis gas, a mix of H<sub>2</sub> and CO, instead of being oxidized into CO<sub>2</sub> and H<sub>2</sub>O;
- In order not to fully oxidize the fuel, the air to fuel ratio is kept low in the CLR-System, as represented in Figures Figure 16 and Figure 15;
- Lower air to fuel ratios result in lower operating temperatures;
- Pure oxygen production plant, which is needed in normal natural gas reforming, is avoided.

The advantages gained in CLC-System which result from the absence of contact between combustion air and fuel are maintained for the CLR-System.



**Figure 15** - Equilibrium gas composition of the fuel reactor (FR) exhaust depending on the air/fuel ratio for pure methane according to J. Bolhar-Nordenkamp et al. (40)



**Figure 16** - The necessary heat extraction from the reactor system versus the global air/fuel ratio for pure methane according to J. Bolhar-Nordenkamp et al. [65]

The detailed description of the CLR-System at Chalmers' components, operational principals and running operations is present in the next chapter of the thesis, along with description of the measurements of gases and tars and evaluation of the available data.

### 1.3.2. Oxygen Carriers

The key issue for a good performance of both the CLC- and CLR-Systems is to find an oxygen carrier which is:

- Reactive towards the fuel gas and air;
- High oxygen transport capacity;
- Resistant towards attrition;
- Not apt to agglomerate;
- Possible to produce at reasonable cost.

In the last decade, a number of researches on oxygen carriers for chemical-looping combustion have been performed. The major affiliations have been Chalmers University of Technology, CSIC in Zaragoza, Spain, Tokyo Institute of Technology in Japan and Korea Institute of Energy Research [31].

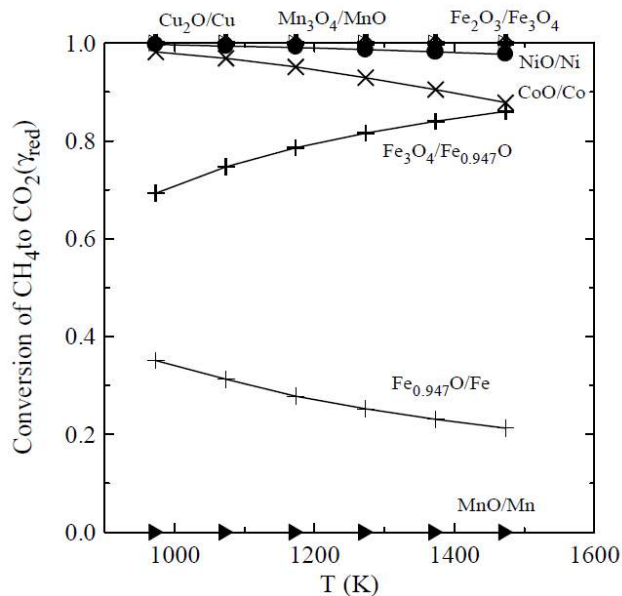
Mattisson and Lyngfelt [32] found that some metal oxides of the transition state metals Fe, Mn and Ni were among the feasible candidates to be used as oxygen carriers in CLC run at higher temperatures. In this previous study, Mattisson and Lyngfelt performed a thermodynamic analysis of different oxygen carriers. This was a primary study on the affinity to the fuel (methane), capacity for conversion of the fuel and mass ratio of active oxygen for different metal oxide pairs – Fe<sub>2</sub>O<sub>3</sub>/Fe<sub>3</sub>O<sub>4</sub>; CuO/Cu; Mn<sub>3</sub>O<sub>4</sub>/MnO and NiO/Ni.

The results showed that most systems have high affinities for reaction with methane. It also showed that the methane conversion, represented in Figure 17, was completed for the Cu<sub>2</sub>O/Cu, Mn<sub>3</sub>O<sub>4</sub>/MnO and Fe<sub>2</sub>O<sub>3</sub>/Fe<sub>3</sub>O<sub>4</sub> and it was above 97% for NiO/Ni. The degree of methane conversion to carbon dioxide was calculated thermodynamically using a method of minimization of Gibbs free energy and was carried out with 100% methane over the metal oxide (Me<sub>x</sub>O<sub>y</sub>) at different temperatures at 1bar total pressure. The oxygen transport capacity or mass ratio of active oxygen was calculated by Equation 6 ( $m_{ox}$  and  $m_{red}$  meaning the mass of oxidized and reduced oxygen carrier) and the results are shown in Figure 18.

$$R_o = \frac{m_{ox} - m_{red}}{m_{ox}} \quad (6)$$

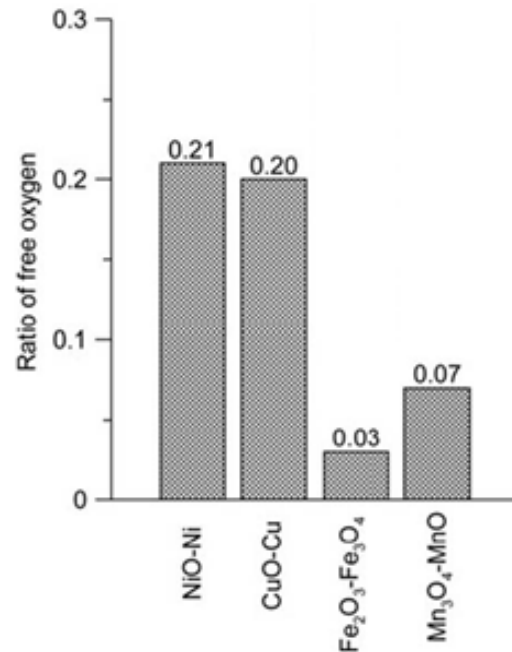
Four different oxygen carriers were investigated for chemical-looping combustion applications (Adánez et al. [34]; Cho et al. [35] and [36]; Mattisson et al. [37]; Johansson et al. [38]; among many others) and it was verified that usually the nickel oxide is the most active carrier. However, some drawbacks were the high level of toxicity as well as the fact that it is not able to convert the fuel (methane) to 100% CO<sub>2</sub> and H<sub>2</sub>O. On the other hand, iron oxide is not toxic, is the hardest and is much cheaper. The setbacks of this carrier were the low reactivity it presented and that, due to thermodynamic limitations, it is not possible to reduce iron further than magnetite, Fe<sub>3</sub>O<sub>4</sub>, and still

achieve full conversion of the fuel to  $\text{CO}_2$  and  $\text{H}_2\text{O}$ , which results in a rather low usable oxygen ratio (only 3% as shown in Figure 18) [30,38].



Nickel- and iron-oxides have been more extensively

**Figure 17** - Conversion of  $\text{CH}_4$  to  $\text{CO}_2$  versus the temperature for different metal oxides [32]



**Figure 18** - Mass ratio of active oxygen for different systems of metal oxides [38]

Copper oxides' main disadvantage is the low melting point of Cu ( $1089^\circ\text{C}$ ) which prevents a high reaction temperature.

A manganese based oxygen carrier showed no obvious disadvantage as it is not toxic, can totally convert the fuel to  $\text{CO}_2$  and  $\text{H}_2\text{O}$ ; has a high melting point and has twice the amount of free oxygen as the iron-oxide. As  $\text{MnO}_2$  decomposes to  $\text{Mn}_2\text{O}_3$  at about  $500^\circ\text{C}$  and  $\text{Mn}_2\text{O}_3$  decomposes to  $\text{Mn}_3\text{O}_4$  at approximately  $900^\circ\text{C}$  in air, the system  $\text{Mn}_3\text{O}_4/\text{MnO}$  is the most likely system to be used in chemical-looping combustion and is, therefore, the system at which studies refer to [34,38].

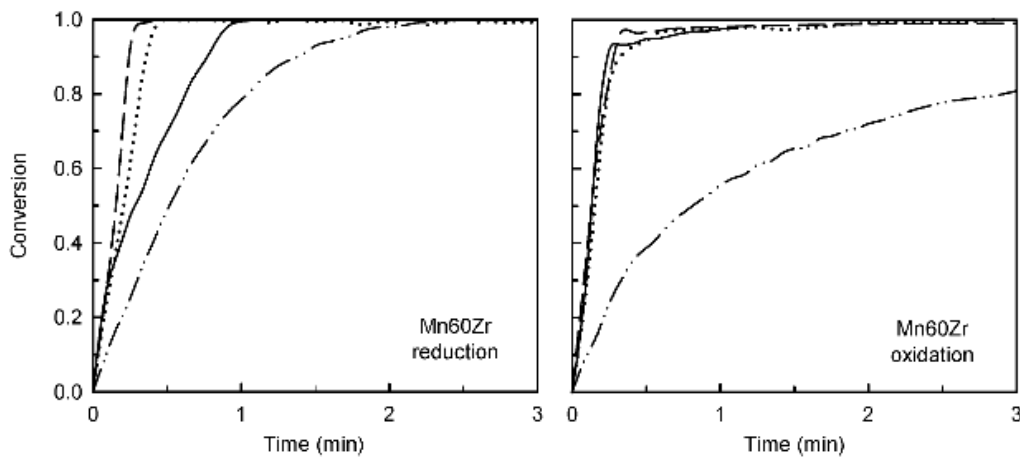
From the study performed by Mattisson and Lyngfelt [32], it was possible to conclude also that these metal oxides should be preferably supported by an inert material which is believed to increase the reactivity and help to maintain the internal structure of the particles throughout the redox reactions. The inert material also provides the oxygen carrier a porous structure which, in turn, increases the surface area for reaction [16,30].

Manganese oxides were studied on five different inert materials by Adánez et al. [34]. The studied inert materials were  $\text{Al}_2\text{O}_3$ , sepiolite,  $\text{SiO}_2$ ,  $\text{TiO}_2$  and  $\text{ZrO}_2$  sintered at four temperatures. These authors performed crushing strength tests, using the ASTM D-4179 method which allows the measurement of the minimum normal force required to crush a cylindrical extrudate placed between two plates in horizontal position, and reactivity tests, carried out in a thermo-gravimetric analyzer (TGA), CI Electronics type. Results from the crushing strength test showed that it was highly dependent on the

concentration of the metal oxide, the inert used as a binder and the sintering temperature. More concretely, Mn-based oxygen carriers only had high crushing strengths when using SiO<sub>2</sub> or TiO<sub>2</sub> sintered at 1100°C and ZrO<sub>2</sub> sintered at temperatures higher than 1100°C. Reactivity tests demonstrated that the Mn-based oxygen carriers showed a different behavior depending on the active metal oxide content, the type of inert and sintering temperature. The results are presented in Figure 19 and Table 7 [34].

**Table 7** - Maximum oxygen transport capacity of different concentrations of manganese based oxygen carriers

Metal oxide (wt %)	Mn <sub>3</sub> O <sub>4</sub> /MnO
100	7.00
80	5.45
60	3.98
40	2.58



**Figure 19** - Reduction and oxidation conversions for Mn-based oxygen carrier supported by ZrO<sub>2</sub> sintered at 950° (-), 1100° (- -), 1200° (...) and 1300°C (- . -) [34]

In general the best performance with complete utilization of the manganese used and reaction times less than 1min was obtained when ZrO<sub>2</sub> was used as the inert material. Further investigation of this oxygen carrier stabilized on several particles, CaO, MgO and CeO<sub>2</sub>, was performed by Johansson and Mattisson [38] which enable a better characterization. All the particles exhibited high reactivity and limited physical changes during the cyclic reactions. However, the particle that showed the highest reactivity among the four was MgO, which makes ZrO<sub>2</sub> stabilized by MgO a good support and inert binder for Mn-based oxygen carriers. Several characteristics of this oxygen carrier, which is the one used in the CLR-System that provided the data for this thesis are summarized in Table 8.

**Table 8** - Summary of properties of M4MgZ1150 particles [38]

<b>Metal oxide</b>	Mn <sub>3</sub> O <sub>4</sub>
<b>Wt % of the metal oxide</b>	40
<b>Inert material</b>	Mg-ZrO <sub>2</sub>
<b>Wt % of the inert</b>	60
<b>Nomenclature</b>	M4MgZ1150
<b>Sintering temperature [°C]</b>	1150
<b>Density [kg m<sup>-3</sup>]</b>	2260

<b>Porosity</b>	0.58
<b>Crushing strength [N]</b>	0.7
<b>Rate index</b>	4.60

Investigation of the behavior of these particles performed by Cho et al. [36] and by Abad et al. [39], confirmed that no sign of agglomeration occurred. Also, since de-fluidization in the experiments performed did not result in a sintering but rather a soft cake, severe problems with de-fluidization at much higher velocities in a real application are not expected. However, further investigation should be carried in order to determine the de-fluidization origin for manganese-based carriers [38].

Although only data of the manganese-based catalyst is available for this thesis, experiments with iron- and nickel-based catalysts are also expected to be carried out at the CLR-System at Chalmers. The operational conditions at which they will occur are summarized in Table 9. All the catalysts are to be supported on a silica-sand bed material which was proven to have no activity on the tar cracking by previous reference studies of the system using only silica-sand [33]. These results for the silica sand study can be seen in Appendix IV.

**Table 9** - Oxygen carriers tested at Chalmers University of Technology

<b>Parameter</b>	<b>Ilmenite</b>	<b>Manganese</b>	<b>Nickel</b>
Active bed material [wt %]	20, 40, 60	23	23
Temperatures in FR [°C]	680, 700, 750, 800, 815	700, 750, 800	600, 700, 750, 800
Oxygen concentration in AR [mole %]	0.4, 0.5, 0.7, 1, 1.75, 2, 4.1	1, 2.2	1, 2.3, 2.7, 2.9
Bed material diameter [μm]	125<dp<180	212<dp<250	212<dp<250

### **1.3.3. Tar Models**

In order to develop a tar decomposition model, literature review was required to get acquainted with the state of the art in research done in the tar reforming field of studies.

Articles produced by Coll and Markevich [40], Narváez and Corella [41] and others (such as references [42,43,44,45]) described the destruction of tars through steam reforming mechanisms. These models were discarded as the system under study works via catalytic cracking. The same happened for several articles referring to thermal cracking of tars, such as the articles produced by Egsgaard and Larsen [46] or by Taralas and Kontominas [47] among others. Thermal cracking of the tars was confirmed to be insignificant in this system by the previous studies performed with the silica-sand. However, some information from the first of these articles, [46], was taken into consideration as it concerns phenolic compounds, which are known to be of a fragile structure and easy to decompose. Therefore, this information was considered to be applicable to the catalytic cracking as well. More information on the tar compounds is given in the next chapters and in Appendix V.

Nevertheless, many articles were found on the subject of catalytic cracking of tar molecules from different fuels. From the papers reviewed, Dou and Gao [48], Simell and Kurkela [49], Dou and Pan [50] and Kumar and Klein [51] wrote about the catalytic destruction of tars from fossil fuel conversions which demand for higher temperatures than biomass conversions. For this reason they were not considered as relevant sources. Also, they described a specific compound's decomposition (1-Methylnaphthalene in two of them) which restrains the modeling criteria, or they performed an evaluation of the heating value which was not done in this thesis due to insufficient data on the operating system.

From all reviewed literature on biomass catalytic cracking of tars, some referred to a single compound's destruction, such as Simell and Hakala [52], while others studied a higher variety of molecules, Li and Suzuki [23], Corella and Caballero [53] and other references [27,54,55,56,57]. All these articles were taken into account in the decision making process while developing the decomposition model applied to the CLR-System at Chalmers. One article by Corella [58] discussed the kinetics of catalytic cracking more extensively. However, this article was not considered, due to the complexity of the described reactions, as it was neither compatible nor feasible to apply those kinetics to such a complex system as the one at Chalmers. Detailed reasons for the consideration of some more relevant data are given when the development of the decomposition model is described (which is done in chapter 3).

## **1.4. Objective**

The objective of this work is to derive a model for tar decomposition using data available from experiments conducted in the Chemical-Looping Reformer (CLR) System at Chalmers, operated with the producer gas coming through a slip stream from the Chalmers 2-4MW<sub>th</sub> biomass gasifier. The model is developed with the objective to increase knowledge on the decomposition mechanisms taking place within the system, as well as understanding how they may be influenced by the operating conditions. Data is available for one bed material in the fuel reactor, using a manganese-based catalyst, and for three different operating temperatures and two oxygen concentrations in the air reactor. After future implementation of the developed model in the system, it should be possible to predict results of further operations, such as velocity of reactions and improvement of operating conditions.

## **1.5. Methodology**

The methodology used in this thesis consisted on a primary study of the system components, execution and available data, to get acquainted with the procedures, problems evolved and the objective of the work.



A literature review was done as to search for information on the tar components and already existing solutions for the modeling of the compounds from different cleaning processes. One model was considered adequate and was adapted for the decomposition model for this work's system. Grouping of the tar compounds was performed according to three main criteria and a diagram of the decomposition paths between different groups was drawn. Kinetic first order reactions were established involving these groups. These reactions represent the ruling network of reactions that occur inside the CLR-System and describe the interrelation between the groups' own decompositions.

The system of kinetic reactions proposed was implemented and solved using the software MatLab and using sets of experimental data as input. The best fitting kinetic constants for each operating conditions of the system was found. In particular, this happened once the model constants yield was a suitable match with the experimental data. Graphics representing the evolution of the concentrations of each group of tars were produced by the program, together with the values of the best fitting kinetic constants and the calculated error between the experimental data and the points calculated by the model.

Evaluation of the results was performed and some conclusions were drawn. Also, some recommendations for future work were made.

## **1.6. Thesis Outline and Structure**

This thesis presents some of the results obtained so far within the experimental setup at Chalmers CLR-System. In chapter 2 the process of the working system is described in detail, along with the measurement procedures for both permanent gases and tar compounds and is followed by the evaluation of the available data. The methodological approach used to develop the decomposition model and the simulation program is detailed in chapter 3. A comparison between results from simulations and experimental ones is performed in chapter 4. Finally, conclusions on the developed model and CLR-System operating conditions are mentioned in chapter 5, as well as a reference to future work for improvement of the model.



## 2. CHEMICAL-LOOPING REFORMING (CLR) SYSTEM AT CHALMERS

The system investigated in this thesis is based on the principle of Chemical Looping Reforming (CLR). This system was developed by Chalmers with the objective of reducing the tar fraction in product gas from biomass gasification through the reforming of the tar components ( $C_nH_m$ ) into useful gas molecules [28,59]. The main reactions involved in the process are partial oxidation, steam reforming and catalytic cracking of the compounds, with the use of a metal oxide catalyst circulating between the two fluidized bed reactors which constitute the system.

The dual fluidized bed is placed downstream the gasifier and the catalyst reactor is operated at a temperature thermally integrated to the temperature from the gasifier exit [33]. This makes the type of system integration to be referred to as a secondary catalytic cracking of the tars. One of the major advantages of thermally integrating the operation temperature with the gasifier temperature is the possibility of minimizing heat losses. However, the associated costs are still too high for integration of the process in industry.

As a consequence, one of the objectives in such a process evaluation is to minimize the overall costs. In particular, this proceeds by developing the application of cheaper but also less active and less toxic catalysts – compared to the traditional nickel-based ones – and making oxygen an additional driving force for tar removal [28,33].

Chalmers' CLR-System studies the performance of the dual fluidized bed process for decomposition of tars, working with different materials such as the natural ore Ilmenite (see Table 9), but also manufactured particles such as a manganese oxide called M4MgZ1150 which consists of 40% Manganese Oxide ( $Mn_3O_4$ ) supported on 60% Magnesium-Zirconium Oxide ( $MgZrO_2$ ), as the catalyst. This is the catalyst investigated in this thesis. Operating conditions during the experiments were characterized by a bed material composed of 23%<sub>mass</sub> catalyst and 77%<sub>mass</sub> silica-sand with operating FR temperatures between 700°C and 800°C and for each temperature two different oxygen concentrations (molar) of 1% and 2.2%. Again, the silica-sand bed has been proven to have no activity on the tar cracking by previous reference studies of the system using only silica-sand [33].

These results for the silica sand study can be seen in Appendix IV. The final purpose is to evaluate the applicability of the system in industry.

## 2.1. Description of Experimental Set-up

The complete system is composed of two fluidized beds, one being the reformer or catalyst reactor (FR), designed as a bubbling fluidized bed, and the other being the regenerator or air reactor (AR), a circulating fluidized bed. The fluidized bed reactor is usually preferred, as coke formation on the catalyst surfaces and consequent catalyst deactivation is contained [5].

The system is supervised by 10 pressure taps (inclined at 45° to prevent blockage by particles) and 10 thermocouples. The raw gas feed into the FR from the gasifier is controlled by a gas pump at the exit of the reactor, which maintains the outflow constant. The gas feed into the AR is controlled by two separate mass flow regulators (for air and nitrogen) to make possible the generation of different oxygen concentrations. The raw gas from the gasifier and the air blend enter the FR and AR (respectively) through wind boxes, reducing pressure fluctuations in the gas feed and the raw gas feeding pipe from the gasifier is pre-heated in order not to have condensation of tars inside the pipe.

Both reactors are placed inside an oven, consisting of two halves, and are kept at sub-atmospheric pressure of -4 to -6kPa as a safety measure. It is possible to obtain separate heating of the two reactors with a difference up to 200°C in between. Despite this possibility, experiments made to the date did not contemplate this, working with both reactors at the same temperature.

Both reactors are linked through two gas tight loop seals: the inferior or lower loop seal (ILS/LLS) which transports the catalyst from the FR to the AR and the superior or upper loop seal (SLS/ULS) which returns the catalyst back to the FR. On both loop seals an inert gas (helium) is introduced and controlled by two independent mass flow regulators, to prevent gas cross-contamination from the respective reactors while enabling the catalyst to circulate.

Table 10 represents the geometrical characteristics of the system and Figure 20 the system components as following: (1) reformer or catalyst reactor (FR); (2) regenerator or air reactor (AR); (3) inferior or lower loop seal (ILS/LLS); (4) superior or upper loop seal (SLS/ULS); (5) oven; (6) and (7) measurement of permanent gases at exiting the FR reactor; (8) and (9) measurement of remaining gases from AR exit; (10) mass flow regulators; (11) SPA port for tar collecting at FR exit; (12) and (13) measurement of inlet permanent gases and SPA port for tar collecting at FR entrance.

**Table 10** - Geometrical measures of the dual-fluidized bed reactor

	Cross-sectional [mm]	Height [mm]
Fuel reactor (FR)	50 x 50	380
Air reactor (AR)	20 x 20	460
Superior loop seal (SLS)	23 x 23	120
Inferior loop seal (ILS)	23 x 23	50

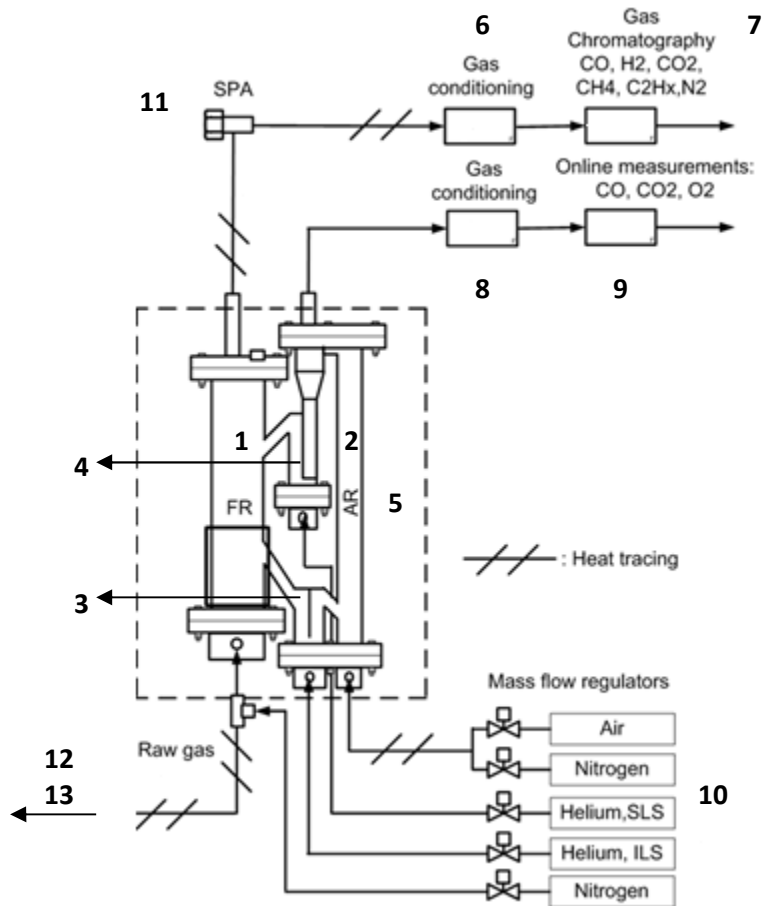
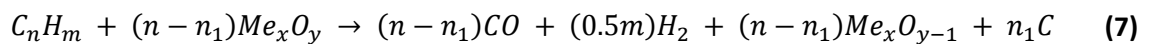


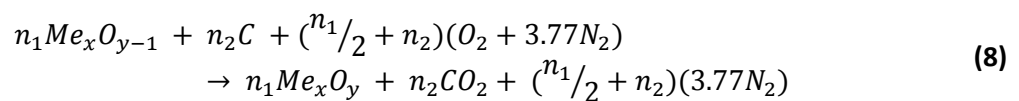
Figure 20 - System Components [17]

More pictures of the system are shown in Appendix III.

In the reformer reactor, FR, the raw gas reacts with the partially oxidized catalyst. This means, that some of the oxygen from the metal oxide ( $Me_xO_y$ ) catalyst is consumed by tar cracking reactions. The reduction of the catalyst is usually an endothermic reaction and has simultaneous carbon forming reactions, which cause for coke to deposit on the surface of the catalyst and deactivate it. The general reaction that represents the tar oxidation and catalyst reduction is represented in Equation 7:

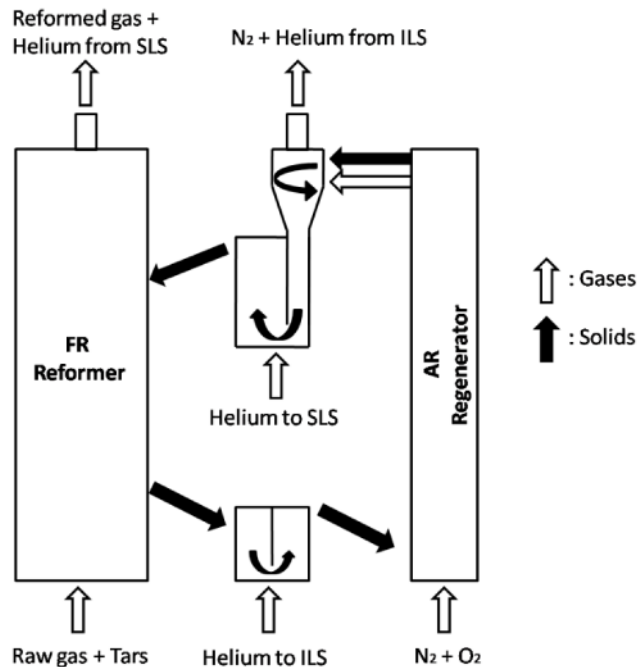


The reformed raw gas leaves the system as cleaned producer gas and the reduced catalyst goes into the air reactor, AR, through the ILS. When the particles reach the regenerator reactor, the re-oxidizing reactions of the metal oxide occur. These are usually strongly exothermic reactions which make the coke deposits on the surfaces of the catalyst to oxidize and produce  $CO_2$ . The general reaction can be described by Equation 8:



The remaining gases leave the AR and the re-oxidized catalyst passes through cyclone recollection and the SLS before the loop seal is fluidized with helium. Additionally, to prevent leakage and mixing

of the gases from the AR to the FR the two reactors are kept with a small difference in pressure, of below 500Pa, being the FR the sub-pressured reactor so that the product gases do not enter the AR. Finally, the reformed catalyst returns to the FR and so forth. The overall process is exemplified in Figure 21.



**Figure 21** - Circulation of the catalyst in the system [16]

As a consequence of the sub-atmospheric operating pressure, the way of introducing the raw gas into the FR is via a pump placed after the outlet of the system. The pump pushes the cleaned producer gas with a constant flow and, therefore, also pushes the inlet raw gas. A consequent problem is that, because of gas expansion and water-gas shift reactions that occur inside the reactor, the volume of gas changes and there is no way of measuring the inlet flow, as the gas is too hot for any flow meter to be able to be mounted.

## 2.2. Measurement Techniques

### 2.2.1. Permanent Gases

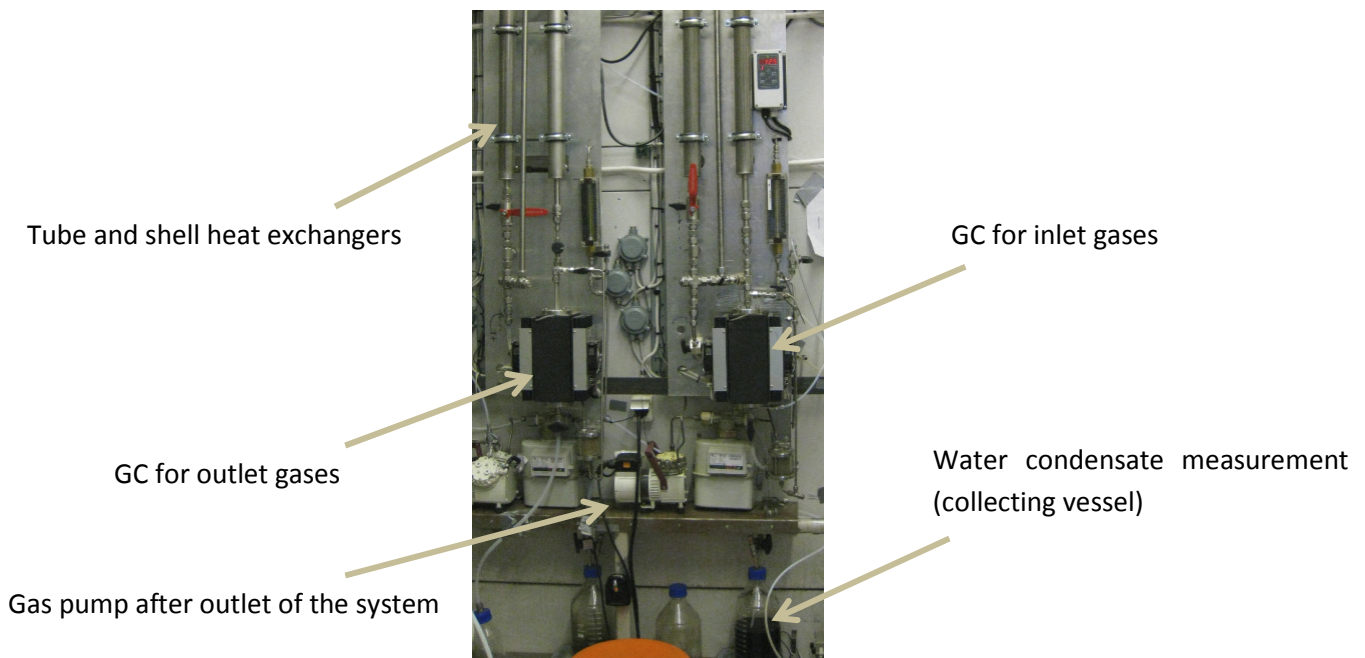
The main components of the permanent gases in the producer gas, that result from the passage of the raw gas through the system, are  $N_2$ ,  $CO$ ,  $H_2$ ,  $CO_2$ ,  $CH_4$  and  $C_2H_n$  and volatile organic compounds.

Both the permanent gases that enter and that leave the FR pass through a venturi nozzle and are mixed with iso-propanol that will act as a solvent for the remaining tars in the gas. This is done as a preventive measure to avoid fouling and clogging in the equipment downstream the CLR. After, the gases are cooled, passing through two tube and shell heat exchangers, and the condensate is

separated by gravity into a collecting vessel. Here the iso-propanol is separated by liquid density difference and is re-circulated into the venturi nozzle. The permanent gases are analyzed by a micro gas chromatograph: Varian 4900. The steps described for this process are seen in Figure 20 in components (6) and (7).

The remaining gases in the AR are measured via on-line measurement by non-dispersive infrared analyzers, for CO and CO<sub>2</sub>, and by paramagnetic analyzer, for O<sub>2</sub>, after passing through a similar cooling and cleaning setup as the one described for the exiting gases from the FR. The steps described for this process are seen in Figure 20 in components (8) and (9).

As before, one of the problems associated with the measurements was that the water content was only measured for the inlet gases, through the condensate. Another operational problem in last year's experiments was that there was only one gas chromatograph port available and, therefore, it was impossible to measure inlet and outlet conditions at the same time. A picture showing the measurement set is in Figure 22.



**Figure 22** - Permanent gases measurement set

### 2.2.2. Solid-Phase Adsorption (SPA)

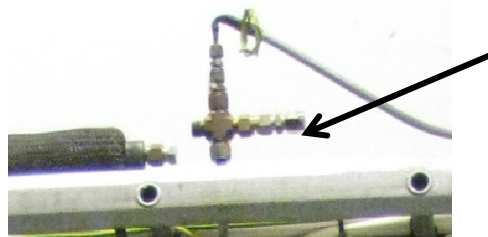
Tars are considered to be the condensable fraction of the organic gasification products and are largely aromatic hydrocarbons, including benzene [13]. The tars composition can provide quantitative and qualitative information on the process conditions, thus making the intermittent trapping and analysis on the compounds an important method to monitor and study the influence of the process parameters and catalysts activity [4,22]. However, unlike permanent gases that can be analyzed through common on-line methods, the complexity of tars makes it impossible to perform an on-line analysis [4].

Development of tar classification systems is especially important for improvement of kinetic models of tar conversion over a catalytic bed and for better understanding of the relationship between the composition of the tar and the operating conditions and design of the gasifier [19].

Researchers at KTH (Royal Institute of Technology, in Stockholm) studied the use of solid-phase adsorption (SPA) on amino-phase to the vapor-phase tar sampling. This was done as an effort to make tar sampling and analysis more efficient and accurate than the traditional techniques, such as cold trapping combined with solvent adsorption and filters. Some of the advantages found for this biomass tar sampling and separation method were the reduction on sampling time and separation time, superior analyte discrimination and accuracy on the investigated tar compounds and possible operating temperature range from 700°-1000°C of the system [22].

On the experimental setup, at Chalmers' CLR-System, sampling was done by SPA upstream and downstream the FR, represented by numbers (11) and (13) in Figure 20. A needle attached to a solid-phase extraction column containing 100mg of amino-phase was connected to a gastight syringe of 100mL and inserted into the septum-tightened ports (as represented in Figure 23 in the raw gas pipe from the gasifier). The samples were taken by manually pulling out the product gases through the column, during approximately 1min. Then, the air tight column was disconnected and stored in a freezer (-18°C).

Overall, the full method includes the solid-phase adsorption (SPA) on amino-phase, for sampling, followed by liquid chromatographic (LC), for group separation, and capillary gas chromatography (GC) with flame-ionization detection (FID), for the individual tar compounds analysis [22]. During the desorption process, an elutropic solvent (solvent of increasing polarity) was used, enabling selective desorption of the tars into aromatic and phenolic fractions. This is the reason why the amino-phase has an excellent LC separation capacity, due to its strong polar properties [22].



**Figure 23** - Septum-tight port for gastight syringe insertion in the raw gas line



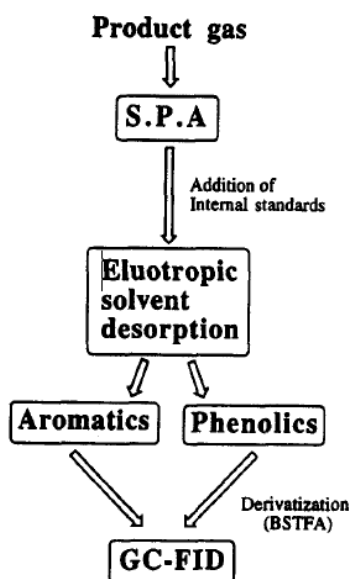


Figure 24 - SPA sampling and analysis scheme for tar components [22]

## 2.3. Experimental Results and Analysis

### 2.3.1. Error Analysis of SPA-Sampling Results

The first step, before simulation of the developed decomposition model, was to calculate the mean and most expected value of each component's concentrations from the raw data obtained by the SPA. The values varied between samples of the same experiment and an error analysis had to be performed. A common error model was considered and the calculus of the relative standard deviation (RSD) was done according to the following Equation 9:

$$RSD [\%] = \frac{\sqrt{\frac{\sum_{i=1}^n (x_i - \bar{x})^2}{n-1}}}{\bar{x}} \times 100 \quad (9)$$

The  $x_i$  stands for the concentrations of each sample, the  $\bar{x}$  stands for the mean value of all the considered samples ( $\bar{x} = \sum_{i=1}^n x_i/n$ ) and the  $n$  for the total number of samples. The results obtained for 700°C, 750°C and 800°C FR temperature and two oxygen concentrations for the operations with the manganese catalyst are shown in Figures 25 to 27 below. The results are presented relatively to tar groups which are defined in the next chapter of the thesis.

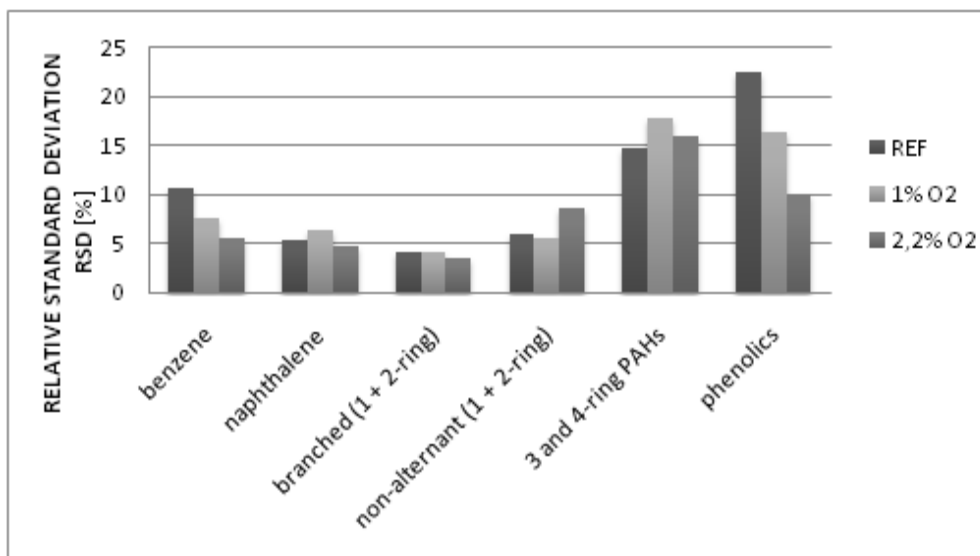


Figure 25 - RSD result values of grouped tars for 23% manganese catalyst at 700°C

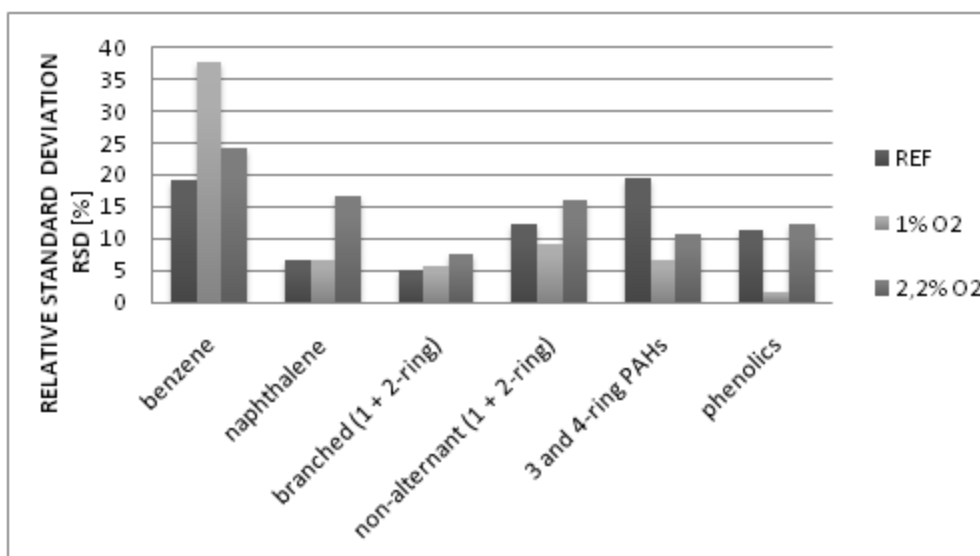


Figure 26 - RSD result values of grouped tars for 23% manganese catalyst at 750°C

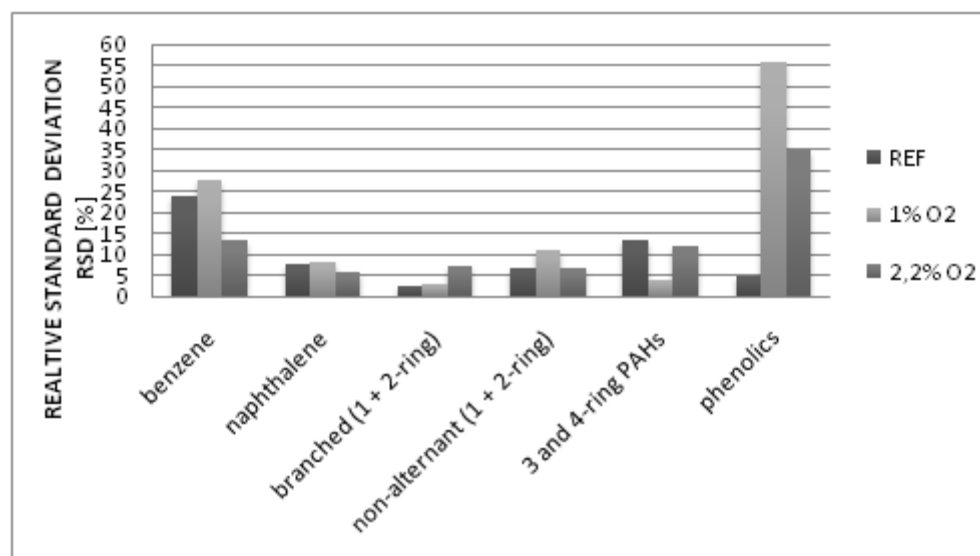


Figure 27 - RSD result values of grouped tars for 23% manganese catalyst at 800°C

As it is possible to perceive from the numbers above, the highest deviation is approximately 15% for all conditions with two exceptions: benzene at 750°C and 800°C and phenolics at 800°C. A possible explanation on why this happened for the benzene, might be the delay between SPA sampling and analysis itself. The waiting time for the samples could have induced the benzene molecules to separate themselves from the amino-phase extraction column, due to the high vapor-pressure. As some particles might have left the column, during the analysis the sampling values for this particular compound would vary in a larger range from sample to sample, increasing the relative error. In the case of the phenolics, looking back at the individual considered samples, presented in Appendix VI, there might be some concentration values for this particular component that lead to believe that some of the sampling considered could have been discharged. This was not noticed at the time and, consequently, the data used has a higher relative error.

Considering the majority of the data has a relative error below 10%, with some exceptions that reach 15 or almost 20%, it is possible to consider that from the collected data a good evaluation of the system can be performed. However, to improve even further this evaluation, the method of extraction of the samples from the SPA port was reformulated this year. In this year's experiments, the 100mL syringe was placed in a pneumatic puller, for a more precise extraction of the raw and producer gas from the lines. Instead, the data available for this work was collected manually which involves a higher induced error from imprecisions on the velocity and volume of extracted gas.

### 2.3.2. Decomposition Trends

In order to make an analysis of the resulting kinetic constants from simulations, described in the next chapter in model development and implementation, it is necessary to previously make an estimation on which trends can be identified for the decomposition of each tar groups. For this purpose, it is necessary to include an analysis of the three different reactor temperatures and two oxygen concentrations. The columns graphic, shown in Figure 28, represents the conversions of each group of tars for the six different operating conditions. The graphics, shown in Figure 29 to Figure 31, represent the concentrations of the tar groups in relative terms, i.e., each group's concentration for each operating condition divided by the total tar concentrations at the same operating condition.

Group conversions were calculated by a simple division of the final and initial group concentrations, as demonstrated in Equation 10:

$$X_i[\%] = \left( \frac{C_{i,0} - C_i}{C_{i,0}} \right) \times 100 = \left( 1 - \frac{C_i}{C_{i,0}} \right) \times 100 \quad (10)$$

Even though the conversions are calculated as shown in the equation, it is important to understand that due to the simultaneous reactions for all tar components occurring inside the reactor these conversions take a broader meaning. This is, when talking about conversion of a group what is being mentioned is the relative velocity at which tars from the group are being decomposed against the velocity of formation of these same molecules originated from other groups' own decompositions.

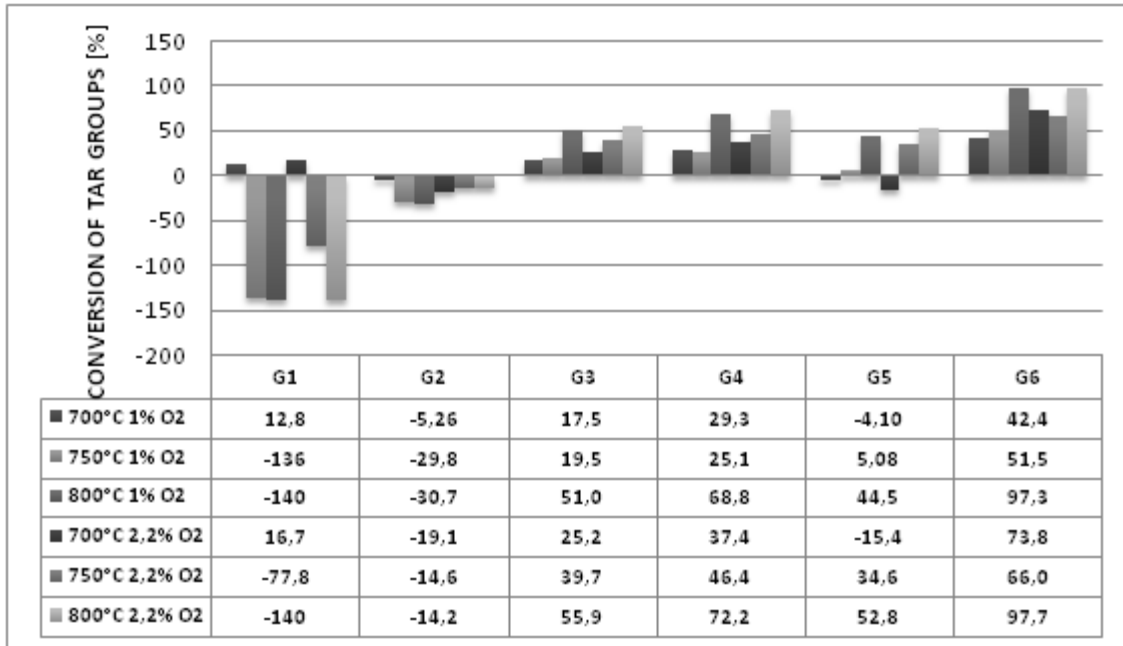


Figure 28 - 23% Manganese tar conversions [%]

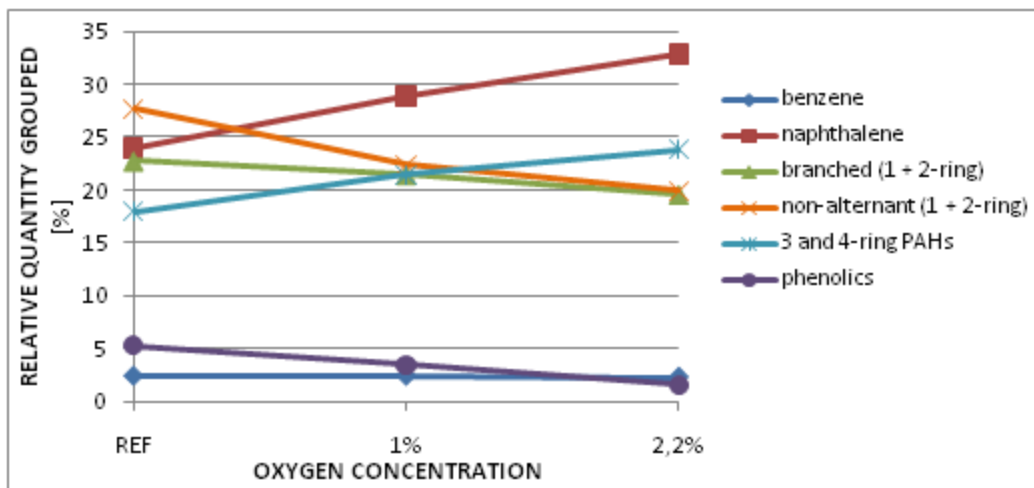


Figure 29 - Relative concentrations of grouped tars for operating temperature 700° at different O<sub>2</sub> concentrations

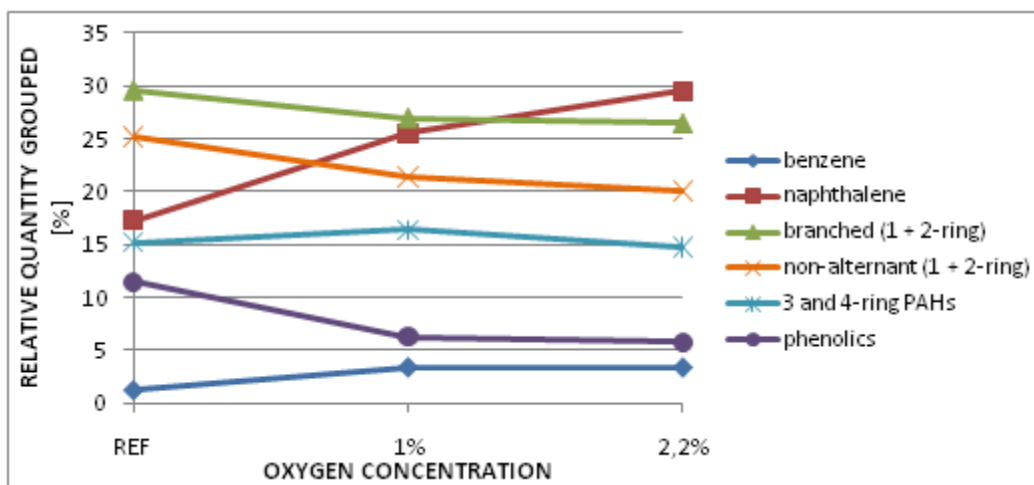
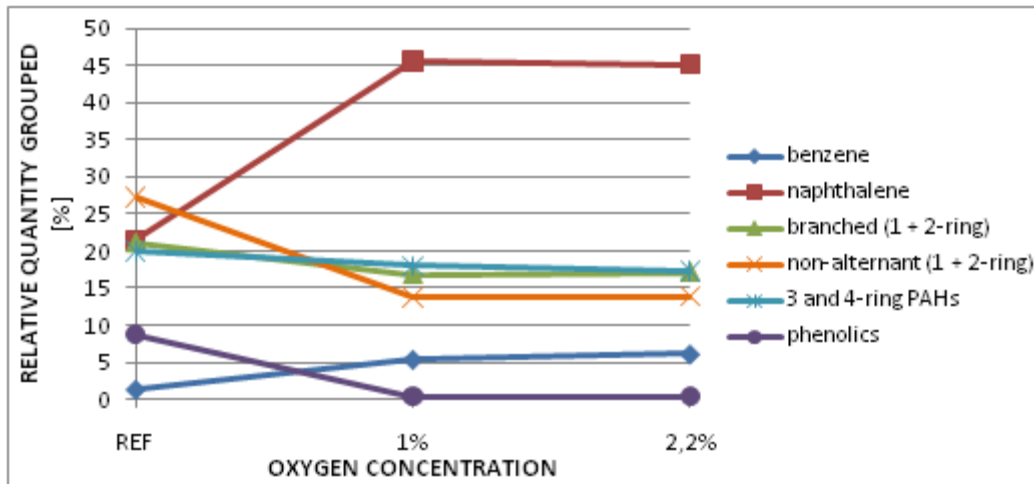


Figure 30 - Relative concentrations of grouped tars for operating temperature 750° at different O<sub>2</sub> concentrations



**Figure 31** - Relative concentrations of grouped tars for operating temperature 800° at different O<sub>2</sub> concentrations

As a result, negative conversions mean that tars are being formed at a higher rate than they are being decomposed, i.e. the velocity of decomposition of other groups in the model is faster than the velocity at which a specific group decomposes. From the previous bars' graphic (Fig. Figure 28) some trends can be proposed for the breakdown of the tar groups with the varying operation conditions:

**1) Benzene:**

- Seems to be "converted" at 700°C, this is, all remaining groups have low conversions at 700°C and the decomposition velocity of benzene is high enough so to compensate for the molecules formation from other tars breakdown;
- However, benzene is produced at a faster rate at higher temperatures;

**2) Naphthalene** always increases in concentration:

- For lower oxygen concentrations, the concentration of naphthalene increases with increasing temperatures;
- But with higher oxygen concentrations, the concentration increases with decreasing temperatures, meaning that probably higher O<sub>2</sub> and higher temperatures are the most favorable conditions to have higher decomposition of naphthalene, along with/besides the forming from other groups;

**3) Branched** compounds always breakdown:

- Increasing temperatures and increasing oxygen concentrations lead to higher conversions, this is, even if there is high formation of these compounds from other molecules, as they have more fragile structures they have a higher tendency to breakdown and compensate the previous effect;

**4) Non-alternant** molecules behave similarly to the branched compounds;

**5) 3 and 4 rings PAHs:**

- Increase concentrations at 700°C for both oxygen concentrations, this might be because at 700°C the unknown molecules\* from that group, which most probably have larger and branched structures, decompose first (on elemental conversions

they have positive values, meaning cracking) giving formation to the other molecules from the same group;

- However, for the remaining conditions they decompose with increasing conversion for increasing temperatures and increasing O<sub>2</sub> concentrations;

**6) Phenolics** always decompose with the largest conversions of the whole present compounds in the raw gas, meaning that they are the easiest to decompose, as suggested in previous works [53].

Although these trends can be verified by the conversions for each situation, it is not possible to take any correlations from them, as they do not vary in any particular proportion between oxygen concentrations or temperatures and are rather “random” depending on the experience conditions. Moreover, when put under relative terms for the group concentrations, as shown in the graphs in Figures Figure 29 to Figure 31, it is possible to see that not always the variation of the concentrations from a whole tar amount perspective follows any particular “path”. This confirms that the proportion of tars that enter the system and that are decomposed inside it cannot be linearly related with the working temperatures and oxygen concentrations.

Despite these conclusions, the trends can be somehow validated by the results shown in the graphics obtained by implementation of the model, shown in chapter 4, for each operating conditions and also by the kinetic constants that were obtained of each situation. The results will show that there is a variation in shape of the decomposition lines (from Figures Figure 37 to Figure 48) and in value and order of magnitude of the kinetic constants (in Table 12 - Set of kinetic constants and respective simulation relative errors for all operating conditions' best results) accordingly to the conversions for each situation.

\*Unknown molecules are compounds, which are not the representative molecules chosen for the tars, present in this group. The selection of these molecules is described in the next chapter.

## 3. DECOMPOSITION MODEL

### 3.1. Development of Model


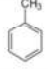
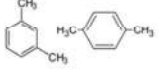
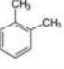
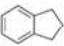
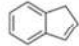
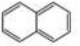
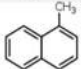
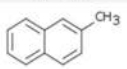


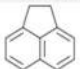
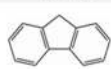

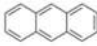
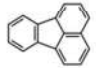


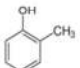
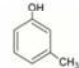
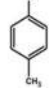
One catalyst was studied for different temperatures, one bed material concentration, described next, and different oxygen concentrations. Therefore, the operating conditions during the experiments were characterized by a bed material composed of 23%<sub>mass</sub> catalyst and 77%<sub>mass</sub> silica-sand with operating FR temperatures between 700°C and 800°C and for each temperature two different oxygen concentrations (molar) of 1% and 2.2%. The catalyst used (M4MgZ1150) consists of 40% Manganese Oxide ( $Mn_3O_4$ ) supported on 60% Magnesium-Zirconium Oxide ( $MgZrO_2$ ).

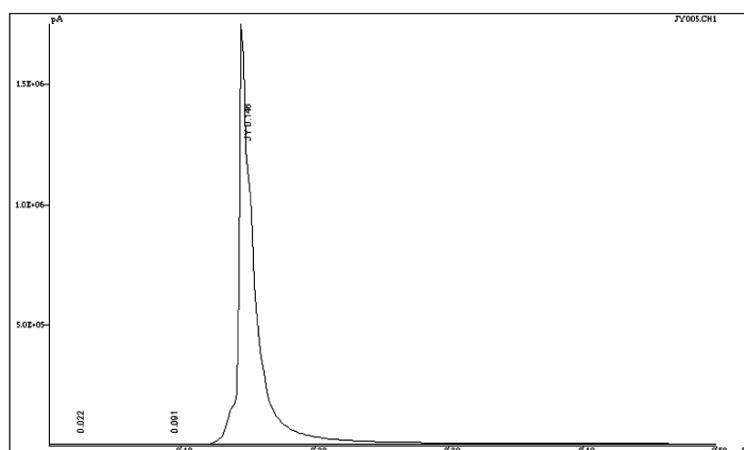
Tar samples were taken every one hour or one hour and a half after changes in the operating conditions, so that the system could reach steady-state. These samples were taken in sets of between three to six SPA-samples of both inlet and outlet of the CLR-System. After GC-FID analysis, it was possible to have the composition, amount and characteristics of the hydrocarbons present in these two gas streams. 21 known molecules were chosen to be the representative tar molecules for the whole system, which are shown in Table 11 below, and approximately 170 unknown compounds with molecular weights spread between benzene and higher than pyrene were detected in between. More detailed information on each chosen compound is described in Appendix V.

In the gas chromatography and the flame-ionization detection, molecules were identified by their length and polarity while being processed (Fig. Figure 32 - FID signal during analysis cycle ). Hence, they are organized from the smaller ones (benzene), that are the first to be measured, till the largest ones (bigger than pyrene), which are the last ones to be identified. This means that the unknown molecules, which are listed in times between other known compounds, have, most probably, similar sizes to the known molecules adjacent to them. With this conclusion, it was decided that, in order to group the tars, the unknown molecules would be divided according to their position between the known compounds and only after the grouping of the 21 known molecules was made.



**Table 11** - Representative tar molecules present in gas

<b>Benzene</b>	<b>Toluene</b>	<b>m/p-Xylene</b>	<b>o-Xylene</b>	<b>Indan</b>	<b>Indene</b>	<b>Naphthalene</b>
$C_6H_6$	$C_7H_8$	$C_8H_{10}$	$C_8H_{10}$	$C_9H_{10}$	$C_9H_8$	$C_{10}H_8$
						
<b>1-Methyl naphthalene</b>	<b>2-Methyl naphthalene</b>	<b>Biphenyl</b>	<b>Acenaphthylene</b>	<b>Acenaphthene</b>	<b>Fluorene</b>	<b>Phenanthrene</b>
$C_{11}H_{10}$	$C_{11}H_{10}$	$C_{12}H_{10}$	$C_{12}H_8$	$C_{12}H_{10}$	$C_{15}H_{10}$	$C_{14}H_{10}$
						
<b>Anthracene</b>	<b>Fluoranthene</b>	<b>Pyrene</b>	<b>Phenol</b>	<b>o-Cresol</b>	<b>m-Cresol</b>	<b>p-Cresol</b>
$C_{14}H_{10}$	$C_{16}H_{10}$	$C_{16}H_{10}$	$C_6H_6O$	$C_7H_8O$	$C_7H_8O$	$C_7H_8O$
						

**Figure 32** - FID signal during analysis cycle [60]

Considering the raw data from the analysis, samples were organized and the mean and most expected value of concentrations of each known compound was calculated, followed by calculation of their respective conversions. The tar concentrations were He-corrected, i.e., they were normalized with regards to the helium dilution from the SLS to the FR (measured to approximately 15~19%, depending on the experiment). Tables of the concentrations, relative weight in the total tar amount and conversions are shown in Appendix VII.

Summarizing, grouping the tars had to take into consideration the aforementioned three parameters:

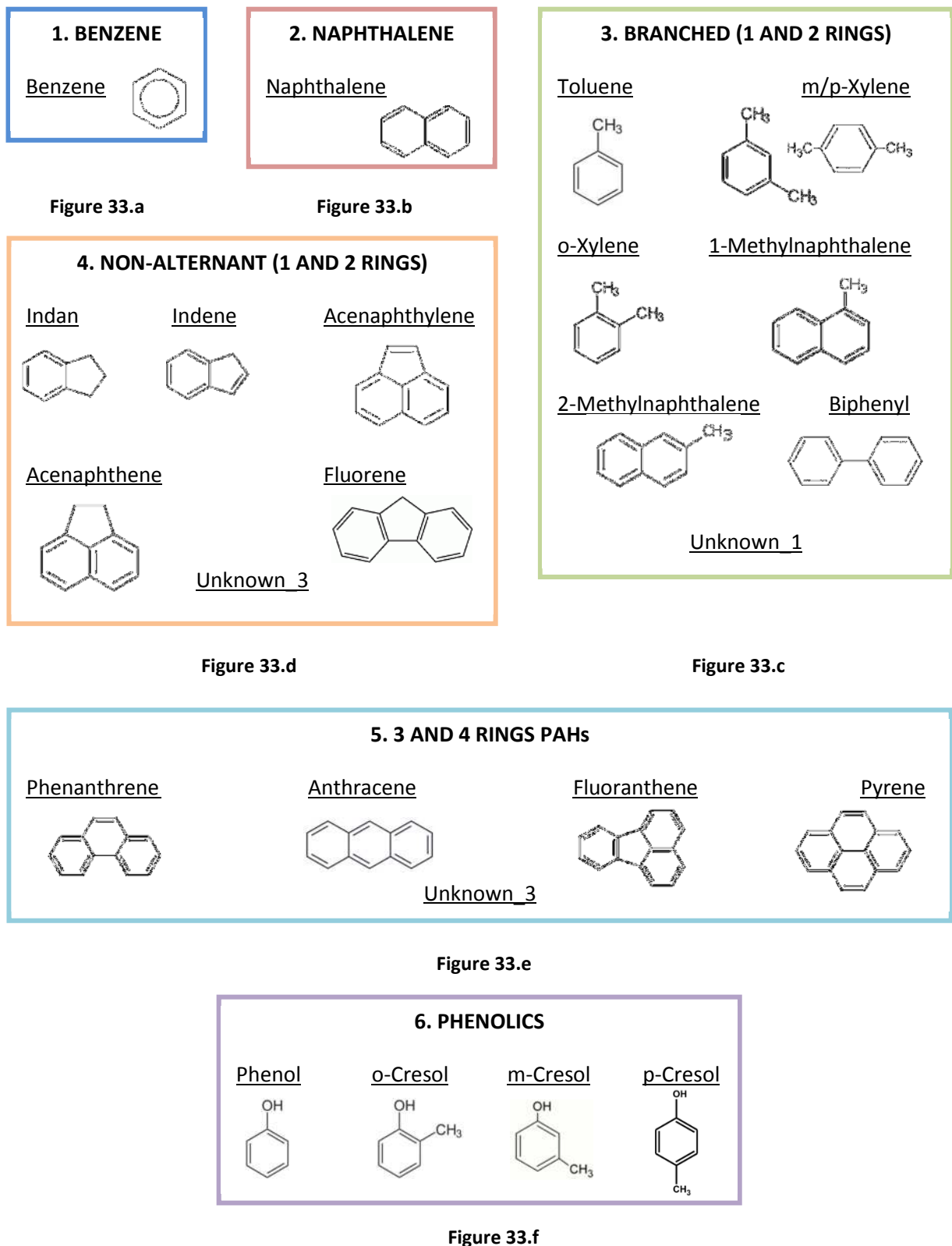
1. The individual conversion and, therefore, each tar concentrations:
  - o Faster decomposing molecules with higher conversions, this is, that the rate of decomposition is higher than the rate at which they are being formed;

- Slower decomposing molecules with very small conversions or even negative conversions, such as benzene and naphthalene, which means that the rate at which they are being formed is much higher than the rate at which they are decomposing;
2. The molecular structure, i.e., the size and type of links between elements:
    - Branched molecules which tend to be easier to breakdown as the branched link is more fragile than the links in the molecules;
    - Non-alternant compounds that have one or more rings which are not benzene (six membered);
    - Polycyclic Aromatic Hydrocarbons (PAHs) which contain two or more fused benzene rings;
    - Phenolics which have one hydroxyl group (-OH) after the branch;
  3. And, finally, the “weight” in the whole tar group, i.e., the relative percentage according to the total number of existing tars.

With these three parameters in mind, the known molecules were grouped and the unknown molecules were arranged and placed according to these groups. The scheme of groups shown in Figure 33 resulted from this process (each group color will from now forward be representative of the group).

Group concentrations were calculated by addition of each group component's individual concentration and group conversions were calculated as already demonstrated in the previous chapter. Graphs showing both initial and final group concentrations and graphs representing group conversions, for the studied catalyst in every different operating condition are shown in Appendix VI.

The important thing to keep in mind, as it was previously referred, is that when talking about conversion of a group what is being mentioned is the relative velocity at which tars from the group are being decomposed against the velocity of formation of these same molecules originated from other groups' own decompositions. For this reason, it is important that the developed model can translate correctly the simultaneousness of the reactions and the interaction between groups.



**Figure 33** - Tar groups: a) Benzene; b) Naphthalene; c) Branched molecules of 1 and 2 rings; d) Non-alternant molecules of 1 and 2 rings; e) Polycyclic Aromatic Hydrocarbons (PAHs) of 3 and 4 rings; f) Phenolic compounds

A first approach to the problem was the simulation of the kinetics of the network of tar groups by considering the Arrhenius' Law (Eq.11). For this it was necessary to have the apparent activation energies of each group (which would be simulated by the most influencing compound of each group) and the pre-exponential factors to obtain the reaction rate constant in order of the temperature. The use of catalyst has already proven to have an influence by decreasing the activation energy necessary and, therefore, increase the velocity of reaction and, consequently, the reaction rate constant. This hypothesis was discarded as these necessary parameters were not of relevance. The reason why was, as all tars are formed by the same elements, namely carbon and hydrogen, and the majority of links between these elements is the same for all compounds (either single or double), the activation energy would not vary for almost any group and any conclusion would be possible to be withdrawn.

$$k = Ae^{-E_a/RT} \quad (11)$$

After a further literature survey, two previously studied models for tar decomposing were found the most suitable and were further considered. They are represented in Appendix III. The first is a two-lump model by Corella et al. [27] where each lump represents two different "classes" of species: the more reactive tar compounds, with faster reactions, and the less reactive tar molecules, with slower reactions. This model was proven unsuitable for this work. The reason is it gives high importance to the thermal breakdown of tars, whereas in this work thermal breakdown is insignificant and the whole cracking process can be considered as mainly catalytic elimination. This was proven with the study with the inert bed material (silica-sand), where there is no change in concentrations due only to the temperature of the system.

The second model considered, also by Corella et al. [53], divided the tars into six different groups – (1) Benzene; (2) One-ring compounds; (3) Naphthalene; (4) Two-ring compounds; (5) Three- and four-ring compounds; (6) Phenolic compounds – according only to the chemical structure. This model could be adapted and enlarged according to the existing tar compounds in each situation and also considered that both thermal and catalytic mechanisms could occur simultaneously in the tar decomposing reactions. Due to the characteristics of being adaptable to the compounds found present after the SPA/GC-FID analysis and considering that both thermal and catalytic mechanisms are occurring simultaneously, even though the thermal decomposition can be considered insignificant for this work, the six-lump model was chosen as guidance for the development of the model for this thesis and which is represented in Figure 34.

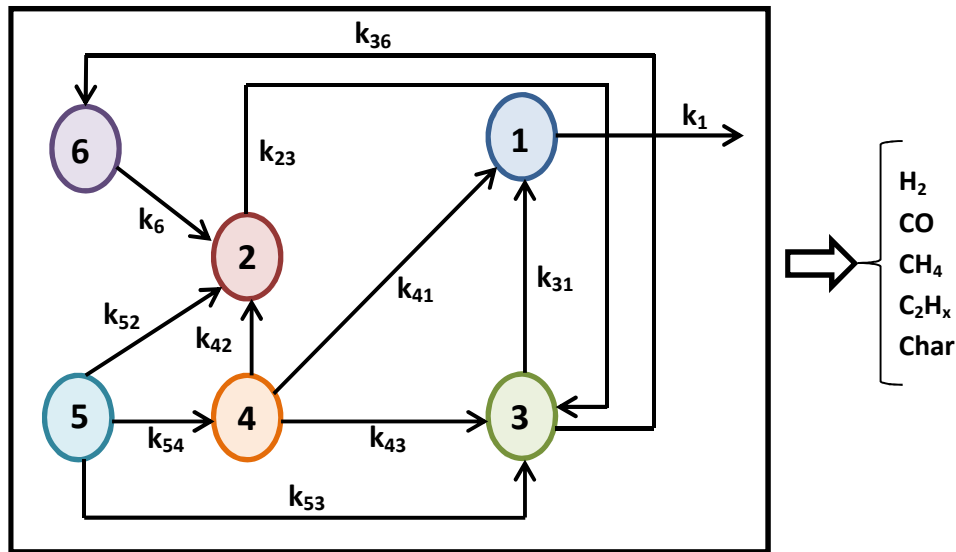
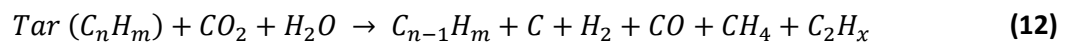


Figure 34 - Developed model for tar breakdown

Some alterations in the tar grouping were made, relatively to the previously existing model, but the general idea for the schematics was maintained. In this work the groups took into consideration more than just the chemical structure of the tars and also included the detected unknown compounds. Some of the “kinetic paths” were changed or confirmed according to some of the several models for individual molecules found in literature during the development of the model. Some of the kinetics between groups were added, in order to give a more general model that can consider the majority of decompositions that might occur in the system. Also the main differing path from Corella’s model and the developed model in this work was the consideration that the major yield after Phenolics’ breakdown would be naphthalene instead of benzene [46] and that toluene and xylenes (both on the group of the Branched compounds) are most likely to crack to benzene [23] than to naphthalene.

As shown in the scheme, the amounts of  $H_2$ ,  $CO$ ,  $CH_4$ ,  $C_2H_x$  and char are calculated from the entire reactions network, as they are resulting components of the cracking of each lump and not only from the decomposition of benzene. The general cracking reaction can be described in Equation 12.



The proposed reaction network has 11 kinetic constants and the set of kinetic equations to describe it is the simplest as possible, as demonstrated in Equation 13. This means that they are based considering each reaction (from the  $i^{\text{th}}$  lump to the  $j^{\text{th}}$  lump) as first-order with respect to the concentration of the species considered [53].

$$r_j = k_{ij}C_i - k_{ji}C_j \quad (13)$$

The decomposition reaction of each group can also be interpreted as a first order differential equation because it describes how the concentration of each group varies in time, i.e. the reaction rate, shown in Equation 14.

$$r_i = \frac{C_{i,0}dX_i}{d\tau} = \frac{dC_i}{d\tau} \quad (14)$$

The previous expression considers a rate (time-related) from the conversion of each group. However, the residence time considered to as the real time that the raw gas is in contact with the catalyst, i.e., the time under which the actual catalytic cracking is being performed, is equal to 1 and, so, it has no influence on the resulting value. Therefore, the previous equation is true. The resulting set of Equations 15 to 20 is the group of equations that describe the kinetics for the developed model.

$$r_1 = \frac{C_{1,0}dX_1}{d\tau} = \frac{dC_1}{d\tau} = k_{31}C_3 + k_{41}C_4 - k_1C_1 \quad (15)$$

$$r_2 = \frac{C_{2,0}dX_2}{d\tau} = \frac{dC_2}{d\tau} = k_{42}C_4 + k_{52}C_5 + k_{62}C_6 - k_{23}C_2 \quad (16)$$

$$r_3 = \frac{C_{3,0}dX_3}{d\tau} = \frac{dC_3}{d\tau} = k_{23}C_2 + k_{43}C_4 + k_{53}C_5 - k_{31}C_3 - k_{36}C_3 \quad (17)$$

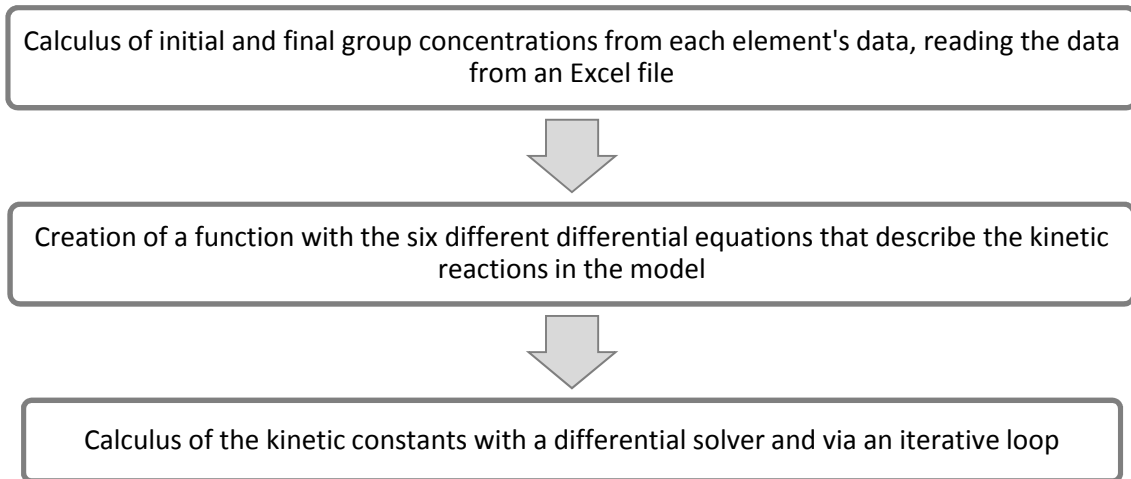
$$r_4 = \frac{C_{4,0}dX_4}{d\tau} = \frac{dC_4}{d\tau} = k_{54}C_5 - k_{41}C_4 - k_{42}C_4 - k_{43}C_4 \quad (18)$$

$$r_5 = \frac{C_{5,0}dX_5}{d\tau} = \frac{dC_5}{d\tau} = -k_{52}C_5 - k_{53}C_5 - k_{54}C_5 \quad (19)$$

$$r_6 = \frac{C_{6,0}dX_6}{d\tau} = \frac{dC_6}{d\tau} = k_{36}C_3 - k_{62}C_6 \quad (20)$$

### 3.2. Implementation of Model in MatLab

In order to estimate the kinetic reaction rate constants in a more effective and automatic way, a program was created using the mathematical software MatLab r2009b and r2010b. Several files were written to make the program more efficient, partitioning the steps to reach the solution. The overall program is constructed as represented in Figure 35.

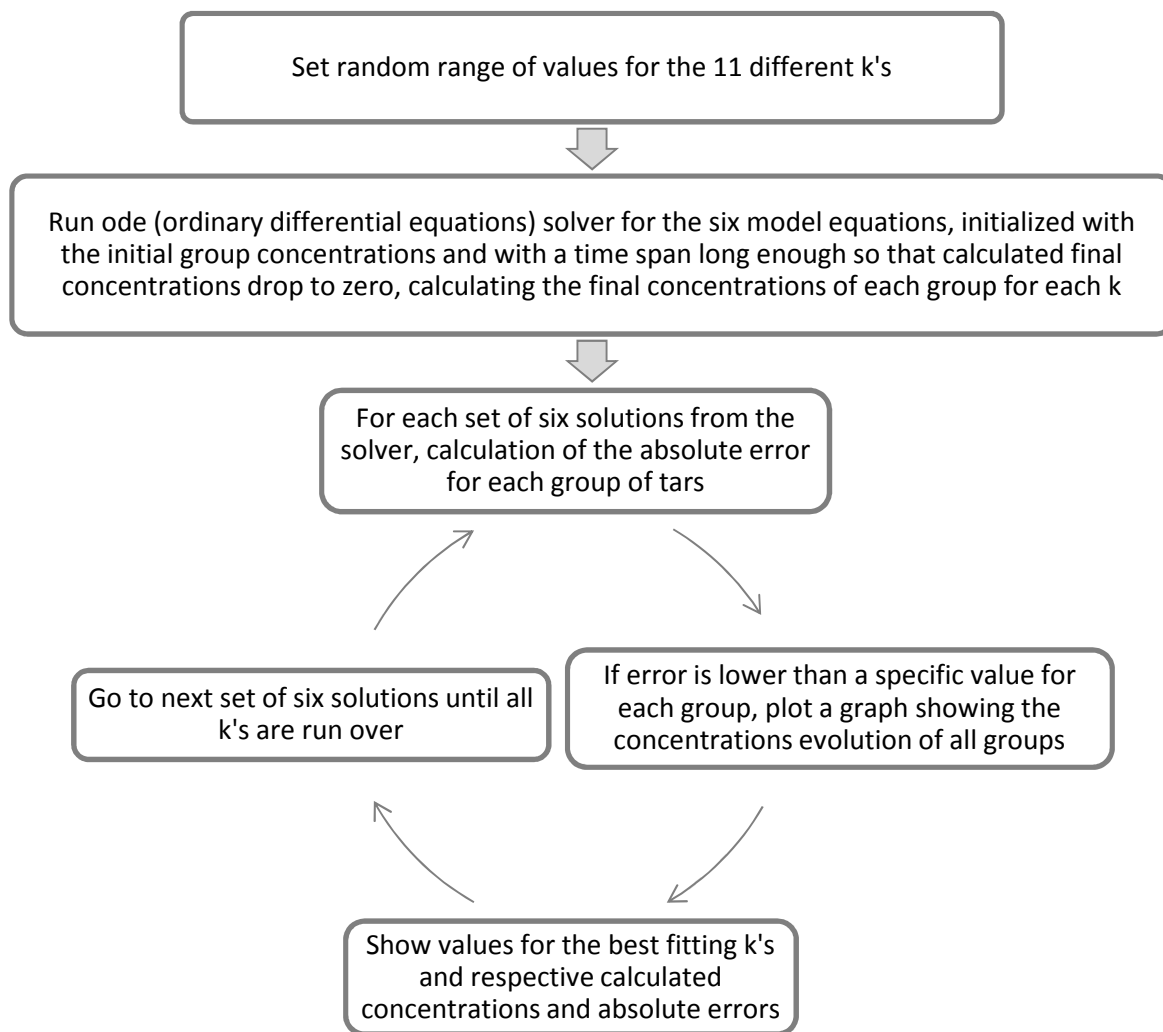


**Figure 35** - Overall view of MatLab model

The third step is, as expected, the most complex and the iterative loop for the manganese catalyst can be described as shown in the scheme in Figure 36.

The choice of the right set of kinetic constants was made by the least square method, calculated by the difference between calculated and experimental final concentrations for each group, and also by the relative error calculated (Eq. 21), for confirmation after results were obtained.

$$relative\_error[\%] = \frac{\sqrt{(calculated\_C_i - experimental\_C_i)^2}}{experimental\_C_i} \times 100 \quad (21)$$



**Figure 36** - Schematics of the calculation of the best kinetic constants on the iterative loop for the manganese catalyst



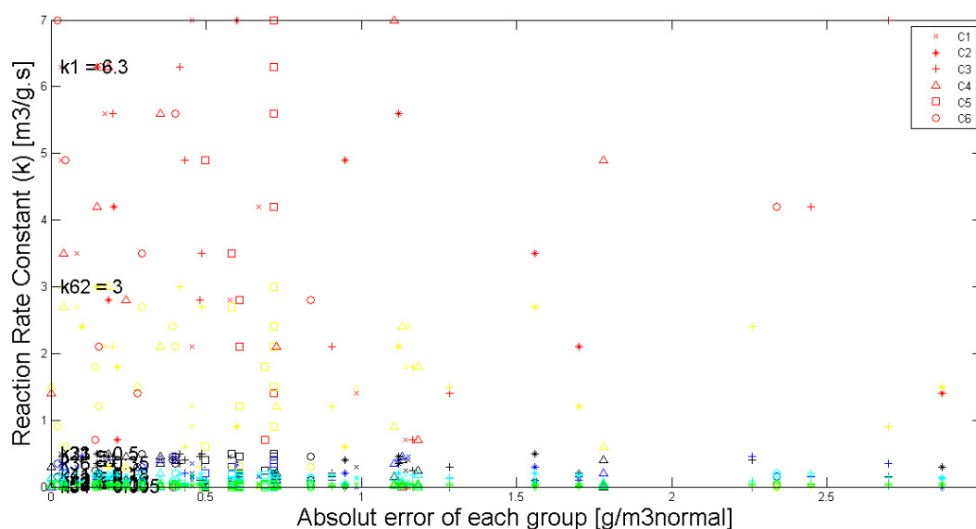


## 4. RESULTS & DISCUSSION

### 4.1. Analysis of Best Results for Each Working System Conditions

#### 700°C and 1% O<sub>2</sub> Concentration

The method used to find the best fitting kinetic constants ( $k$ ) was by plotting graphs of the several groups' errors calculated for the different considered set of kinetic constants, being each of them identified by a different shape and color. It also points out where the best result is encountered. This allowed for manual identification of the best value for each constant and to understand the changes occurred by a change in the range of each  $k$ . One example of this graphic is shown in Figure 37, although it was done as guidance for every solution. A subsequent problem of this method is the necessity of manual identification and intervention and consequent introduction of intrinsic errors of precision.

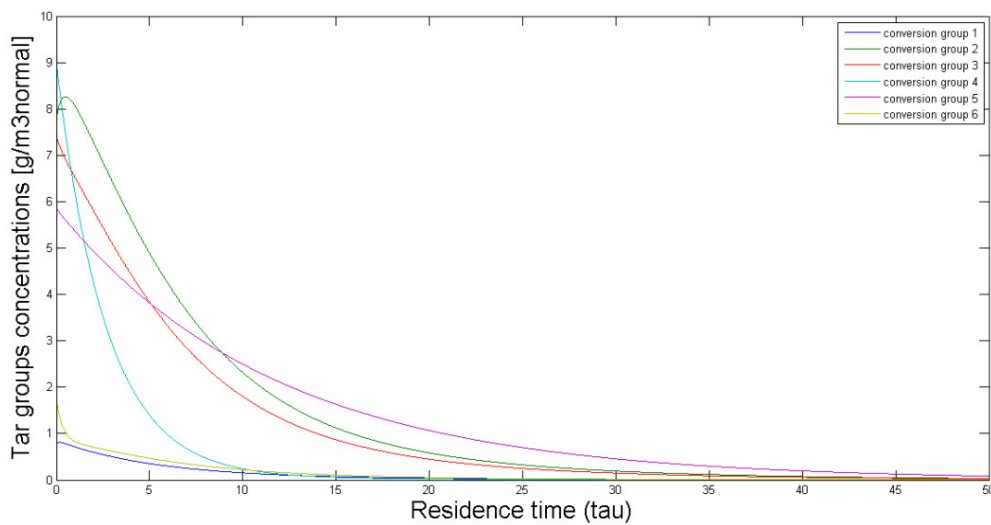


**Figure 37** - Tested set of kinetic constants and respective error for each tar group

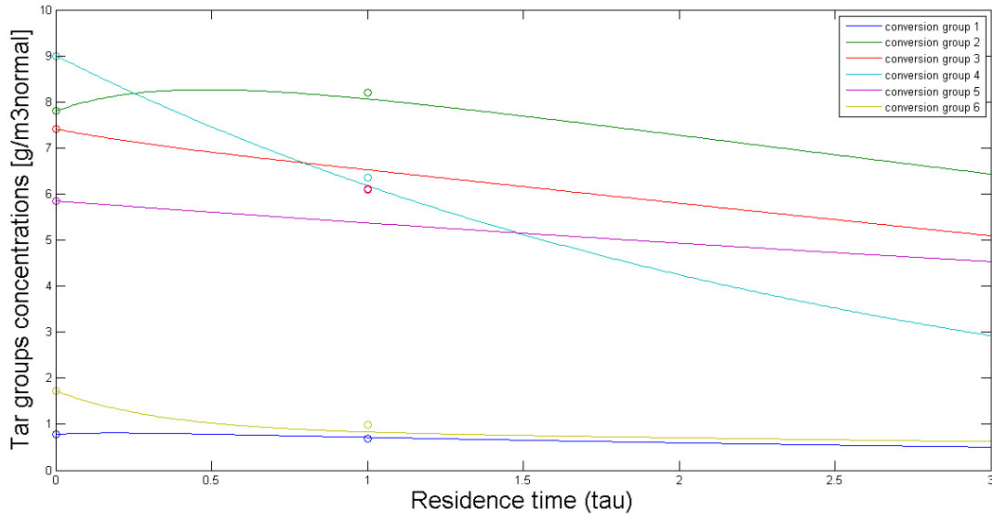
As shown in the legend of Figure 37, each symbol represents one group: the crosses represent group 1 (benzene); the stars group 2 (naphthalene); the pluses group 3 (branched, 1 and 2 rings); the triangles represent group 4 (non-alternant, 1 and 2 rings); the squares group 5 (3 and 4 rings PAHs)

and, finally, the circles group 6 (phenolics). Also, each  $k$  has a correspondent color for an easier verification and is according to the group from where it “departs”:  $k_1$  is shown in red;  $k_{23}$  in dark blue;  $k_{31}$  and  $k_{36}$  in black;  $k_{41}$ ,  $k_{42}$  and  $k_{43}$  in light blue;  $k_{52}$ ,  $k_{53}$  and  $k_{54}$  in green and  $k_{62}$  in yellow.

When a set of kinetic constants is found which provides group absolute errors lower than a determined value (different for each operating conditions so to minimize the error), two different plots are given – the first is an evolution of the concentration of tars on the considered time span for calculations; the second is a zoom on the evolution of the concentration of tars between the initial residence time ( $\tau=0$ ), corresponding to the inlet concentrations in the raw gas, i.e., upstream the FR, and a residence time considered to be representative of the residence time of the raw gas inside the fuel reactor with a bed material of 23% manganese, i.e.,  $\tau=1$ . For this reason, the concentrations marked at  $\tau=1$  in the graphs are the measured concentrations from the SPA/GC-FID analysis for these operating conditions. From observation of the lines/paths that represent the evolution of each tar group’s concentrations and the markers of each measured concentration, it is possible to predict the simulation errors. From these two results from implementation of the model, it is possible to withdraw conclusions on whether the model follows the predicted decomposition paths and, therefore is valid, and whether the system operating conditions should be changed so to have a bigger impact on the decomposition of the tars.

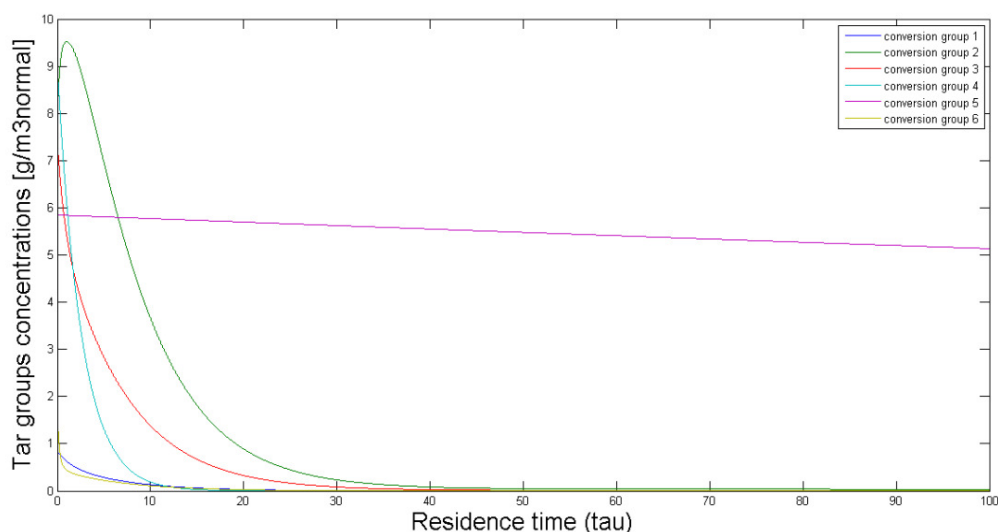


**Figure 38** - Development of each group’s concentrations at 700°C and 1% O<sub>2</sub> on the whole considered time span

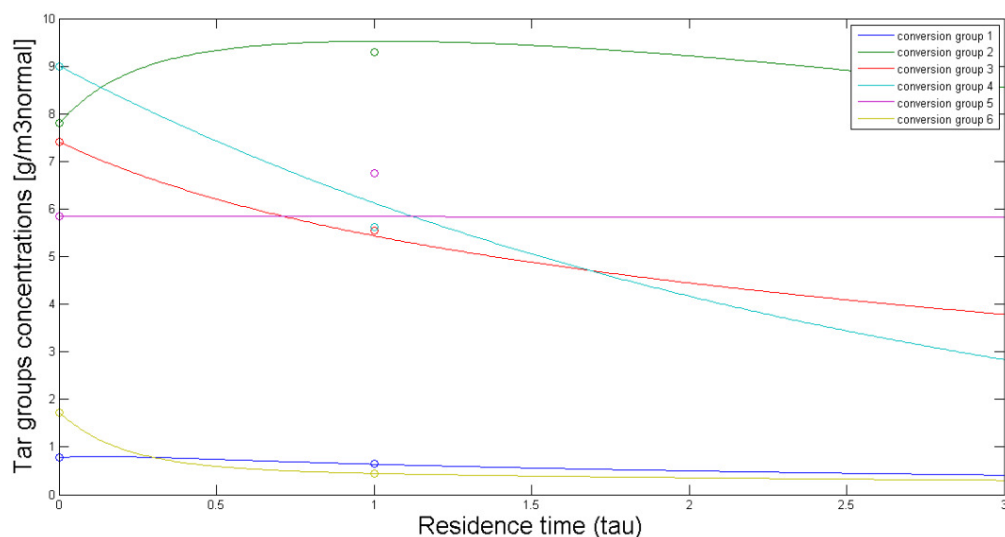


**Figure 39** - Zoom on the development of each group's concentrations at 700°C and 1% O<sub>2</sub>

Figure 38 shows the evolution of the composition of the tar groups in time over the whole considered time span. The residence which is considered to be the contact time between catalyst and raw gas inside the fuel reactor is equal to 1. This means that, if the tars are to be completely decomposed, a fifty times higher residence time is needed. That is, at around  $\tau=1$  the group concentrations already start declining as seen by Figure 39, but even at a residence time 50 times higher not all of the tar groups have reached the complete decomposition into CO, H<sub>2</sub> and lighter hydrocarbons. A potential explanation might be that the operating conditions may not be the most efficient for the process goal that is trying to be achieved. Nevertheless, in spite of the lower conversions, the cracking process is already occurring for all species, since entering the system. It is also perceptible the positive derivative of the green curve (naphthalene) at lower residence times. This means that at lower residence times the formation of this compound from other species is faster than its own decomposition. Consequently, the amount of tars from this group increase and so does the curve. A remark is made for the negative derivative of the blue line (benzene), even at the beginning of reactions. This means that for this temperature the velocity of formation of these molecules is still lower than the velocity of decomposition. This result seems inadequate as benzene is the last group from the model, i.e. the last considered decomposition structure for all species. However, if the remaining species are regarded, it is seen that the velocity of their reactions is still not very high, as the curvatures of the concentration lines are not so big either, which means that their conversions probably are insufficient to equal or superior the conversion of benzene. This corresponds to the trend found before for benzene at 700°C.

700°C and 2.2% O<sub>2</sub> Concentration

**Figure 40** - Development of each group's concentrations at 700°C and 2.2% O<sub>2</sub> on the whole considered time span



**Figure 41** - Zoom on the development of each group's concentrations at 700°C and 2.2% O<sub>2</sub>

From Figure 40 it is concluded that, for this working conditions, the evaluated time span was not enough for the tar groups' concentrations to completely drop to zero. As observed by the different time scale between Figures Figure 38 and Figure 40, which in the last one goes up to  $\tau=100$ , not even with a reaction period inside the FR one hundred times higher, group 5 (3 and 4 rings PAHs) is completely broken down by the catalyst. This means that, probably, at 700°C and with an oxygen supply of 2.2% molar O<sub>2</sub> concentration in the AR, the molecules from this particular group are still being formed. This is clearly seen in Figure 41, where group 5 (represented by the purple line) is always increasing the concentration, even at a residence time three times higher than the considered  $\tau=1$ . One possible explanation is that the unknown tars belonging to this group, which most reasonably have bigger, branched and, therefore, more fragile structures are decomposing at this conditions and are giving place to the formation of the remaining molecules from this group. It is also observed by both Figures Figure 40 and Figure 41, compared to Figures Figure 38 and Figure 39, that the curve increase of the green line (naphthalene) is bigger with these operating conditions, as it

reaches concentrations around  $9.5 \text{ g/m}^3_{\text{normal}}$  of tars, and it only starts declining after  $\tau=1$  which means that decomposition of these tars does not even overcome the self formation rate inside the reactor. Hence, it can be predicted that the formation of these compounds from other species is even faster with a higher oxygen concentration than its decomposition into other species and molecules. As a consequence, it can be said that the conversions of the remaining species are probably higher. Again, benzene at  $700^\circ\text{C}$  still does not have a rate of formation as high as its rate of decomposition, seen from the negative slope at zero residence time.

### 750°C and 1% O<sub>2</sub> Concentration

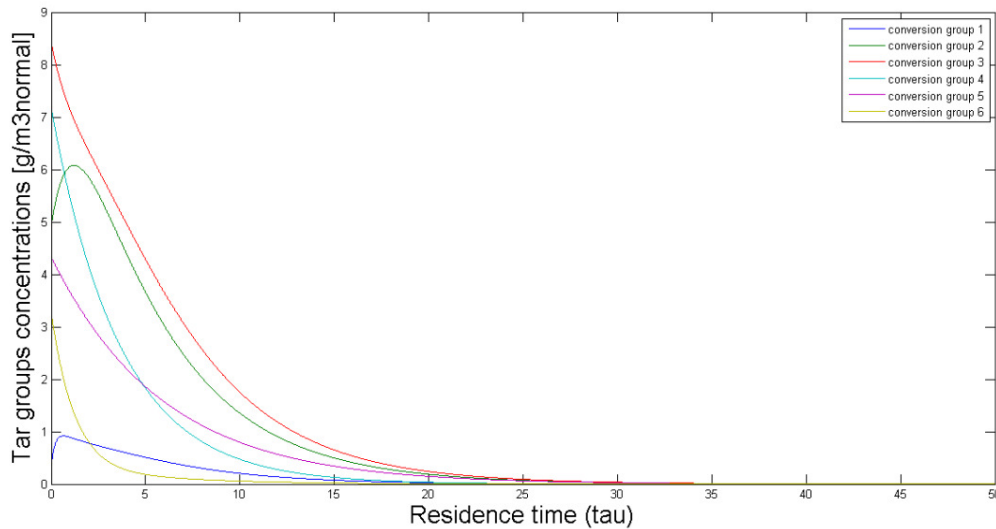


Figure 42 - Development of each group’s concentrations at 750°C and 1% O<sub>2</sub> on the whole considered time span

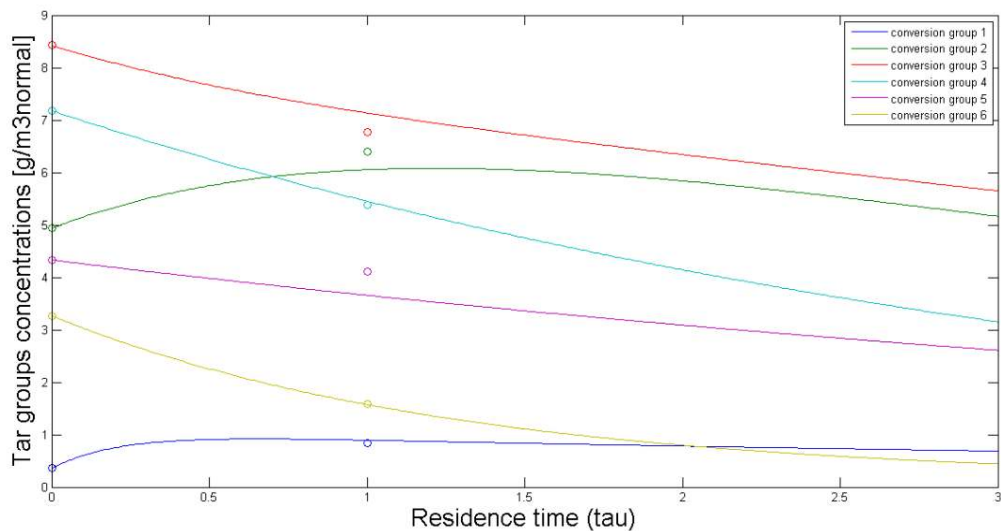


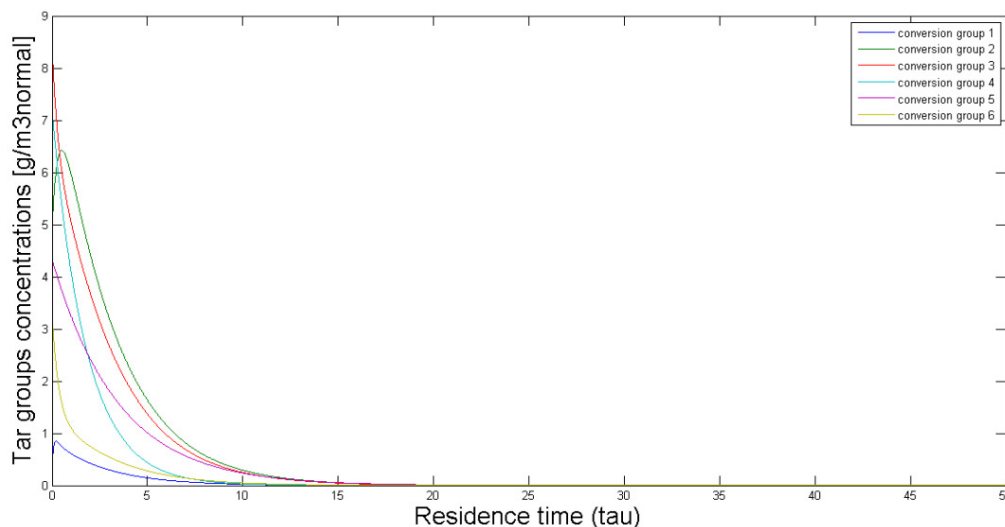
Figure 43 - Zoom on the development of each group’s concentrations at 750°C and 1% O<sub>2</sub>

From Figure 42 it is possible to confirm that the time span considered in this particular simulation was long enough so that all concentrations would level out. Comparing with the previous graphs, it is even possible to see that this “necessary” residence time is lower for this temperature, which means reactions are faster at higher temperatures. Faster reactions also mean higher curvature of the lines, which is visible for all species. As before, the green curve (naphthalene) increases at lower residence

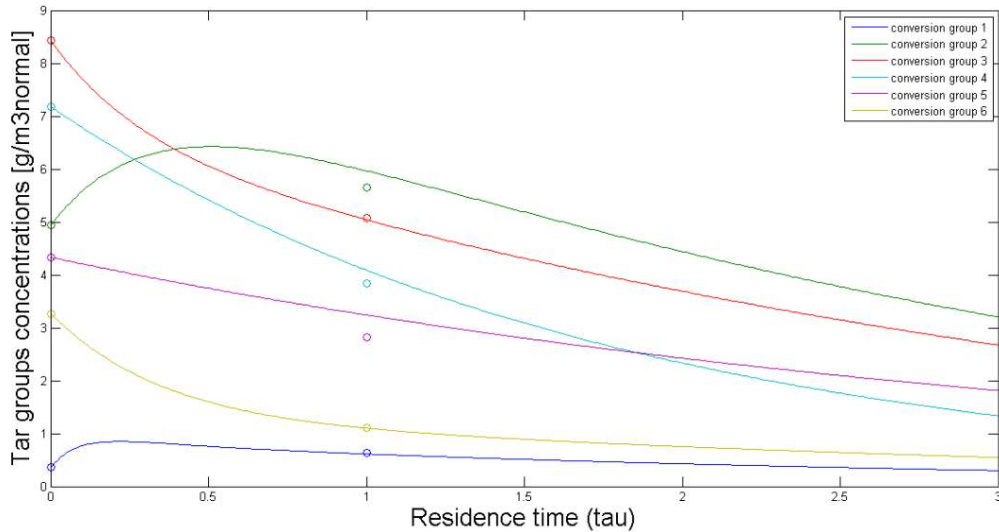
times. This results from a higher formation velocity of these compounds, from the decomposition of the remaining species, than the own decomposition velocity. At 750°C it is possible to observe the same happening to the blue curve, i.e. benzene. The formation of benzene from other species is faster than its own decomposition into other molecules. This was expected, as, in the model, benzene is considered the last decomposition structure of all existing tar compounds. Observing the yellow line (phenolics) at low residence times in this graph and all the previous ones, it is noticeable that it probably is the group with the highest conversions, as it always has the biggest initial gradient. However, it is important to notice that the initial concentration of phenolics in this experiment was higher than for the previous situations, meaning that the raw gas probably had a higher percentage of phenolic compounds from gasification.

### 750°C and 2.2% O<sub>2</sub> Concentration

From Figure 44 below, it is possible to draw the same conclusion as before – the time span was long enough so that if there would be an “infinite” residence time (much larger compared to  $\tau=1$ , considered to be the real residence time) inside the fuel reactor all the tars could be decomposed. A first conclusion to be taken, comparing Figures Figure 42 and Figure 44, is the fact that with a higher oxygen concentration in the AR at the same temperature the conversion of tars increases. This is seen from the curves, which have much higher slopes in the case of 2.2% O<sub>2</sub> rather than in at 1% O<sub>2</sub> concentration. This can also be observed looking at the green line (naphthalene) between Figures Figure 43 and Figure 45. At 2.2% O<sub>2</sub> naphthalene does increase concentration at an initial rate much higher than it does at 1% O<sub>2</sub> but it also has a higher drop after the initial step. This means that the velocity of decomposition increases at higher oxygen concentrations, as for the initial step all other compounds decompose at a higher rate, making naphthalene and benzene have a sharper increase but also making it possible for these molecules to overcome the formation rate faster, as it is seen by the rapid decrease in the curves after their maximum points. This is expected, as in combustion when the oxygen concentration is increased the oxidation reactions increase and, therefore, more components are burnt. As all groups have higher decomposition rates, benzene is expected to have an increase in concentration as it is the last stage of decomposition. Again, this can be seen by the sharper gradient at zero residence time of the blue line.



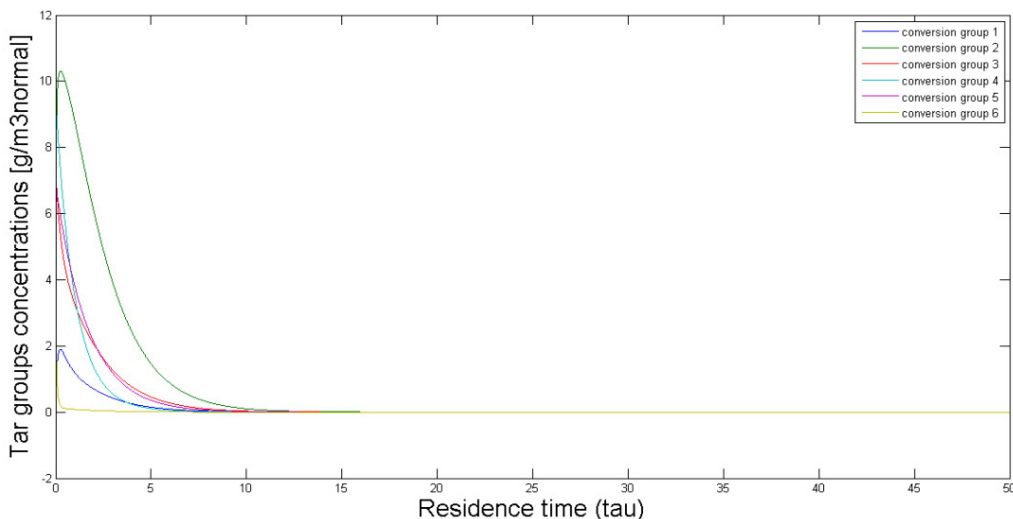
**Figure 44** - Development of each group's concentrations at 750°C and 2.2% O<sub>2</sub> on the whole considered time span



**Figure 45** - Zoom on the development of each group’s concentrations at 750°C and 2.2% O<sub>2</sub>

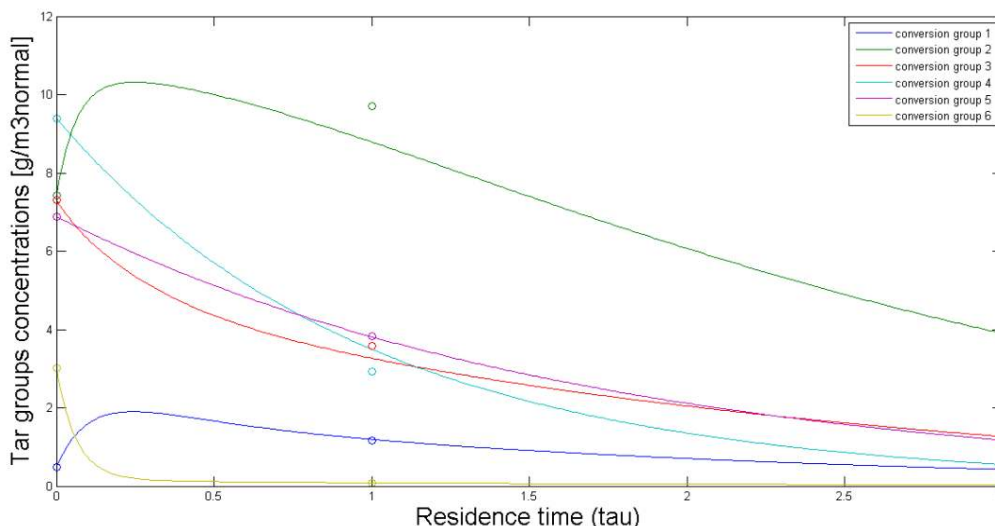
**800°C and 1% O<sub>2</sub> Concentration**

Analyzing Figure 46, below, it is seen that the time span was once again long enough for all tar groups to level out. Actually, it takes even lower times for this to happen – at around  $\tau=10$  all groups have already dropped to zero. Therefore, a trend in the decomposing process can be confirmed: with increasing temperatures the decomposition becomes faster even at the same oxygen concentrations. All slope curvatures are bigger than for previous cases, which mean higher reaction velocities. The blue line (benzene) follows the same trend already picked up at 750°C. The green line (naphthalene) has here the sharpest inclination of all previous cases at initial residence times. This can be confirmed by the conversion value that is also the highest for all cases, which means that the formation rate at the highest studied temperature but lowest oxygen concentration is the fastest and overcomes highly the decomposition rate of these molecules. Special attention is paid to the yellow line (phenolics). Phenolic compounds are expected to be the fastest at reacting and breaking down, already at low temperatures. Therefore, at a higher temperature, this is 800°C, they are expected to breakdown almost instantly, which is seen by the gradient close to 90° at zero residence time.



**Figure 46** - Development of each group’s concentrations at 800°C and 1% O<sub>2</sub> on the whole considered time span

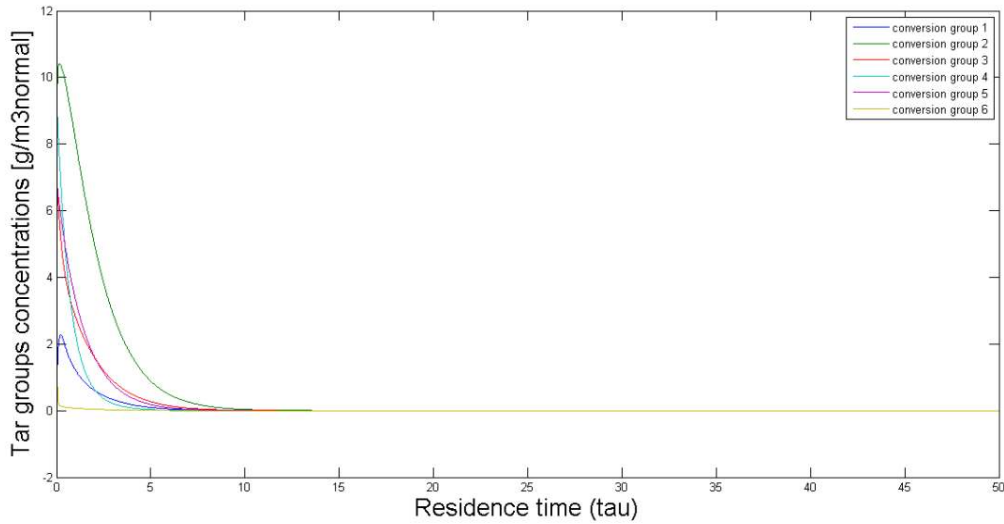




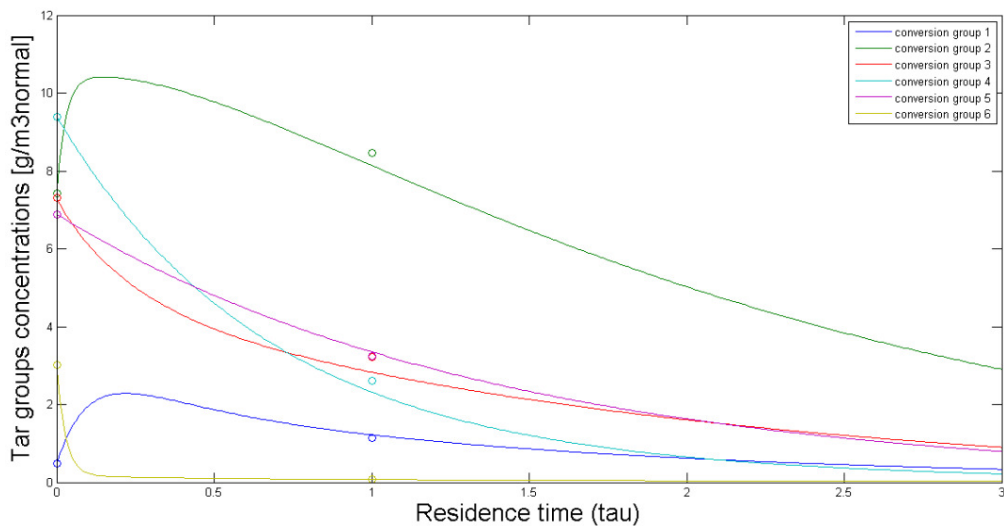
**Figure 47** - Zoom on the development of each group's concentrations at 800°C and 1% O<sub>2</sub>

### 800°C and 2.2% O<sub>2</sub> Concentration

From Figure 48, below, and in comparison with Figures Figure 40 and Figure 44, the same conclusion as in the 1% O<sub>2</sub> concentration can be withdrawn. With increasing temperature and the same oxygen concentrations the reaction velocity increases. Moreover, if a closer attention is paid at the residence time scale for the two cases at 800°C, it is also possible to conclude that at the same temperature with increasing oxygen concentrations the decomposing is also faster. This conclusion had already been taken at 750°C, and validates once again. This results that probably the best conditions for the system to perform are characterized by higher temperatures and higher oxygen concentrations. This has the same effect as explained before – higher oxygen concentrations and especially at higher temperatures, the burning reactions are faster, which make the velocity of tar breakdown increase. It is visible that the curvature of naphthalene is even sharper at initial residence times but the decomposition rate surpasses the formation rate more rapidly and, therefore the conversion of this group should be higher (or less negative) which is confirmed by Figure 28. The blue line (benzene) seems to have a bigger increase in concentrations. It seems reasonable, as all other groups breakdown even at a faster rate than before and, most probably, there is an increase of the percentage of tars that decompose until the benzene structure. But looking at the conversion values in Figure 28, the benzene conversion is the same for both oxygen concentrations at 800°C. This means that the increase in oxygen concentration will make the benzene also decompose faster so that the proportion of tars formed against tars broken is the same as for the previous operating conditions. Finally, in this case the phenolics' line has again the highest slope, which is confirmed by its conversion that reaches almost 98%.



**Figure 48** - Development of each group's concentrations at 800°C and 2.2% O<sub>2</sub> on the whole considered time span



**Figure 49** - Zoom on the development of each group's concentrations at 800°C and 2.2% O<sub>2</sub>

## 4.2. Evaluation of Kinetic Constants and Simulation Errors for all Best Results

All previous graphs show the best results for each operating condition, this is, the results which in implementation of the model gave the least absolute and relative error on the calculations of the concentrations of each tar group. Therefore, along with each best result, the set of kinetic constants that best fit the model and the coupled simulation errors are shown in Table 12 - Set of kinetic constants and respective simulation relative errors for all operating conditions' best results and further discussed.

It is possible to compare the relative error of each group's calculated values during simulation, shown in Table 12 below, with the relative standard deviation of the SPA-samples for the groups at the same operating conditions, in Figures Figure 25 to Figure 27.

**Table 12** - Set of kinetic constants and respective simulation relative errors for all operating conditions' best results

	BEST SETS OF k VALUES [ $\text{m}^3_{\text{tars}}/\text{g}_{\text{catalyst}}\text{s}$ ]							
	700°C		750°C		800°C			
	1% O <sub>2</sub>	2,2% O <sub>2</sub>	1% O <sub>2</sub>	2,2% O <sub>2</sub>	1% O <sub>2</sub>	2,2% O <sub>2</sub>	1% O <sub>2</sub>	2,2% O <sub>2</sub>
<b>k<sub>1</sub></b>	6,3	6,2	4,5	11,6	9	9,5		
<b>k<sub>23</sub></b>	0,5	0,3	0,36	1,05	0,75	1		
<b>k<sub>31</sub></b>	0,5	0,56	0,48	1,1	2,7	3,1		
<b>k<sub>36</sub></b>	0,35	0,4	0,02	0,65	0,4	0,95		
<b>k<sub>41</sub></b>	0,18	0,12	0,09	0,33	0,35	0,82		
<b>k<sub>42</sub></b>	0,1	0,09	0,12	0,155	0,35	0,24		
<b>k<sub>43</sub></b>	0,1	0,175	0,07	0,085	0,38	0,5		
<b>k<sub>52</sub></b>	0,05	0,0012	0,14	0,1	0,34	0,42		
<b>k<sub>53</sub></b>	0,03	0	0,021	0,18	0,15	0,15		
<b>k<sub>54</sub></b>	0,005	0,0001	0,008	0,01	0,1	0,15		
<b>k<sub>62</sub></b>	3	5,2	0,8	3,5	16,1	37		
RELATIVE EVALUATION ERROR [%]								
	1% O <sub>2</sub>	2,2% O <sub>2</sub>	1% O <sub>2</sub>	2,2% O <sub>2</sub>	1% O <sub>2</sub>	2,2% O <sub>2</sub>	1% O <sub>2</sub>	2,2% O <sub>2</sub>
<b>G1</b>	4,71	1,75	5,88	4,38	3,39	6,02		
<b>G2</b>	1,83	2,58	5,46	5,42	9,43	3,97		
<b>G3</b>	6,71	1,88	5,31	0,89	8,79	12,1		
<b>G4</b>	2,99	8,81	1,30	6,26	19,1	11,2		
<b>G5</b>	11,8	13,4	11,2	14,6	0,17	3,17		
<b>G6</b>	16,2	1,16	0,57	0,63	0,97	2,86		

Looking first at the cases at 700°C, it is possible to verify that every group's error is lower or similar to the error obtained from the calculation of the concentrations from sampling. This means that, in principle, the model works according to what is expected to happen as the errors in simulations are lower than experimental errors. The only exception is group 3 at 1% O<sub>2</sub>, which has a slightly higher error from the model than from the sampling. This could be due to the degree of uncertainty that is present in the simulation because of the required manual process of choosing the kinetic values' range. Also, this could be due to the sampling itself, as the concentrations for the various elements result from the mean value of the several considered samples. Therefore, if in any of the groups one or more elements have higher relative deviations, this can affect the deviation of the whole group.

Looking at the values at 750°C, it is possible to see that every group's error for these particular solutions for the model are lower than the error present on the calculation of the concentrations from experimental data with the exception of the 5<sup>th</sup> group. The same conclusion for all the good results can be taken from the previous temperature. The higher error observed might be slightly toned if the SPA relative standard deviation for the initial concentrations of this specific group is taken into account. As the initial concentrations (reference values) are the input data for the differential equations solver in the model program, a higher uncertainty in these values (around 19%) can lead to an underestimation of the final concentrations and, therefore, to an increase in the difference between experimental and simulated results of the final concentrations.

Finally for the 800°C, it is possible to see that all simulation errors have lower or similar values for groups 1, 2, 5 and 6 but for the branched molecules (group 3) and non-alternant molecules (group 4) the difference is not so favorable. This might have been influenced by the considered samples, as discussed for 750°C, which could have changed substantially the concentration of the whole group. A second reason is, again, the required manual work for the setting of the values in the program, which introduces by its own a considerable error.

The following Table 13 shows the "intrinsic reactivity rate" of each group, i.e., the relative velocity at which each group is decomposed. This is simply the sum of the kinetic constants that refer to the destruction of each group, i.e., the kinetic constants that represent the path from a specific group to any other groups in the model.

**Table 13** - "Intrinsic reactivity rate" of each group of tars

	"INTRINSIC REACTIVITY RATE" OF EACH GROUP [ $\text{m}^3_{\text{tars}}/\text{g}_{\text{catalyst}} \text{s}$ ]							
	700°C		750°C		800°C			
	1% O <sub>2</sub>	2,2% O <sub>2</sub>	1% O <sub>2</sub>	2,2% O <sub>2</sub>	1% O <sub>2</sub>	2,2% O <sub>2</sub>		
<b>G1</b>	6,3	6,2	4,5	11,6	9	9,5		
<b>G2</b>	0,5	0,3	0,36	1,05	0,75	1		
<b>G3</b>	0,85	0,96	0,5	1,75	3,1	4,05		
<b>G4</b>	0,38	0,385	0,28	0,57	1,08	1,56		
<b>G5</b>	0,085	0,0013	0,169	0,29	0,59	0,72		
<b>G6</b>	3	5,2	0,8	3,5	16,1	37		

It is seen that all kinetic constants increase from the lowest oxygen concentration in the AR to the highest, as well as, from the lowest to the highest FR working temperature, as it is a general trend for all groups to have higher conversions and, therefore, faster reactions at the maximum operating conditions.

A first remark is done for the results at 750°C and 1% O<sub>2</sub>, as it seems to be the only differing case, because they seem to have lower values than both the results at 700°C and 1% O<sub>2</sub>. This is explained by what was previously discussed about the conversions at 700°C. At 700°C the decomposition of all groups is lower due to the lower temperature, which makes the "following" groups' tar formations to be lower as well. This happens especially to the benzene that at this temperature has such a low

formation rate that the decomposition rate can compensate this formation. Therefore, the higher velocity represented by the higher values of the “intrinsic reactivity rates” for this group only mean that the decomposition velocity comparatively to the formation velocity is higher. The same happens for all groups as their surrounding groups have lower conversions. The only lower values at 700°C with 1% O<sub>2</sub> than at 750°C with 1% O<sub>2</sub> are actually from group 5. This is the special case where the formation of tars inside its own group from the unknown molecules might be so high that the decomposition into other structures is not fast enough to make it a positive conversion. This is translated by the very low “intrinsic reactivity rate” meaning low velocity of decomposition to other groups.

A second remark is done at 750°C and 2.2% O<sub>2</sub>, where the reactivity rate for group 1 seems to be much higher than the same figure at 750°C and 1% O<sub>2</sub>. This is explained by the higher conversion (less negative), i.e. the decomposition rate is so that it can more successfully compensate the formation rate from other groups. Therefore, the reaction velocities are higher and so is the kinetic constant. This is most probably an effect of the higher oxygen concentration, as discussed before. This effect also is noticeable on all remaining groups which confirm the higher “intrinsic reactivity rate” values.

At 800°C all results are higher than for the lower temperatures and oxygen concentrations, respectively. The only less immediate result is, again, the “intrinsic reactivity rates” for the benzene, which are lower at 800°C and 2.2% O<sub>2</sub> than at 750°C with 2.2% O<sub>2</sub>. This could happen because at higher temperatures the decomposition of tars is much faster for all groups, which increases the formation of benzene as the last considered structure. Therefore, a smaller relative velocity is in order as the decomposition rate might not be fast enough to overcome the formation rate.

Finally, the differences between the reactivity rates at 700°C, 750°C and 800°C are higher than the differences between different oxygen concentrations for each temperature. This means that, probably, the working temperature of the FR has a bigger influence on the decomposition process than the oxygen concentration in the AR.

It is important to keep in mind that all these kinetic constants are affected by the simulation errors and that a small change in one group decomposition velocity can change significantly all other kinetic constants. This happens because the model is a net of interrelated reactions and every change in one group has consequences on the behavior of all the remaining ones. Nevertheless, the kinetic constants obtained seem realistic, even though their order of magnitude is small. The reason for this is that the units chosen are not the conventional units from the international system (SI), but are units chosen according to the data at which would be most representative for this particular system. This way, the numbers obtained represent the decomposition of cubic meter of tars per gram of catalyst and per second, which corresponds to a very small time scale and a low amount of catalyst in the bed material. Consequently, the orders of magnitude of the reaction velocities are according to what should be realistic from a reactor system like the one studied.

Hence, from all the previous discussion and validation of both experimental data and results from the model simulation program, it could be said that the developed model for this system describes relatively well the decomposition of tar compounds inside the fuel reactor and their change of behavior depending on changing operating conditions both from the FR and the AR.



## 5. CONCLUSIONS & FUTURE WORK

The main aim of this work has been to develop a tar decomposition model for application in a Chemical-Looping Reformer system at Chalmers University of Technology. The study was carried out with data available from previous running of the system by the research group that gave support to this work at Chalmers. The CLR-System was developed with the scope of reducing the tar fraction in product gas from biomass gasification. This was to be achieved by reforming the tar components into useful gas molecules through catalytic cracking of the compounds. The system works with a dual-fluidized bed setup, where raw gas from Chalmers' biomass gasifier entered the system and catalytic cracking reactions between gas components and a metal-oxide catalyst occurred. A manganese-based catalyst was chosen and was introduced in the reactor in a silica-sand bed.

The effects of the cracking reactions inside the system were measured by collecting samples from the raw gas line (directly from the gasifier) and from the product gas line (out of the system) by a KTH developed method called Solid-Phase Adsorption sampling, followed by gas-chromatography and flame-ionization detection. 21 tar molecules were chosen to be representative of the whole tar products in the raw and product gases and a remaining 170 unknown compounds were detected. Error analysis on the SPA-samples demonstrated that for the majority of situations, grouping of tar samples and grouping of the tars for development of model showed an error below 15%. Exceptions were observed for benzene, which were explained by the possibility of detachment of the molecules from the amino-phase extraction column, due to the high vapor-pressure at which they are submitted.

The decomposition model was developed after a literature survey on previous works with tars. Several models were found but only one model by Corella [53] was considered applicable to this work. Tars were grouped according to three criteria – individual conversions, molecular structure and relative percentage in the whole tar amount – and a reaction network was developed to represent the relation between tar decompositions inside the fuel reactor. Kinetic equations of the first order were withdrawn and implementation was done in the mathematical software MatLab.

Results from implementation of the model were found to be conclusive. The comparison between results and previous decomposition trends from work done only with the conversion values and

concentration values of the tar groups validated the model. Naphthalene is always formed at higher rates than it is decomposed, for all operating temperatures and oxygen concentrations. This is confirmed by the positive gradients at low residence times in all graphics of evolution of tars' concentrations and by the low values of the "intrinsic reaction rates", especially at higher temperatures, although at higher temperatures the decomposition is more easily promoted. Benzene also has higher formation rates than decomposition rates in most working conditions with exception of lower operating FR temperatures. This is also translated by the negative slopes of the benzene curves for 700°C and both oxygen concentrations and can be explained by a lower conversion from other tar groups at the same conditions. For higher temperatures, it is expected the growth in concentration of benzene as it is the last considered stage of decomposition in the developed model. On the other hand, branched compounds and non-alternant molecules seem to have higher decomposition rates than formation rates at all FR and AR conditions. This is reasonable as they have the most fragile structures from the whole tar representatives. Phenolic compounds seem to be the easier compounds to breakdown, which is supported by the highest conversions from all tar groups in all situations and the sharpest gradients in all simulation results.

As expected, general trends were possible to be withdrawn from the conversions and evolution of concentrations of tars but no correlation was possible to be made. The proportion of tars that entered the system and that were decomposed inside it could not be linearly related with operating conditions, i.e. FR temperatures or AR oxygen concentrations. However, FR operating temperatures seem to have a higher influence on the decomposition process than the AR oxygen concentrations.

Simulation results had lower relative errors than SPA-sampling standard deviations. The existing errors present in the simulations should mainly be from two sources: from the SPA-sampling deviations of the reference concentration values, which are the input data during the implementation of the model, and, therefore, could lead to an underestimation of the final calculated concentrations; some errors can also come from the manual process required to change, adapt and interpret the inserted set of kinetic constants into the model, providing in this way small precision errors into the results.

Overall, the model seems adequate to represent the reaction network and tar relative decomposition velocity inside the fuel reactor. Hence, from simulation results, conjectures of the behavior of tars with changing operating conditions could be made. It was observed the trend that higher temperatures and higher oxygen concentrations seem to improve the system performance. For these conditions, the model predicted that with a residence time inside the reactor of around 20 times higher it seemed possible the production of tar free producer gas. This could be achieved by increasing catalyst concentration in the bed material or by increasing the length of the fluidized bed. However, with these working conditions the permanent gases composition would probably be largely affected. This means that a compromising situation could be reached, which could highly improve the performance of the system.

This opens the way for suggestions for future work, where operational changes in the system could be studied in order to improve the prototype for further implementation in industry. Also, changes in the model implementation, such as making the introduction of kinetic constants an automatized system so to prevent precision errors and to make the selective process faster. The model should be tested with this year's experiments. The extraction method for the SPA-sampling has already been



changed and deviations in the samplings should be lower, giving a more accurate view on the decomposition of tars inside the reactor. Finally, the model should be implemented in the software Aspen-Plus where models for the permanent gases already exist or are being developed. This could bring a higher accuracy to the model describing the CLR-System and make online evaluations possible for the system, depending on the raw gas feed and desired gas composition output.



---

## REFERENCES

- [1] C.M. van der Meijden, H.J. Veringa, and L.P.L.M. Rabou, "The production of synthetic natural gas (SNG): a comparison of three wood gasification systems for energy balance and overall efficiency," *Biomass and Bioenergy*, pp. 302-311, 2010.
- [2] "BP Statistical Review of World Energy," London, United Kingdom, June 2011.
- [3] R.W.R. Zwart, H. Boerrigter, E.P. Deurwaarder, C.M. van der Meijden, and S.V.B. van Paasen, "Production of synthetic natural gas (SNG) from biomass - development and operation of integrated bio-SNG system," Biomass, Coal and Environmental Research, Energy Research Center of the Netherlands (ECN), November 2006.
- [4] C. Brage, Q. Yu, and K. Sjöström, "Characteristics of evolution of tar from wood pyrolysis in a fixed-bed reactor," *Fuel*, vol. 75, no. 2, pp. 213-219, 1996.
- [5] S. Heyne and S. Harvey, "Methane from biomass: process-integration aspects," *Energy*, vol. 162, pp. 13-22, February 2009.
- [6] S. Heyne, H. Thunman, and S. Harvey, "Extending existing combined heat and power plants for synthetic natural gas production," *International Journal of Energy Research*, vol. 33, 2011.
- [7] S. Heyne and M. C. Seemann, "Integration study for alternative methanation technologies for the production of synthetic natural gas from gasified biomass," *Chemical Engineering Transactions*, vol. 21, 2010.
- [8] M. Mozaffarian, R.W.R. Zwart, H. Boerrigter, E.P. Deurwaarder, and S.R.A. Kersten, "'Green gas' as SNG (synthetic natural gas) - a renewable fuel with conventional quality," Victoria, Vancouver Island, BC, Canada, Contribution to the "Science in Thermal and Chemical Biomass Conversion" Conference August-September 2004.
- [9] (2010) Biomass, an important source of renewable energy. [Online]. <http://www.biomass.net/Biomass-Advantages.html> (visited in April 2011)
- [10] A. Fargette, P. Le Feuvre, K. MacLennan, K. MacKay, and G. Wallis. University of Strathclyde's Sustainable Engineering MSc in "Energy Systems and the Environment". [Online]. [http://www.esru.strath.ac.uk/EandE/Web\\_sites/06-07/Biomass/HTML/index.htm](http://www.esru.strath.ac.uk/EandE/Web_sites/06-07/Biomass/HTML/index.htm) (visited in September 2011)
- [11] (2010) Union of Concerned Scientists, Citizens and Scientists for Environmental Solutions. [Online]. [http://www.ucsusa.org/clean\\_energy/technology\\_and\\_impacts/energy\\_technologies/how-biomass-energy-works.html](http://www.ucsusa.org/clean_energy/technology_and_impacts/energy_technologies/how-biomass-energy-works.html) (visited in April 2011)

- [12] C.A. Miller, "Environmental impacts of biofuel production and use," *Preprints. American Chemical Society. Division of Fuel Chemistry*, vol. 54, 2009.
- [13] D. Dayton, "A review of the literature on catalytic biomass tar destruction," National Renewable Energy Laboratory, U.S. Department of Energy Laboratory, operated by Midwest Research Institute, Golden, Colorado, December 2002.
- [14] L. Devi, K.J. Ptasinski, and F.J.J.G. Janssen, "A review of the primary measures for tar elimination in biomass gasification processes," *Biomass and Bioenergy*, pp. 125-140, 2003.
- [15] (2010) Biomass, an important source of renewable energy. [Online]. <http://www.biomass.net/Biomass-Gasification.html> (visited in April 2011)
- [16] "Final Report: ERA-NET," Sweden, 2010.
- [17] M.A. Gerber, "Review of novel catalysts for biomass tar cracking and methane reforming," Pacific Northwest National Laboratory, Richland, Washington, Prepared for the U.S. Department of Energy October 2007.
- [18] C. Pfeifer and H. Hofbauer, "Development of catalytic tar decomposition downstream from a dual fluidized bed biomass steam gasifier," *Powder Technology*, vol. 180, pp. 9-16, 2008.
- [19] N. Sundac, "Catalytic cracking of tar from biomass gasification," Department of Chemical Engineering, Lund University, Lund, Sweden,.
- [20] G. Taralas, M.G. Kontominas, and X. Kakatsios, "Modeling the thermal destruction of toluene (C<sub>7</sub>H<sub>8</sub>) as tar-related species for fuel gas cleanup," *Energy and Fuels*, vol. 17, pp. 329-337, 2003.
- [21] P.C.A. Bergman, S.V.B. van Paasen, and H. Boerrigter, "The novel "OLGA" technology for complete tar removal from biomass producer gas," in *Paper presented at: Pyrolysis and Gasification of Biomass and Waste, Expert meeting*. Strasbourg, France, 30 September - 1 October 30 September - 1 October 2002.
- [22] C. Brage, Q. Yu, G. Chen, and K. Sjöström, "Use of amino phase adsorbent for biomass tar sampling and separation," *Fuel*, vol. 76, no. 2, pp. 137-142, 1997.
- [23] C. Li and K. Suzuki, "Tar property, analysis, reforming mechanism and model for biomass gasification - an overview," *Renewable and Sustainable Energy Reviews*, vol. 13, pp. 594-604, 2009.
- [24] T.A. Milne, R.J. Evans, and N. Abatzoglou, "Biomass gasifier "tars" their nature, formation, and conversion," U.S. Department of Energy, National Renewable Energy Laboratory, Golden, Colorado, NREL/TP-570-25357, 1998.
- [25] E.G. Baker, M.D. Brown, D.C. Elliott, and L.K. Mudge, "Characterization and treatment of tars from biomass gasifiers," Summer National Meeting, Denver CO, 1988.

- 
- [26] (2010) Biomass Power & Thermal. [Online]. <http://biomassmagazine.com/articles/3451/syngas-tasks> (visited in April 2011)
- [27] J. Corella, J.M. Toledo, and M.P. Aznar, "Improving the modeling of the kinetics of the catalytic tar elimination in biomass gasification," *Industrial & Engineering Chemistry Research*, vol. 41, pp. 3351-3356, 2002.
- [28] F. Lind, M. Israelsson, M. Seemann, and H. Thunman, "Tar cleaning in a dual fluidized bed with  $Mn_3O_4$  on  $Mg-ZrO_3$  as catalyst," The Swedish and Finnish National Committees of the International Flame Research Foundation, Scandinavian-Nordic Section of the Combustion Institute, Göteborg, Sweden, 2010.
- [29] A. Lyngfelt, B. Leckner, and T. Mattisson, "A fluidized-bed combustion process with inherent  $CO_2$  separation; application of chemical-looping combustion," *Chemical Engineering Science*, vol. 10, pp. 3101-3113, 2001.
- [30] M. Johansson, T. Mattisson, and A. Lyngfelt, "Comparison of oxygen carriers for chemical-looping combustion," *Thermal Science*, vol. 10, pp. 93-107, 2006.
- [31] H. Fang, L. Haibin, and Z. Zengli, "Advancemens in development of chamilal-looping combustion: a review," *International Journal of Chemical Engineering*, 2009.
- [32] T. Mattisson and A. Lyngfelt, "Capture of  $CO_2$  using chemical-looping combustion," Department of Energy Conversion, Chalmers University of Technology, Göteborg, Sweden, 2001.
- [33] F. Lind, M. Seemann, and H. Thunman, "Continuous catalytic tar reforming of biomass derived raw gas with simultaneous catalyst regeneration," Department of Energy and Environment, Chalmers University of Technology, Göteborg, Sweden, 2010.
- [34] J. Adánez, L.F. de Diego, F. García-Labiano, P. Gayán, and A. Abad, "Selection of oxygen carriers for chemical-looping combustion," *Energy & Fuels*, pp. 371-377, 2004.
- [35] P. Cho, T. Mattisson, and A. Lyngfelt, "Comparison of iron-, nickel-, copper- and manganese-based oxygen carriers for chemical-looping combustion," *Fuel*, pp. 1215-1225, 2004.
- [36] P. Cho, T. Mattisson, and A. Lyngfelt, "Defluidization conditions for a fluidized bed of iron oxide-, nickel oxide-. and manganese oxide-containing oxygen carriers for chemical-looping combustion," *Industrial and Engineering Chemistry Research*, vol. 45, pp. 968-977, 2006.
- [37] T. Mattisson, A. Järnäs, and A. Lyngfelt, "Reactivity of some metal oxides supported on alumina with alternating methane and oxygen - application for chemical-looping combustion," *Energy and Fuels*, vol. 17, pp. 643-651, 2003.
- [38] M. Johansson, T. Mattisson, and A. Lyngfelt, "Investigation of  $Mn_3O_4$  with stabilized  $ZrO_2$  for chemical-looping combustion," *Chemical Engineering Research and Design*, pp. 807-818, 2006.

- [39] A. Abad, T. Mattisson, A. Lyngfelt, and M. Rydén, "Chemical-looping combustion in a 300W continuously operating reactor system using a manganese-based oxygen carrier," *Fuel*, vol. 9, pp. 1174 - 1185, 2006.
- [40] R. Coll, M. Marquevich, J. Salvadó, and D. Montané, "Steam reforming of biomass gasification tars using model compounds," 1st World Conference on Biomass for Energy and Industry, Sevilla, Spain, 2001.
- [41] I. Narváez, J. Corella, and A. Orío, "Fresh tar (from a biomass gasifier) elimination over a commercial steam-reforming catalyst. Kinetics and effect of different variables of operation," *Industrial and Engineering Chemistry Research*, pp. 317-327, 1997.
- [42] A. Łamacz, A. Krztoń, A. Musi, P. Da Costa, and G. Djéga-Mariadassou, "Reforming of model gasification tar compounds," *Catalysts for Environment Depollution, Renewable Energy and Clean Fuels*, 2008.
- [43] R. Coll, J. Salvadó, X. Farriol, and D. Montané, "Steam reforming model compounds of biomass gasification tars: conversion at different operating conditions and tendency towards coke formation," *Fuel Processing Technology*, pp. 19-31, 2001.
- [44] D. Świerczynski, S. Libs, C. Courson, and A. Kiennemann, "Steam reforming of tar from a biomass gasification process over Ni/olivine catalyst using toluene as a model compound," *Applied Catalysts B: Environmental*, pp. 211-222, 2007.
- [45] D. Swierczynski, C. Courson, and A. Kiennemann, "Study of steam reforming of toluene used as model compound of tar produced by biomass gasification," *Chemical Engineering and Processing*, pp. 508-513, 2008.
- [46] H. Egsgaard and E. Larsen, "Thermal transformation of light tar - specific routes to aromatic aldehydes and PAH," in *1st World Conference on Biomass for Energy and Industry*. Sevilla, Spain: James & James (Science Publishers) Ltd, 2000, pp. 1468-1471.
- [47] G. Taralas, M.G. Kontominas, and X. Kakatsios, "Modeling the thermal destruction of toluene (C<sub>7</sub>H<sub>8</sub>) as tar-related species for fuel gas cleanup," *Energy & Fuels*, pp. 329-337, 2003.
- [48] B. Dou, J. Gao, X. Sha, and S.W. Baek, "Catalytic cracking of tar component from high-temperature fuel gas," *Applied Thermal Engineering*, pp. 2229-2239, 2003.
- [49] P. Simell, E. Kurkela, P. Stahlberg, and J. Hepola, "Catalytic hot gas cleaning of gasification gas," *Catalysts Today*, pp. 55-62, 1996.
- [50] B. Dou et al., "Removal of tar component over cracking catalysts from high temperature fuel gas," *Energy Conversion and Management*, pp. 2247-2253, 2008.

- 
- [51] A. Kumar and M.T. Klein, "Molecule-based modeling of gasoil fluid catalytic cracking," *Preprints of Papers - American Chemical Society. Division of Fuel Chemistry*, pp. 485-489, 1999.
- [52] P.A. Simell, N.A.K. Hakala, H.E. Haarlo, and A.O.I. Krause, "Catalytic decomposition of gasification gas tar with benzene as the model compound," *Industrial and Engineering Chemistry Research*, pp. 42-51, 1997.
- [53] J. Corella, M. A. Caballero, M. P. Aznar, and C. Brage, "Two advanced models for the kinetics of the variation of the tar composition in its catalytic elimination in biomass gasification," *Industrial & Engineering Chemistry Research*, vol. 42, pp. 3001-3011, 2003.
- [54] J. Corella, M.A. Caballero, M.P. Aznar, J. Gil, and C. Brage, "A 6-lump model for the kinetics of the catalytic tar removal in biomass gasification," Proceedings of the 1st World Conference on Biomass for Energy and Industry, London, 2001.
- [55] M.A. Caballero, J. Corella, M.P. Aznar, and J. Gil, "Biomass gasification with air in fluidized bed. Hot gas cleanup with selected commercial and full-sized nickel-based catalysts," *Industrial and Engineering Chemistry Research*, pp. 1143-1154, 2000.
- [56] C. Myrén, C. Hörnell, E. Björnbom, and K. Sjöström, "Catalytic tar decomposition of biomass pyrolysis gas with a combination of dolomite and silica," *Biomass and Bioenergy*, pp. 217-227, 2002.
- [57] W. Torres, S.S. Pansare, and Jr., J.G. Goodwin, "Hot gas removal of tars, ammonia and hydrogen sulfide from biomass gasification gas," *Catalysis Reviews*, pp. 407-456, 2007.
- [58] J. Corella, "On the modeling of the kinetics of the selective deactivation of catalysts. Application to the fluidized catalytic cracking process," *Industrial and Engineering Chemical Research*, pp. 4080-4086, 2004.
- [59] F. Lind, "Catalytic tar cleaning of biomass-derived gas with simultaneous catalyst regeneration," Department of Energy and Environment, Chalmers University of Technology, Gothenburg, Sweden, Licentiate thesis 2011.
- [60] T. Wang, J. Chang, P. Lv, and J. Zhu, "Novel catalyst for cracking of biomass tar," *Energy & Fuels*, vol. 19, pp. 22-27, 2005.
- [61] Aromatics Producers Association, a sector group of Cefic, aromatics online.
- [62] (2000-2010) Chemical Land 21.com. [Online]. <http://www.chemicalland21.com/industrialchem/organic/PHENANTHRENE.htm> (visited in April 2011)
- [63] "Public Health Statement, Polycyclic Aromatic Hydrocarbons," U.S. Department of Health and Human Services, Agency for Toxic Substances and Disease Registry (ATSDR), Atlanta, 1990.

- [64] A. Dufour et al., "Comparison of two methods of measuring wood pyrolysis tar," *Journal of Chromatography A*, vol. 1164, pp. 240-247, 2007.
- [65] J. Bolhar-Nordenkamp, T. Pröll, P. Kolbitsch, and H. Hofbauer, "Comprehensive modeling tool for chemical-looping based processes," *Chemical Engineering & Technology*, vol. 3, pp. 410-417, 2009.



## APPENDIX I – WORLD SHARES OF FUELS’ PRODUCTION

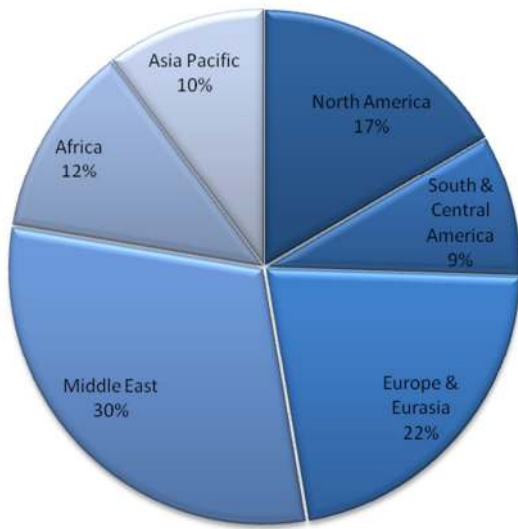


Figure 50.a

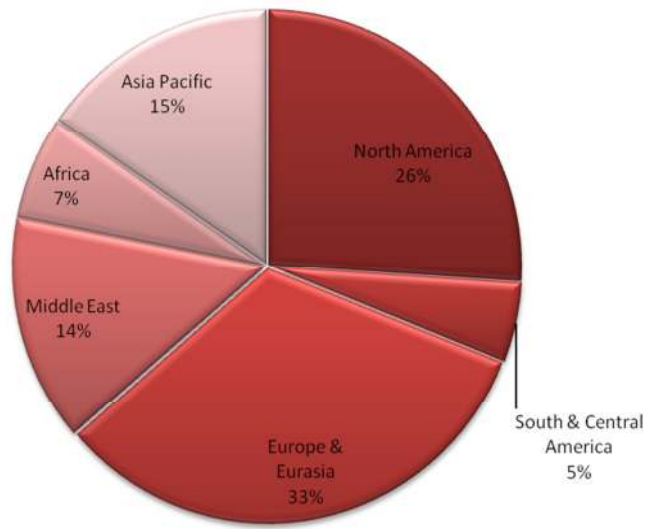


Figure 50.b

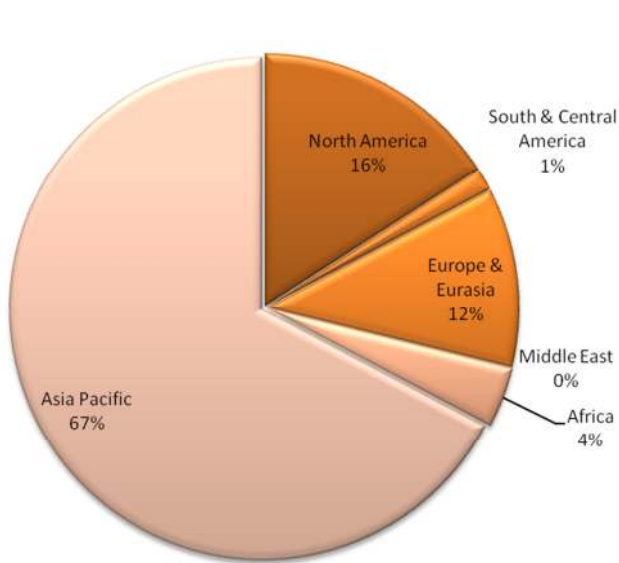


Figure 50.c

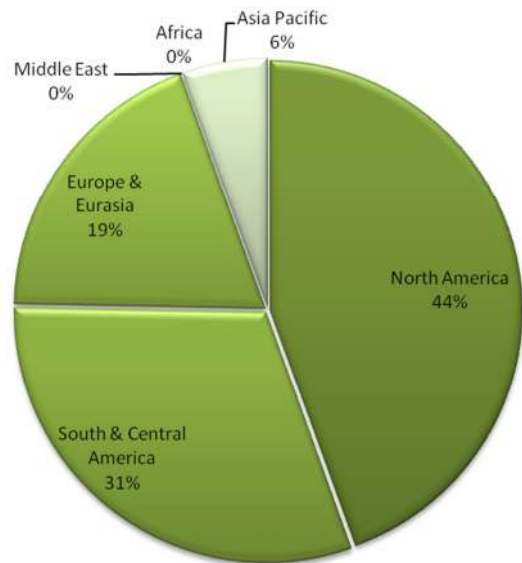


Figure 50.d

**Figure 50** - World energy production shares of: a) coal; b) natural gas; c) oil; d) biofuels

## **APPENDIX II – GAS CLEANING TECHNOLOGIES**

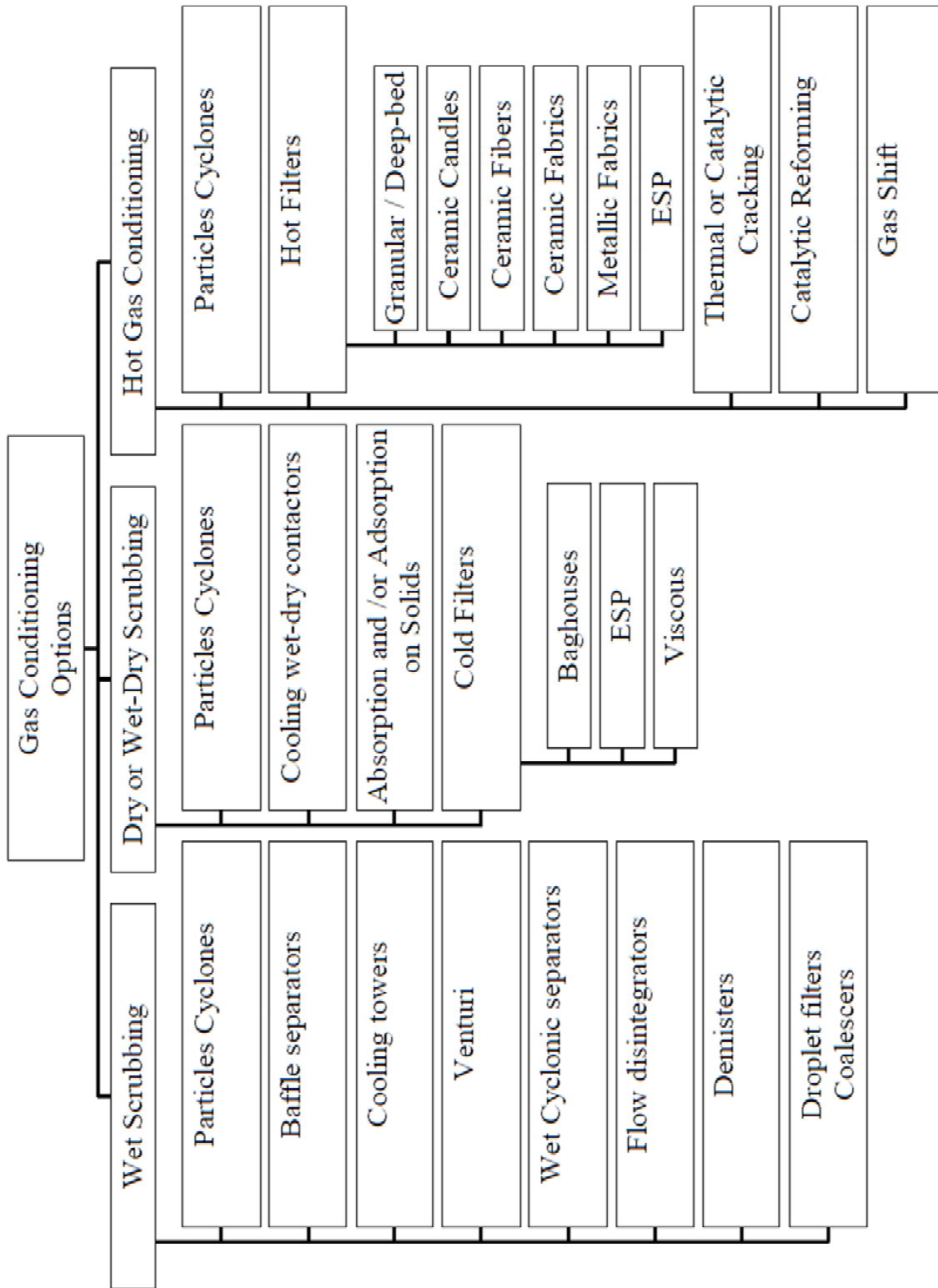
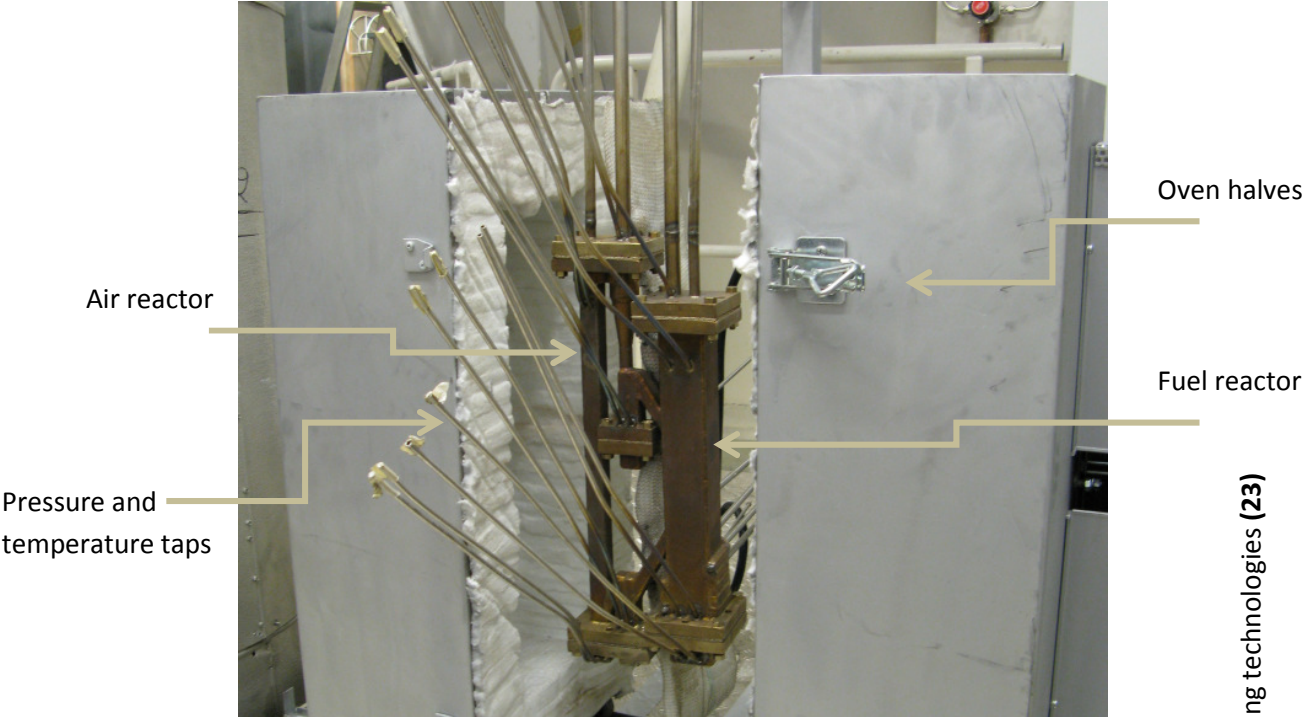


Figure 51 - Gas cleaning technologies (23)

**APPENDIX III – CLR SYSTEM**



**Figure 52** - CLR-System

**Figure 51** - Gas cleaning technologies (23)



**Figure 53** - CLR-System after operation

## APPENDIX IV – RESULTS OF PREVIOUS STUDIES

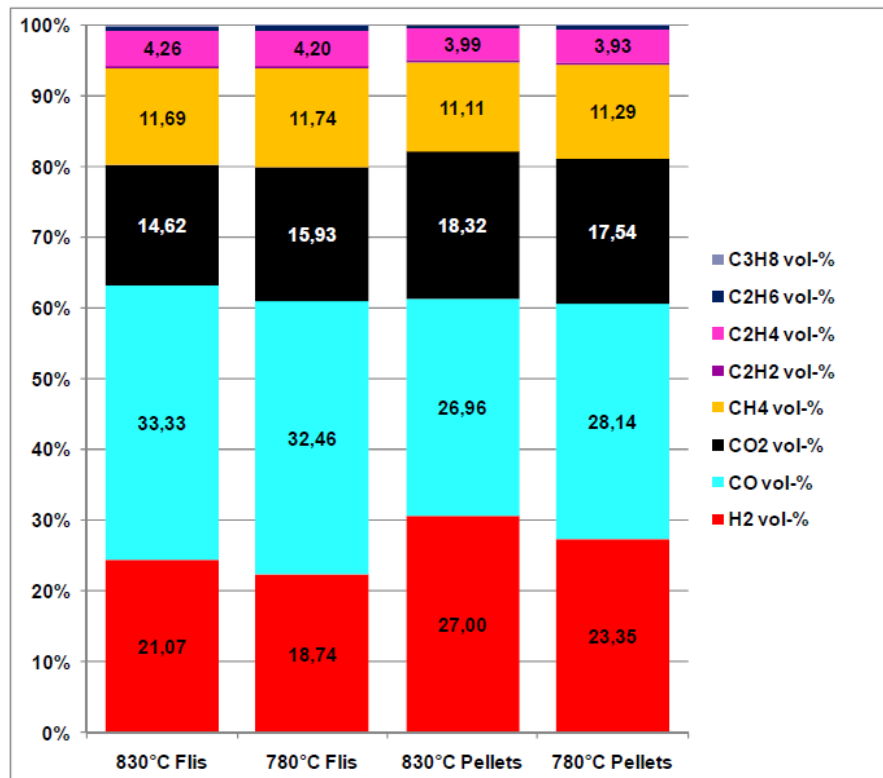


Figure 54 - Chalmers gasifier product gas from gasification of wood chips and wood pellets

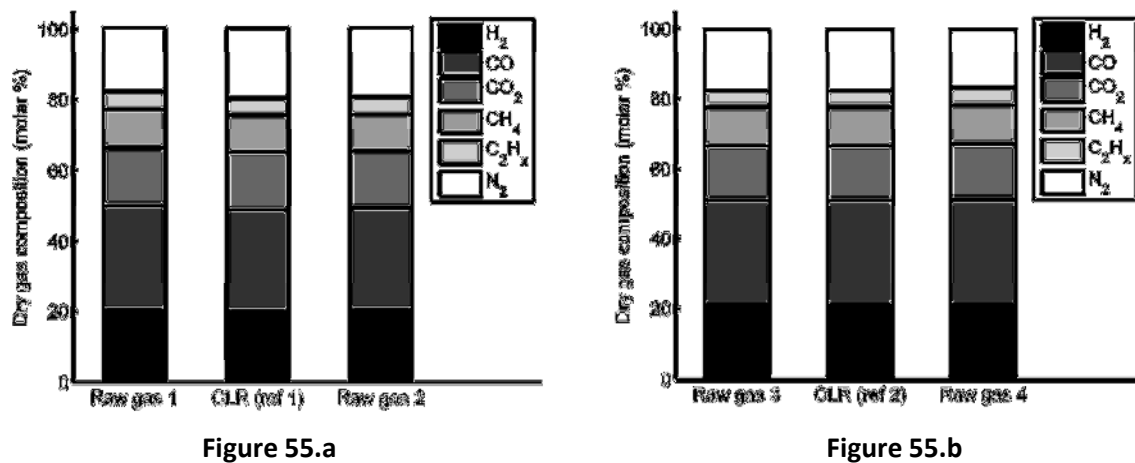


Figure 55 - CLR reference experiments with silica-sand [33]: a) at 740°C; b) at 815°C

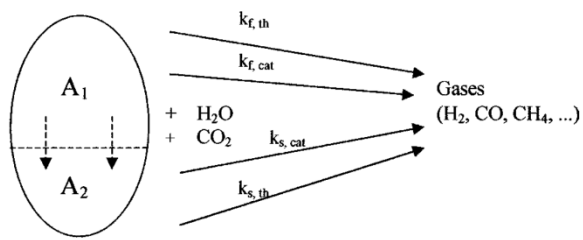


Figure 56.a

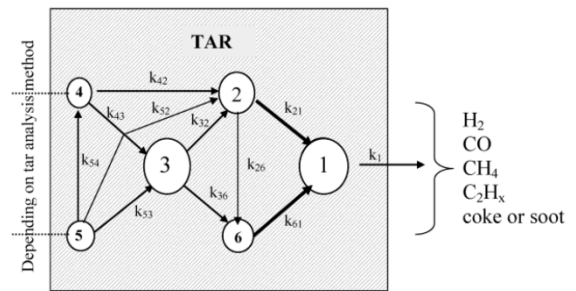



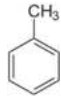

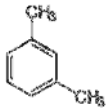
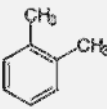
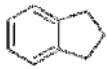
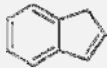
Figure 56.b

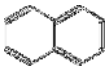
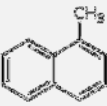
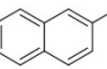
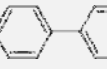
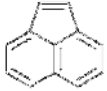

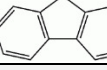
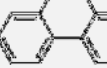
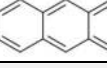
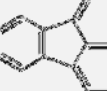
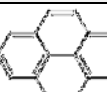
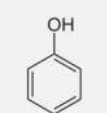
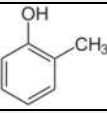
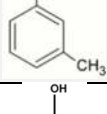
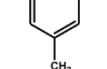
Figure 56 - Previous models by Corella et al.: a) Two-Lump model [27]; b) Six-Lump model [53]

## APPENDIX V – DETAILED INFORMATION ON IDENTIFIED TAR MOLECULES

Aromatic hydrocarbons are organic compounds that consist exclusively of the elements carbon (C) and hydrogen (H). The word “aromatic” means that the compound have similar properties to benzene, such as, a ring-like structure and the carbon atoms being interchangingly linked together via simple and double bonds [61]. Polycyclic aromatic hydrocarbons (PAHs) consist of fused aromatic rings and do not contain heteroatoms, this is, any atom that is not carbon or hydrogen, or carry any substituents. They have two or more single or fused aromatic rings, if a pair of carbon atoms is shared between rings in their molecules [62]. Naphthalene and Biphenyl are the simplest examples of a PAH. The PAHs composed only of six-membered rings (fused benzene rings in a rectilinear arrangement) are called alternant PAHs, while the ones containing one ring other than benzene are called non-alternant. PAHs may contain four-, five- or six-rings, called “small” PAHs or even seven-rings, called “large” PAHs. Five or six ringed PAHs are the most common. PAHs are solid and range in appearance from colorless to white or pale yellow-green [63].

**Table 14** - Information on identified tar molecules

Molecule name	Chemical Symbol	Structure	Relevant Properties
<b>Benzene</b>	C <sub>6</sub> H <sub>6</sub>		<ul style="list-style-type: none"> <li>Is the simplest aromatic hydrocarbon (recognized as the first);</li> <li>Highly polyunsaturated structure, with just one hydrogen atom for each carbon atom;</li> <li>High carbon-hydrogen ratio.</li> </ul>
<b>Toluene</b>	C <sub>7</sub> H <sub>8</sub>		<ul style="list-style-type: none"> <li>Is a mono-substituted benzene derivative (a single hydrogen atom has been replaced by an univalent group, in this case CH<sub>3</sub>);</li> <li>Toluene hydrodealkylation converts toluene to benzene and methane.</li> </ul>
<b>p-Xylene</b>	C <sub>8</sub> H <sub>10</sub>		<ul style="list-style-type: none"> <li>Derivative from benzene with two methyl substituents;</li> <li>The “p” stands for <i>para</i>, identifying the location of the methyl groups as across one from another.</li> </ul>
<b>m-Xylene</b>	C <sub>8</sub> H <sub>10</sub>		<ul style="list-style-type: none"> <li>Derivative from benzene with two methyl substituents;</li> <li>The “m” stands for <i>meta</i>, meaning the two methyl groups are at locants 1 and 3 on the aromatic ring.</li> </ul>
<b>o-Xylene</b>	C <sub>8</sub> H <sub>10</sub>		<ul style="list-style-type: none"> <li>Derivative from benzene with two methyl substituents;</li> <li>The “o” stands for <i>ortho</i>, as the two methyl groups are bonded to adjacent carbon atoms in the aromatic ring.</li> </ul>
<b>Indan</b>	C <sub>9</sub> H <sub>10</sub>		<ul style="list-style-type: none"> <li>Is a hydrocarbon petrochemical compound;</li> <li>Can be converted in a catalytic reactor to other aromatics such as Xylenes.</li> </ul>
<b>Indene</b>	C <sub>9</sub> H <sub>8</sub>		<ul style="list-style-type: none"> <li>Is a polycyclic hydrocarbon;</li> <li>It is composed of a benzene ring fused with a cyclopentene ring.</li> </ul>

<b>Naphthalene</b>	$C_{10}H_8$		<ul style="list-style-type: none"> <li>• Its structure consists of a fused pair of benzene rings;</li> <li>• The simplest of fused aromatic rings PAHs;</li> <li>• The carbon-carbon bonds are not of the same length (unlike benzene).</li> </ul>
<b>1-Methylnaphthalene</b>	$C_{11}H_{10}$		<ul style="list-style-type: none"> <li>• Is a bicyclic aromatic hydrocarbon (PAH);</li> <li>• Is a methyl substituted naphthalene;</li> <li>• It is found in crude oil and other petroleum products.</li> </ul>
<b>2-Methylnaphthalene</b>	$C_{11}H_{10}$		<ul style="list-style-type: none"> <li>• Is a bicyclic aromatic hydrocarbon (PAH);</li> <li>• Is a methyl substituted naphthalene;</li> <li>• It is found in crude oil and other petroleum products.</li> </ul>
<b>Biphenyl</b>	$C_{12}H_{10}$		<ul style="list-style-type: none"> <li>• Simplest of single aromatic rings PAHs;</li> <li>• Molecule consists of two connected phenyl rings;</li> <li>• Lacking functional groups;</li> </ul>
<b>Acenaphthylene</b>	$C_{12}H_8$		<ul style="list-style-type: none"> <li>• PAH consisting of naphthalene with an ethylene bridge connecting positions 1 and 8;</li> <li>• Constituent of coal tar.</li> </ul>
<b>Acenaphthene</b>	$C_{12}H_{10}$		<ul style="list-style-type: none"> <li>• PAH consisting of naphthalene with an ethylene bridge connecting positions 1 and 8;</li> <li>• Constituent of coal tar.</li> </ul>
<b>Fluorene</b>	$C_{13}H_{10}$		<ul style="list-style-type: none"> <li>• Non-alternant PAH;</li> <li>• Constituent of coal tar.</li> </ul>
<b>Phenanthrene</b>	$C_{14}H_{10}$		<ul style="list-style-type: none"> <li>• PAH composed of three fused benzene rings;</li> <li>• The name is a composite of phenyl and Anthracene;</li> </ul>
<b>Anthracene</b>	$C_{14}H_{10}$		<ul style="list-style-type: none"> <li>• PAH consisting of three fused benzene rings;</li> <li>• Linear isomer of Phenanthrene and less stable.</li> </ul>
<b>Fluoranthene</b>	$C_{16}H_{10}$		<ul style="list-style-type: none"> <li>• Non-alternant PAH consisting of a naphthalene and a benzene unit connected by a five-membered ring;</li> <li>• Structural isomer of Pyrene and less stable.</li> </ul>
<b>Pyrene</b>	$C_{16}H_{10}$		<ul style="list-style-type: none"> <li>• Alternant PAH consisting of four fused benzene rings;</li> <li>• Flat aromatic system;</li> </ul>
<b>Phenol</b>	$C_6H_6O$		<ul style="list-style-type: none"> <li>• Is an organic compound consisting of a phenyl (<math>-C_6H_5</math>) group bonded to a hydroxyl (<math>-OH</math>) group;</li> <li>• It has weak tendencies to lose the <math>H^+</math> ion from the hydroxyl group.</li> </ul>
<b>o-Cresol</b>	$C_7H_8O$		<ul style="list-style-type: none"> <li>• Organic compound which is a methyl phenol;</li> <li>• The "o" stands for <i>ortho</i>, or the methyl group is on the second position.</li> </ul>
<b>m-Cresol</b>	$C_7H_8O$		<ul style="list-style-type: none"> <li>• Organic compound which is a methyl phenol;</li> <li>• The "m" stands for <i>meta</i>, or the methyl group is on the third position.</li> </ul>
<b>p-Cresol</b>	$C_7H_8O$		<ul style="list-style-type: none"> <li>• Organic compound which is a methyl phenol;</li> <li>• The "p" stands for <i>para</i>, or the methyl group is on the fourth position.</li> </ul>



## APPENDIX VI – RELATIVE STANDARD DEVIATION TABLES

**Table 15** - RSD result values for the samples of manganese catalyst at 700°C

700°C						
NAME	RELATIVE STANDARD DEVIATION - RSD [%]					
	REF	1% O <sub>2</sub>	2,2% O <sub>2</sub>	REF	1% O <sub>2</sub>	2,2% O <sub>2</sub>
Benzene	10,75	7,62	5,55	10,75	7,62	5,55
Naphthalene	5,26	6,31	4,72	5,26	6,31	4,72
Toluene	5,56	4,48	6,71	4,14	4,17	3,41
m/p-Xylene	10,70	5,55	9,46			
o-Xylene	13,26	9,46	10,51			
1-Methylnaphthalene	5,30	7,88	6,89			
2-Methylnaphthalene	4,68	7,41	7,27			
Biphenyl	7,06	1,81	6,61			
Unknown_1	5,29	8,11	3,22			
Indan	7,38	84,53	2,73	5,87	5,61	8,68
Indene	1,51	12,86	7,07			
Acenaphthylene	7,81	1,86	9,53			
Acenaphthene	7,96	4,87	7,00			
Fluorene	9,67	6,28	11,52			
Unknown_2	12,53	4,36	12,05			
Phenanthrene	13,61	11,47	11,00	14,78	17,78	16,03
Anthracene	13,06	11,21	12,46			
Fluoranthene	17,93	13,97	17,35			
Pyrene	16,76	14,16	16,60			
Unknown_3	14,92	27,00	21,69			
Phenol	24,49	16,45	11,08	22,56	16,46	10,05
o-Cresol	0,00	0,00	0,00			
m-Cresol	15,70	14,05	3,52			
p-Cresol	22,92	28,25	0,00			
<b>Total</b>	<b>4,29</b>	<b>4,47</b>	<b>6,87</b>	<b>4,29</b>	<b>4,47</b>	<b>6,87</b>

**Table 16** - RSD result values for the samples of manganese catalyst at 750°C

23% MANGANESE @ 750°C							
NAME	RELATIVE STANDARD DEVIATION - RSD [%]						
	REF	1% O <sub>2</sub>	2,2% O <sub>2</sub>	REF	1% O <sub>2</sub>	2,2% O <sub>2</sub>	
Benzene	19,01	37,78	24,19	19,01	37,78	24,19	
Naphthalene	6,74	6,64	16,66	6,74	6,64	16,66	
Toluene	8,72	27,23	12,18	4,92	5,66	7,63	
m/p-Xylene	7,02	20,80	13,67				
o-Xylene	5,29	16,19	9,28				
1-Methylnaphthalene	9,06	6,74	17,75				
2-Methylnaphthalene	8,76	7,63	17,79				
Biphenyl	11,28	5,72	15,36				
Unknown_1	7,07	11,24	15,92	12,13	9,13	15,99	
Indan	9,24	9,63	9,71				
Indene	4,74	9,96	17,84				
Acenaphthylene	12,19	7,16	15,08				
Acenaphthene	12,91	7,18	15,67				
Fluorene	14,39	9,69	16,75				
Unknown_2	21,55	11,05	18,76	19,33	6,75	10,68	
Phenanthrene	16,61	6,39	9,48				
Anthracene	15,91	7,80	10,01				
Fluoranthene	20,30	5,86	10,64				
Pyrene	17,79	5,57	12,12				
Unknown_3	21,10	8,11	14,55	11,45	1,44	12,39	
Phenol	11,34	0,26	11,14				
o-Cresol	0,00	0,00	25,80				
m-Cresol	9,32	5,60	73,32				
p-Cresol	8,72	13,79	44,01				
<b>Total</b>	8,44	4,16	10,24	8,44	4,16	10,24	

**Table 17** - RSD result values for the samples of manganese catalyst at 800°C

800°C							
NAME	RELATIVE STANDARD DEVIATION - RSD [%]						
	REF	1% O <sub>2</sub>	2,2% O <sub>2</sub>	REF	1% O <sub>2</sub>	2,2% O <sub>2</sub>	
Benzene	23,85	27,76	13,22	23,85	27,76	13,22	
Naphthalene	7,55	8,10	5,68	7,55	8,10	5,68	
Toluene	17,23	19,02	10,69	2,66	3,02	7,09	
m/p-Xylene	16,71	18,63	11,58				
o-Xylene	21,23	12,14	7,60				
1-Methylnaphthalene	6,80	20,67	10,18				
2-Methylnaphthalene	7,03	16,99	8,89				
Biphenyl	9,61	9,31	6,49				
Unknown_1	3,97	28,37	7,01				
Indan	31,46	11,14	6,20	6,82	11,16	6,52	
Indene	3,42	9,11	6,50				
Acenaphthylene	9,88	10,29	7,49				
Acenaphthene	8,70	14,70	7,90				
Fluorene	11,08	22,97	51,97				
Unknown_2	11,88	19,13	18,40				
Phenanthrene	13,77	6,66	10,11	13,52	3,99	12,03	
Anthracene	13,59	5,17	10,24				
Fluoranthene	16,52	3,44	12,54				
Pyrene	15,71	3,06	13,72				
Unknown_3	12,84	19,13	16,62				
Phenol	3,26	55,84	35,07	5,00	55,84	35,07	
o-Cresol	16,83	0,00	0,00				
m-Cresol	6,79	0,00	0,00				
p-Cresol	8,60	0,00	0,00				
<b>Total</b>	5,35	4,76	6,49	5,35	4,76	6,49	

## APPENDIX VII - ADDITIONAL RESULTS FOR TARS CALCULATIONS

**Table 18** - Tar values and grouping for 23% manganese at 700°C and three situations: reference from the gasifier, 1% oxygen concentration and 2,2% oxygen concentration

NAME	QUANTITY [g/m <sup>3</sup> normal]			RELATIVE PERCENTAGE IN TOTAL TARS [%]			CONVERSIONS [%]			QUANTITY GROUPED [g/m <sup>3</sup> normal]			CONVERSIONS GROUPED [%]					
	REF	1%	2,2%	REF	1%	2,2%	1%	2,2%	REF	1%	2,2%	REF	1%	2,2%	REF	1%	2,2%	
	Benzene	0,78	0,68	0,65	2,39	2,40	2,30	12,4	16,7	0,78	0,68	0,65	12,4	16,7	0,78	0,68	0,65	12,4
Naphthalene	7,80	8,21	9,29	24,0	28,9	32,8	-5,26	-19,1	7,80	8,21	9,29	-5,26	-19,1	7,80	8,21	9,29	-5,26	-19,1
Toluene	0,81	0,73	0,64	2,48	2,55	2,25	10,1	21,3										
m/p-Xylene	0,20	0,18	0,14	0,62	0,62	0,50	13,2	30,6										
o-Xylene	1,26	1,16	1,01	3,86	4,06	3,58	8,13	19,5										
1-Methylnaphthalene	0,80	0,66	0,61	2,44	2,34	2,16	16,5	23,1	7,41	6,11	5,54	17,6	25,3	7,41	6,11	5,54	17,6	25,3
2-Methylnaphthalene	1,24	1,07	1,00	3,82	3,75	3,52	14,0	19,9										
Biphenyl	0,53	0,60	0,75	1,63	2,12	2,65	-13,7	-41,4										
Unknown_1	2,57	1,71	1,39	7,90	6,03	4,92	33,4	45,9										
Indan	0,04	0,06	0,03	0,13	0,22	0,10	-51,7	33,9										
Indene	3,80	2,08	1,45	11,7	7,31	5,11	45,2	61,9										
Acenaphthylene	2,31	2,22	2,34	7,11	7,81	8,27	3,99	-1,12	9,00	6,36	5,63	29,3	37,5	9,00	6,36	5,63	29,3	37,5
Acenaphthene	0,16	0,09	0,09	0,50	0,33	0,31	42,5	46,8										
Fluorene	0,79	0,57	0,48	2,41	2,00	1,68	27,5	39,4										
Unknown_2	1,90	1,33	1,25	5,83	4,69	4,42	29,6	34,0										
Phenanthrene	1,50	1,85	2,28	4,62	6,51	8,07	-23,1	-51,8										
Anthracene	0,45	0,55	0,64	1,39	1,92	2,28	-20,3	-42,2										
Fluoranthene	0,43	0,52	0,64	1,32	1,82	2,25	-20,3	-47,7	5,85	6,09	6,75	-4,12	-15,4	5,85	6,09	6,75	-4,12	-15,4
Pyrene	0,48	0,59	0,74	1,48	2,07	2,60	-22,0	-52,4										
Unknown_3	2,98	2,58	2,45	9,14	9,08	8,64	13,2	17,8										
Phenol	1,39	0,89	0,42	4,28	3,14	1,47	35,8	70,1										
o-Cresol	0,07	0,00	-	0,20	-	-	-	-	1,72	0,99	0,45	42,4	73,8	1,72	0,99	0,45	42,4	73,8
m-Cresol	0,20	0,08	0,04	0,62	-	-	-	-										
p-Cresol	0,06	0,02	-	0,19	-	-	-	-										
<b>Total</b>	<b>32,6</b>	<b>28,4</b>	<b>28,3</b>	<b>100</b>	<b>100</b>	<b>100</b>			<b>32,6</b>	<b>28,4</b>	<b>28,3</b>			<b>32,6</b>	<b>28,4</b>	<b>28,3</b>		

**Table 19** - Tar values and grouping for 23% manganese at 800°C and three situations: reference from the gasifier, 1% oxygen concentration and 2,2% oxygen concentration

NAME	QUANTITY [g/m <sup>3</sup> normal] He-corrected			PERCENTAGE IN TOTAL TARS [%]			CONVERSIONS [%]			QUANTITY GROUPED [g/m <sup>3</sup> normal]			CONVERSIONS GROUPED [%]						
	REF	1%	2,2%	REF	1%	2,2%	REF	1%	2,2%	REF	1%	2,2%	REF	1%	2,2%				
	Benzene	0,36	0,84	0,64	1,25	3,36	3,35							0,36	0,84	0,64	-137	-79,9	-137
Naphthalene	4,94	6,41	5,66	17,3	25,5	29,5							4,94	6,41	5,66	-29,8	-14,6	-29,8	-14,6
Toluene	0,60	0,99	0,69	2,12	3,95	3,59										-63,9	-13,8		
m/p-Xylene	0,23	0,26	0,19	0,82	1,05	0,98										-13,6	19,1		
o-Xylene	0,99	1,29	0,97	3,46	5,13	5,06										-30,6	1,61		
1-Methylnaphthalene	0,79	0,63	0,48	2,76	2,51	2,51							8,42	6,78	5,08	19,9	38,8	19,5	39,7
2-Methylnaphthalene	1,23	1,07	0,82	4,32	4,25	4,27										13,3	33,6		
Biphenyl	0,36	0,48	0,43	1,27	1,90	2,24										-31,4	-18,1		
Unknown_1	4,22	2,06	1,51	14,8	8,21	7,87										51,2	64,3		
Indan	0,04	0,04	0,03	0,15	0,15	0,15										14,0	32,2		
Indene	2,88	1,93	1,37	10,1	7,70	7,15										33,0	52,5		
Acenaphthylene	1,41	1,64	1,30	4,94	6,52	6,77										-16,4	7,77		
Acenaphthene	0,19	0,09	0,07	0,65	0,36	0,38										51,3	61,4		
Fluorene	0,46	0,43	0,27	1,63	1,70	1,43										7,85	41,0		
Unknown_2	2,19	1,25	0,80	7,70	5,00	4,19										42,8	63,4		
Phenanthrene	0,91	1,28	0,99	3,21	5,11	5,14										-40,3	-7,82		
Anthracene	0,27	0,39	0,28	0,95	1,53	1,46										-42,9	-4,14		
Fluoranthene	0,26	0,34	0,25	0,90	1,34	1,31										-32,2	1,71		
Pyrene	0,30	0,37	0,26	1,05	1,48	1,38										-24,2	11,6		
Unknown_3	2,59	1,74	1,05	9,10	6,92	5,46										33,0	59,6		
Phenol	2,18	1,29	0,95	7,66	5,12	4,94										41,1	56,6		
o-Cresol	0,18	0,03	0,02	0,61	-	-										-	-		
m-Cresol	0,50	0,20	0,08	1,77	-	-										-	-		
p-Cresol	0,40	0,07	0,07	1,41	-	-										-	-		
<b>Total</b>	<b>28,5</b>	<b>25,1</b>	<b>19,2</b>	<b>100</b>	<b>100</b>	<b>100</b>							<b>28,5</b>	<b>25,1</b>	<b>19,2</b>				

**Table 20** - Tar values and grouping for 23% manganese at 750°C and three situations: reference from the gasifier, 1% oxygen concentration and 2,2% oxygen concentration

NAME	QUANTITY [g/m <sup>3</sup> normal]			RELATIVE PERCENTAGE IN TOTAL TAR [ % ]			CONVERSIONS [ % ]			QUANTITY GROUPED [g/m <sup>3</sup> normal]			CONVERSIONS GROUPED [ % ]		
	He-corrected			TOTAL TAR [ % ]			1,0% 2,2%			REF 1% 2,2%			1% 2,2%		
	REF	1%	2,2%	REF	1%	2,2%	REF	1,0%	2,2%	REF	1%	2,2%	REF	1%	2,2%
Benzene	0,48	1,15	1,15	1,41	5,42	6,13		-138	-137		0,48	1,15	1,15	-138	-137
Naphthalene	7,42	9,70	8,47	21,5	45,6	45,1		-30,8	-14,2		7,42	9,70	8,47	-30,8	-14,2
Toluene	0,63	0,65	0,61	1,82	3,03	3,25		-2,95	2,58						
m/p-Xylene	0,18	0,07	0,07	0,53	0,35	0,39		59,0	59,9						
o-Xylene	1,05	0,81	0,86	3,06	3,80	4,58		23,3	18,5						
1-Methylnaphthalene	0,81	0,24	0,18	2,35	1,13	0,95		70,4	78,1		7,30	3,58	3,22	51,0	55,9
2-Methylnaphthalene	1,29	0,51	0,38	3,74	2,40	2,04		60,4	70,4						
Biphenyl	0,52	0,80	0,66	1,51	3,77	3,52		-53,9	-26,9						
Unknown_1	2,82	0,50	0,45	8,16	2,34	2,41		82,4	83,9						
Indan	0,04	0,17	0,16	0,12	0,78	0,83		-289	-266						
Indene	3,74	0,65	0,62	10,8	3,06	3,32		82,6	83,3						
Acenaphthylene	2,30	1,46	1,28	6,66	6,85	6,81		36,6	44,4		9,40	2,93	2,61	68,8	72,2
Acenaphthene	0,17	0,06	0,05	0,50	0,26	0,24		67,9	73,7						
Fluorene	0,82	0,13	0,09	2,38	0,63	0,48		83,6	89,1						
Unknown_2	2,32	0,47	0,42	6,72	2,21	2,22		79,8	82,0						
Phenanthrene	1,64	1,77	1,52	4,76	8,32	8,11		-7,85	7,28						
Anthracene	0,49	0,41	0,34	1,43	1,91	1,82		17,8	30,7						
Fluoranthene	0,48	0,42	0,37	1,39	1,96	1,98		13,2	22,7		6,88	3,82	3,25	44,5	52,8
Pyrene	0,53	0,42	0,37	1,55	1,98	1,97		21,2	30,9						
Unknown_3	3,73	0,81	0,64	10,82	3,80	3,42		78,4	82,8						
Phenol	2,15	0,08	0,07	6,22	0,39	0,38		96,1	96,7						
o-Cresol	0,25	-	-	0,73	-	-		-	-		3,02	0,08	0,07	97,3	97,6
m-Cresol	0,47	-	-	1,36	-	-		-	-						
p-Cresol	0,15	-	-	0,43	-	-		-	-						
<b>Total</b>	<b>34,5</b>	<b>21,3</b>	<b>18,8</b>	<b>100</b>	<b>100</b>	<b>100</b>					<b>34,5</b>	<b>21,3</b>	<b>18,8</b>		

As explained in the methodology, grouped quantities are simply the sum of all the elements concentrations from that specific group, as to be representative of the “size” and “composition” of the group and grouped conversions is the conversion calculated from the grouped quantities. Negative conversions mean tar forming instead of decomposing.

The color scheme was chosen according to the previous table:

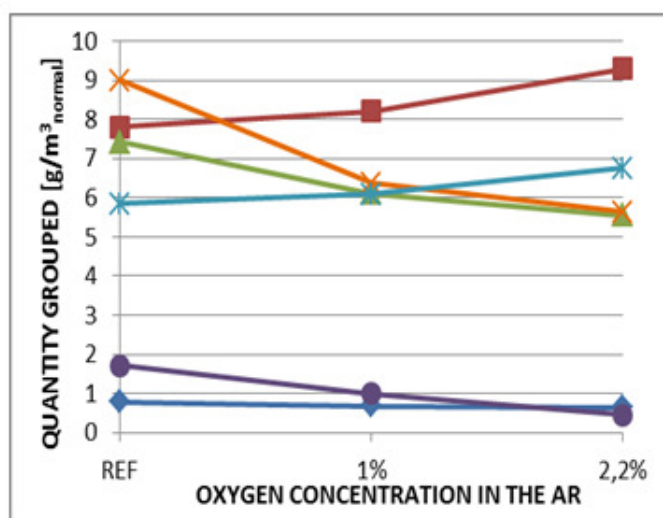
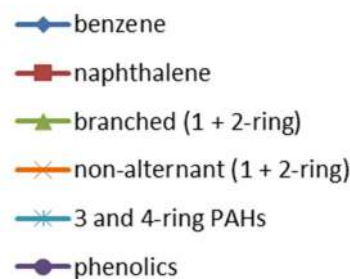


Figure 57.a

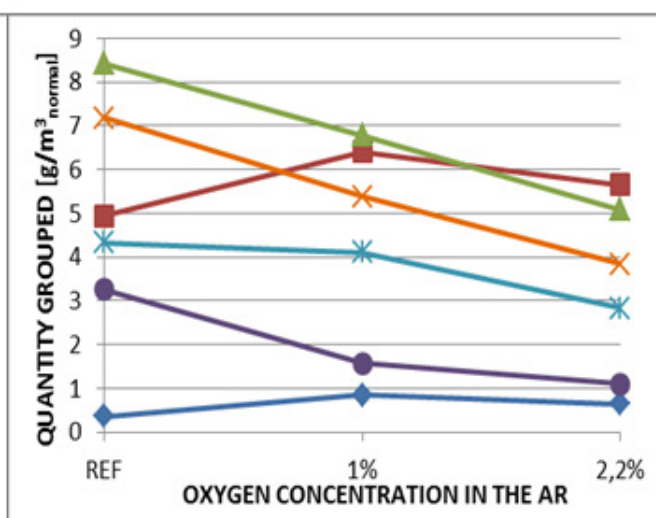


Figure 57.b

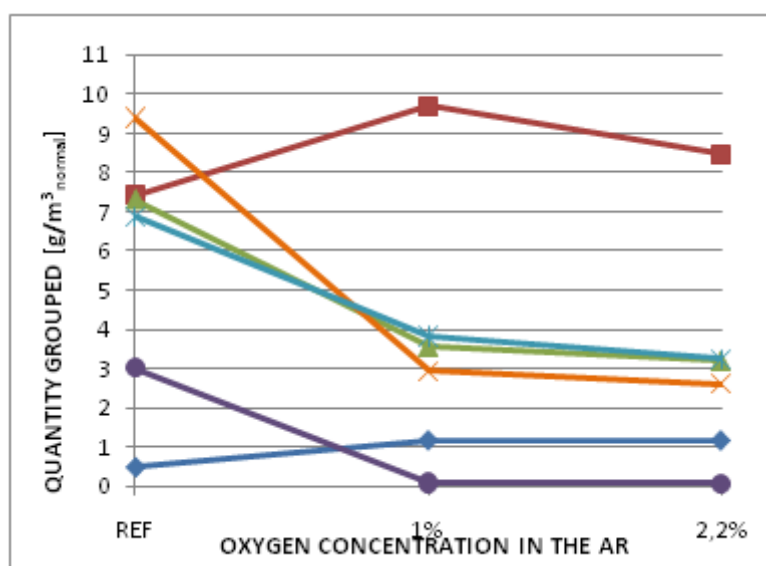


Figure 57.c

**Figure 57** - Group concentrations before and after CLR-System on the two oxygen concentrations and at: a) 700°C; b) 750°C; c) 800°C

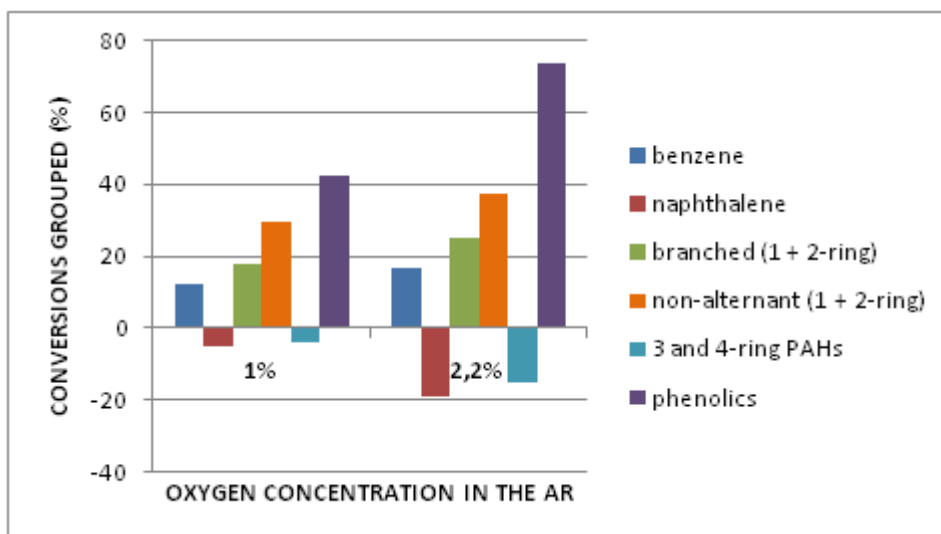


Figure 58.a

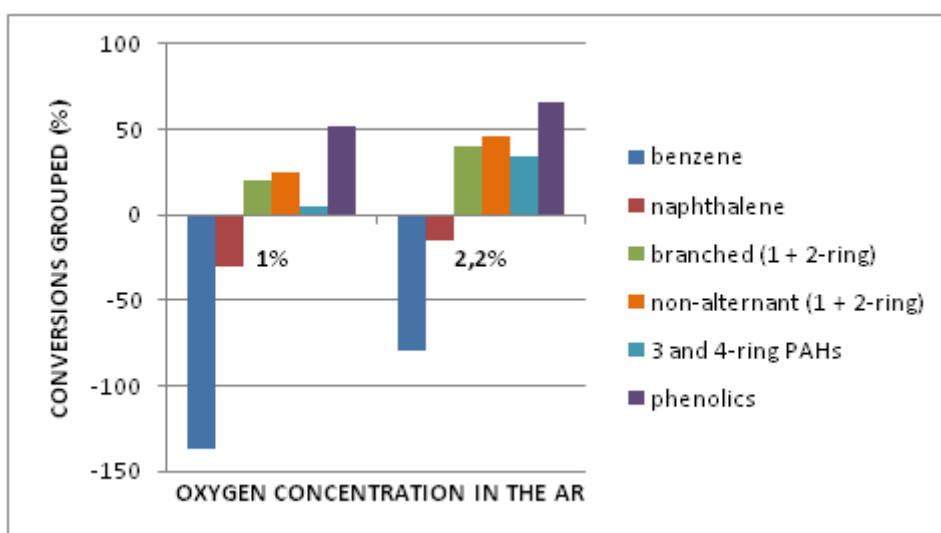


Figure 58.b

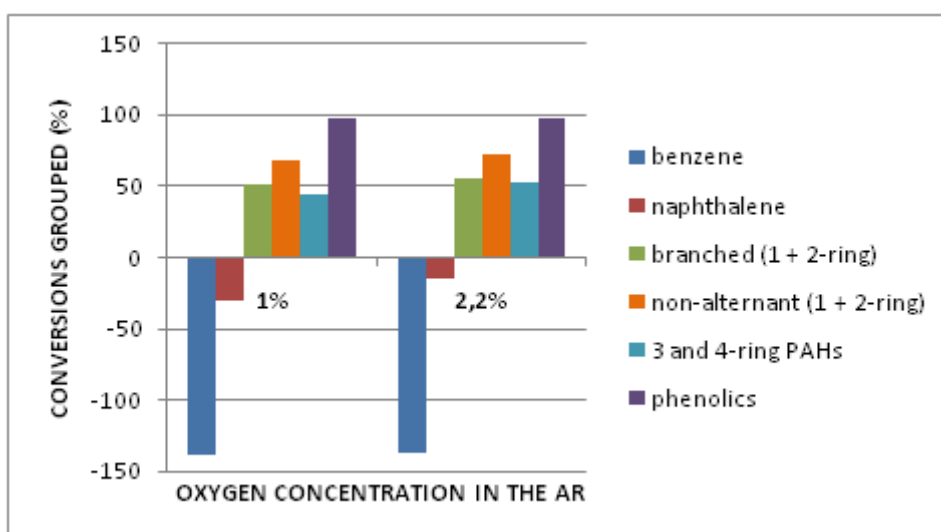


Figure 58.c

Figure 58 - Group conversions of total amount of tars on the two oxygen concentrations and at: a) 700°C; b) 750°C; c) 800°C